Master's Thesis

M.Sc. Course "Actuarial Science"

Pandemics, Wars and More: How to Correct for Singular Events in Mortality Forecasting Models

submitted by:

Thom van Rijn

Matriculation No.: 20-059-184

Address:

Basel

Telephone No.:

Email: teb.vanrijn@gmail.com

supervised by:

Dr. Frank Weber

Submission date, place:

06.10.2022, Basel

Abstract

Historic events such as pandemics (COVID-19 or AIDS), wars (World War I or World War II) or other anomalies (Year Without a Summer) can have large impacts on the observed mortality frequencies. When left uncorrected, these impacts can distort parameters of mortality forecasting models. This has multiple negative implications, such as a decreased fitting and projection quality. This thesis attempts to set up a framework to deal with these historic events (named singular events in the thesis). The thesis shortly covers three well-known mortality forecasting models (Nolfi, Lee-Carter and Renshaw-Haberman). Afterwards, methods for defining and identifying singular events are explored. Finally, the thesis applies several correction methods which show promising results such as an improved estimation quality.

Contents

List of Figures **IV**

List of Abbreviations **XX**

1 Introduction **1**

2 Mortality Forecasting Models **9**
2.1 Nolfi . . . 9
2.1.1 Fitting . . . 10
2.1.2 Projecting . . . 13
2.2 Lee-Carter . . . 14
2.2.1 Fitting . . . 15
2.2.2 Projecting . . . 18
2.3 Renshaw-Haberman . . . 19
2.3.1 Fitting . . . 20
2.3.2 Projecting . . . 23

3 Defining and Identifying Singular Events **26**
3.1 Expert Judgement . . . 30
3.2 Algorithm . . . 32
3.2.1 Part One: Finding the Affected Calendar Years . . . 33
3.2.2 Part Two: Finding the Affected Ages . . . 38

4 Singular Event Corrections **43**
4.1 Single Model Correction . . . 45
4.1.1 Nolfi . . . 50
4.1.2 Lee-Carter . . . 57
4.1.3 Nolfi vs Lee-Carter . . . 63
4.2 Iterative Model Corrections . . . 64
4.2.1 Stationary Singular Event . . . 67
4.2.2 Moving Singular Event . . . 75
4.3 Final Fit Correction . . . 83
4.3.1 Lee-Carter . . . 85
4.3.2 Renshaw-Haberman . . . 88

5 Conclusion **93**

Appendix **96**
Appendix A: WW I (France) . . . 97
Appendix B: WW II (France) . . . 106
Appendix C: Spanish Flu (Switzerland) . . . 115

References **124**

List of Figures

1 Lifespan cumulative distribution function (CDF) for Swiss people for years 1876-1880 and 1998-2003. The left graph shows an infant mortality rate (ages 0-1) of approximately 20%, whereas the right graph shows an infant mortality rate (ages 0-1) of less than 1%. Furthermore, the left graph shows that between 1876-1880 only approximately 30% of the population reached an age of 65 years or older. In the right graph, approximately 90% of people reach an age that is older than 65 years. Source: (cf. [1]). 1

2 Life expectancy for Swiss men and women for generations 1876 until 2020. The graph shows a consistent higher life expectancy for women than for men. Additionally, the Spanish Flu from 1918 can clearly be recognized in the graph. Source: BfS (cf. [2]). 2

3 Errors as defined by Equation (1.3) for the Nolfi Model (introduced in Chapter 2) for Swiss data (Male, years 1950-1980, ages 0-98). Red colours show underestimations, blue colours show overestimations and yellow colours show a relatively accurate estimation. 5

4 Estimated Nolfi Model errors in time periods where there are several historical events with a large impact on mortality. The upper graph shows the mortality model fitted on Swiss data from years 1970-2015 and ages 0-98. In this graph the AIDS effect is visible as a large area of underestimation (i.e. positive errors). The lower graph shows the mortality model fitted on French data from years 1910-2016 and ages 0-98. Here the two World Wars are visible as two large areas of underestimation. Additionally, in the year 1918 one can see the impact of the Spanish Flu, which overlaps with World War I and is therefore more difficult to recognize. 6

5 Overview of the diagram building blocks, which will be explained throughout the thesis. FIT stands for the mortality forecasting model fitting process. SE stands for the singular event detection process. COR stands for the singular event correction process. 8

6 The diagram symbol for the fitting process described in this chapter is a red diamond with “FIT” written in it. This symbol will be relevant for the diagrams in Chapter 4. 9

7 Parameters of the Nolfi Model for calendar years 1970-2010 and ages 0-98 for men in Switzerland. The top left graph shows the starting mortality rate $\hat{q}_x(t_0)$. Here, $t_0 = 1970$. The top right graph shows the logarithm of the starting mortality rate $\hat{\gamma}_x = \ln(\hat{q}_x(t_0))$. The bottom graphs show the half-value period $\hat{\beta}_x$, which is measured in years. The bottom left graph shows the ages 0-90, whereas the bottom right graph shows the ages 0-98. 12
8 Mortality estimation errors of the Nolfi Model for calendar years 1970-2015 and ages 0-98 for men in Switzerland. The final five years were projected. The start of the projection point is shown by the black line in the Figure. 14
9 Parameters of the LC Model for calendar years 1970-2010 and ages 0-98 for men in Switzerland. The top left graph shows the estimated logarithmic mean mortality rate $\hat{\alpha}_x$. The top right graph shows the estimated mean mortality rate $\hat{Q}_x = \exp(\hat{\alpha}_x)$. The bottom left graph shows the estimated age sensitivity for the mortality trend $\hat{\beta}_x$. The bottom right graph shows the estimated mortality trend $\hat{\kappa}_t$. 17
10 Mortality estimation errors of the LC Model for calendar years 1970-2015 and ages 0-98 for men in Switzerland. The last five years were projected. The start of the projection point is shown by the black line in the Figure. 19
11 Parameters of the RH Model for calendar years 1970-2010 and ages 0-98 for men in Switzerland. The top left graph shows the logarithmic mean mortality rate $\hat{\alpha}_x$. The top right graph shows the mean mortality rate $\hat{Q}_x = \exp(\hat{\alpha}_x)$. The middle left graph shows age sensitivity for the mortality trend $\hat{\beta}_x$. The middle right graph shows the mortality trend $\hat{\kappa}_t$. The bottom graph shows the cohort trend $\hat{\iota}_{(t-x)}$. 22
12 Mortality estimation errors of the RH Model for calendar years 1970-2015 and ages 0-98 for men in Switzerland. The last five years were projected. The start of the projection point is shown by the black line in the Figure. 24
13 Observed mortality frequencies (in blue) versus the estimated mortality rates by the Nolfi Model (in orange). The red arrows depict the location of a consistent area of underestimation by the Nolfi Model. 27
14 Nolfi Model effects of singular historic events. Switzerland (Male, 1960-2010) on the right. The black rectangle highlights the age 30, which is shown individually in Figure 13. 28

15 Raw observed mortality frequencies (in blue) versus the estimated mortality rates by the LC Model (in orange). 29
16 Raw observed mortality frequencies (in blue) versus the estimated mortality rates by RH Model (in orange). 30
17 The diagram symbol for the singular event identification process described in this chapter is a red diamond with "SE" written in it. This symbol will be relevant for the diagrams in Chapter 4. . 30
18 Pop-up questions in R which are consecutively shown when the expert judgement method is used. 31
19 Results from the expert judgement pop-up questions. The singular events are now highlighted by black rectangles. Note how event 1 (WW I) matches with the answers given in Figure 18. . 31
20 Fitting errors for the Nolfi Model in time period 1960-2010 for men in Switzerland. The AIDS effect is clearly visible and will be used to explain the algorithm. 33
21 Fitting errors for the Nolfi Model in calendar year 1989, ages 18 until 28 for men in Switzerland. The green check marks identify the data points which contain errors $\geq \varepsilon = 0.3$, thereby counting as large errors. The red crosses indicate the data points which are $< \varepsilon = 0.3$, thereby not counting as large errors. 34
22 Graphical overview of the score calculation. Each data point is represented by a rectangle, the number within the rectangle is the error which is calculated as shown in Equation (3.2). If the data point has an error $\geq \varepsilon = 0.3$ it receives a point. For each of its lateral neighbours that has an error $\geq \varepsilon = 0.3$ it receives half a point. If the score is calculated for finding the affected ages, the upper and lower neighbours are used (not shown in this figure). For each calendar year, the points are summed. This is then divided by the number of data points in calendar year t (i.e. the number of ages), see Equation (3.4). 35
23 Fitting errors for the Nolfi Model in calendar year 1987-1989, ages 0-98 for men in Switzerland. The green check marks identify the calendar years which have a score $\geq \gamma^{year} = 0.33$, thereby counting as a singular event year. The red crosses indicate the calendar years with scores $< \gamma^{year} = 0.33$, thereby not counting as singular event years. 36
24 Fitting errors for the Nolfi Model in calendar year 1985-2001, ages 0-98 for men in Switzerland. Within the dashed lines are the years that exceeded some level γ^{year}, thereby counting as a singular event years. The years between the dashed and filled lines, were lines that passed the easier threshold $\alpha^{year}\gamma^{year}$ and were therefore added to the singular event years (with $\alpha^{year} = 0.5$). 37

25 Fitting errors for the Nolfi Model in calendar year 1985-2001, ages 0-98 for men in Switzerland. The calendar years within the black filled line show the calendar years which are affected by the singular event. This information is used by the second part of the algorithm to calculate the affected ages. 38
26 Fitting errors for the Nolfi Model in calendar year 1987-1996, ages 36-39 for men in Switzerland. The green check marks identify the ages which have a score $\geq \gamma^{age} = 0.66$, thereby counting as a singular event age. The red cross indicates the age with a score $< \gamma^{age}$, thereby not counting as a singular event age. Note, that only the singular event years are considered for defining which ages are affected. These years are contained within the black lines in this figure. 40
27 Fitting errors for the Nolfi Model in calendar year 1987-1996, ages 0-98 for men in Switzerland. Within the dashed vertical lines are the ages with a score $\geq \gamma^{age}$, thereby counting as a singular event years (the right dashed line overlaps with the filled line). The ages between the dashed and filled lines, were the adjacent ages with a score $\geq \alpha^{age}\gamma^{age}$ and were therefore added to the singular event years (with $\alpha^{age} = 0.4$). 41
28 Fitting errors for the Nolfi Model in calendar year 1960-2010, ages 0-98 for men in Switzerland. The black rectangular box now shows the singular event as detected by the aforementioned algorithm. 42
29 Diagram symbol for the correction building block, which corrects the number of deaths data $\tilde{D}_x(t)$. 44
30 Diagram overview of the single model correction. Blue boxes represent obtained data, red diamonds represent different building blocks. The final result is represented by the green box. . . . 45
31 Overview of the single correction steps. The blue line represents the observed mortality frequency. The yellow line shows the estimated Nolfi mortality rate based on the blue line. The red line shows the altered observed mortality frequency. The green line shows the estimated mortality rate based on the red line. The AIDS singular event is within the black lines. 45
32 The error graphs above show the single correction method step-by-step. 47
33 This error graph shows the absolute improvement (shown in green) or deteriorations (shown in red) when correcting for the singular event. The improvement is defined by Equation (4.3). . 49

34 Parameters of the Nolfi Model for calendar years 1970-2010 and ages 0-98 for men in Switzerland. The top left graph shows the starting mortality rate $\hat{q}_x(t_0)$. Here, $t_0 = 1970$. The top right graph shows the logarithm of the starting mortality rate $\hat{\gamma}_x = \ln(\hat{q}_x(t_0))$. The bottom graphs show the half-value period $\hat{\beta}_x$, which is measured in years. The bottom left graph shows the ages 0-90, whereas the bottom right graph shows the ages 0-98. 50
35 Nolfi Model parameter difference for $\hat{q}_x(t_0)$ after the single correction method has been applied. The graph shows the relative difference in the parameter for ages 0-98 for men in Switzerland (calendar years 1970-2010). The relative difference calculation is shown in Equation (4.5). The credibility weight z is shown for values 0.25, 0.5, 0.75 and 1. 52
36 Nolfi Model parameter difference for $\hat{\beta}_x$ after the single correction method has been applied. The graph shows the absolute difference in the parameter for ages 0-98 for men in Switzerland (calendar years 1970-2010). The absolute difference calculation is shown in Equation (4.4). The credibility weight z is shown for values 0.25, 0.5, 0.75 and 1. 53
37 Nolfi Model parameter difference for $\hat{\beta}_x$ after the single correction method has been applied. The graph shows the relative difference in the parameter for ages 0-98 for men in Switzerland (calendar years 1970-2010). The percentage difference calculation is shown in Equation (4.5). The credibility weight z is shown for values 0.25, 0.5, 0.75 and 1. 53
38 Overview of single correction steps for credibility weights z 0.25, 0.5, 0.75 and 1. Explanation similar to Figure 31. The black line represents the boundary between fitted and projected data. The data viewed is from Swiss males aged 30, between calendar years 1970 and 2010. The data is projected until 2015. 55
39 This error graph shows the absolute improvement (shown in green) or deteriorations (shown in red) when correcting for the singular event for different credibility weights z 0.25, 0.5, 0.75 and 1. The improvement is defined by Equation (4.3). The data viewed is from Swiss males aged 30, between calendar years 1970 and 2010. The data is projected until 2015. 56

40 Parameters of the LC Model for calendar years 1970-2010 and ages 0-98 for men in Switzerland. The top left graph shows the logarithmic mean mortality rate $\hat{\alpha}_x$. The top right graph shows the mean mortality rate $\hat{Q}_x = \exp(\hat{\alpha}_x)$. The bottom left graph shows age sensitivity for the mortality trend $\hat{\beta}_x$. The bottom right graph shows the mortality trend $\hat{\kappa}_t$. 57
41 Fitting errors for the LC Model in calendar year 1970-2010, ages 0-98 for men in Switzerland. The black rectangular box now shows the singular event as detected by the algorithm. The ages 20-37 and calendar years 1989-1994 belong to the singular event. 58
42 LC Model parameter $\hat{Q}_x$ difference after the single correction method has been applied. The graph shows the relative difference in the parameter for ages 0-98 for men in Switzerland (calendar years 1970-2010). The relative difference calculation is shown in Equation (4.5). The credibility weight z is shown for values 0.25, 0.5, 0.75 and 1. 59
43 LC Model parameter $\hat{\beta}_x$ difference after the single correction method has been applied. The graph shows the relative difference in the parameter for ages 0-98 for men in Switzerland (calendar years 1970-2010). The relative difference calculation is shown in Equation (4.5). The credibility weight z is shown for values 0.25, 0.5, 0.75 and 1. 59
44 LC Model parameter $\hat{\kappa}_t$ difference after the single correction method has been applied. The graph shows the relative difference in the parameter for ages 0-98 for men in Switzerland (calendar years 1970-2010). The relative difference calculation is shown in Equation (4.5). The credibility weight z is shown for values 0.25, 0.5, 0.75 and 1. 60
45 Overview of single correction steps for the LC Model for credibility weights z equal to 0.25, 0.5, 0.75 and 1. Explanation similar to Figure 31. The black line represents the boundary between fitted and projected data. 61
46 Absolute improvements (shown in green) or deteriorations (shown in red) when correcting for the singular event with different credibility weights $z \in \{0.25, 0.5, 0.75, 1\}$. The improvement is defined by Equation (4.3). 62
47 Fitting errors for the Nolfi Model and the LC Model in calendar year 1970-2010, ages 0-98 for men in Switzerland for credibility weight z values 0 and 1. 63

48 Absolute improvements (shown in green) or deteriorations (shown in red) between Nolfi Model and the LC Model for credibility weight z values 0 and 1. The improvement is defined by Equation. 64
49 Symbol for the first stopping criterion. 66
50 Symbol for the second stopping criterion. 66
51 Diagram overview of the single model correction. Blue boxes represent obtained data, red diamonds represent a calculation step. The purple dashed area is the area in which the iterative process takes places. The purple square represents the stopping criterion for the iterative process. The final estimated mortality rate is shown by the green box. 67
52 Development of the error $\xi^{(i)}$ (Equation (4.6)) as iterations go by. The iteration process is stopped by the stopping criteria at iteration 7. 68
53 Nolfi Model parameters $\hat{q}_x(t_0)$ and $\hat{\beta}_x$ after the stationary iterative correction method has been applied. The graphs show the relative difference (Equation (4.5)) in the parameters for ages 0-98 for men in Switzerland (calendar years 1970-2010). The blue lines show the difference between no correction and the iterative correction. The orange lines show the difference between the single correction and the stationary iterative correction. The stationary iterative and the single correction method use credibility weight $z = 1$. 69
54 Nolfi Model parameter $\hat{\beta}_x$ after the stationary iterative correction method has been applied. The graph shows the relative difference (Equation (4.5)) in the parameter for ages 0-98 for men in Switzerland (calendar years 1970-2010). The blue line shows the difference between no correction and the iterative correction. The orange line shows the difference between the single correction and the iterative correction. The stationary iterative and the single correction method use credibility weight $z = 1$. . 70
55 Absolute improvements (shown in green) or deteriorations (shown in red) between no correction, the single correction and the stationary iterative correction for the Nolfi Model. The improvement is defined by Equation (4.3). 71

56 LC Model parametesr $\hat{Q}_x$ and $\hat{\beta}_x$ after the stationary iterative correction method has been applied. The graphs show the relative difference (Equation (4.5)) in the parameters for ages 0-98 for men in Switzerland (calendar years 1970-2010). The blue lines show the difference between no correction and the stationary iterative correction. The orange lines show the difference between the single correction and the stationary iterative correction. The stationary iterative and the single correction method use credibility weight $z = 1$. 72
57 LC Model parameter $\hat{\kappa}_t$ after the stationary iterative correction method has been applied. The graph shows the relative difference (Equation (4.5)) in the parameter for ages 0-98 for men in Switzerland (calendar years 1970-2010). The blue line shows the difference between no correction and the stationary iterative correction. The orange line shows the difference between the single correction and the stationary iterative correction. The stationary iterative and the single correction method use credibility weight $z = 1$. 73
58 Absolute improvements (shown in green) or deteriorations (shown in red) between no correction, the single correction and the stationary iterative correction for the LC Model. The improvement is defined by Equation (4.3). 74
59 Diagram overview of the single model correction. Blue boxes represent obtained data, red diamonds represent a calculation step. The purple dashed area is the area in which the iterative process takes places. The purple square represents the stopping criterion for the iterative process. The final estimated mortality rate is shown by the green box. The differences with the stationary iterative correction diagram are the added (SE) red diamond before the (COR) red diamond and the different stopping criteria. 75
60 Overview of the changing size of the singular event per iteration. Above each graph, the ages and calendar years which belong to the singular event as defined by the algorithm are written down. 76

61 Nolfi Model parameters $\hat{q}_x(t_0)$ and $\hat{\beta}_x$ after the moving iterative correction method has been applied. The graphs show the relative difference (Equation (4.5)) in the parameter for ages 0-98 for men in Switzerland (calendar years 1970-2010). The blue lines show the difference between no correction and the moving iterative correction. The orange lines show the difference between the single correction and the moving iterative correction. The green lines show the difference between the stationary iterative correction and the moving iterative correction. All correction methods use credibility weight $z = 1$. 77
62 Nolfi Model parameter $\hat{\beta}_x$ after the moving iterative correction method has been applied. The graph shows the absolute difference (Equation (4.4)) in the parameter for ages 0-98 for men in Switzerland (calendar years 1970-2010). The blue line shows the difference between no correction and the moving iterative correction. The orange line shows the difference between the single correction and the moving iterative correction. The green line shows the difference between the stationary iterative correction and the moving iterative correction. All correction methods use credibility weight $z = 1$. 78
63 Absolute improvements (shown in green) or deteriorations (shown in red) between no correction, the single correction, the stationary iterative correction and the moving iterative correction for the Nolfi Model. The improvement is defined by Equation (4.3). 79
64 LC Model parameters $\hat{Q}_x$ and $\hat{\beta}_x$ after the moving iterative correction method has been applied. The graphs show the relative difference (Equation (4.5)) in the parameter for ages 0-98 for men in Switzerland (calendar years 1970-2010). The blue lines show the difference between no correction and the moving iterative correction. The orange lines show the difference between the single correction and the moving iterative correction. The green lines show the difference between the stationary iterative correction and the moving iterative correction. All correction methods use credibility weight $z = 1$. 80

65 LC Model parameter $\hat{\kappa}_t$ after the moving iterative correction method has been applied. The graph shows the relative difference (Equation (4.5)) in the parameter for ages 0-98 for men in Switzerland (calendar years 1970-2010). The blue line shows the difference between no correction and the moving iterative correction. The orange line shows the difference between the single correction and the moving iterative correction. The green line shows the difference between the stationary iterative correction and the moving iterative correction. All correction methods use credibility weight $z = 1$. 81
66 Absolute improvements (shown in green) or deteriorations (shown in red) between no correction, the single correction, the stationary iterative correction and the moving iterative correction for the LC Model. The improvement is defined by Equation (4.3). . 82
67 Diagram overview of the single model correction. Blue boxes represent obtained data, red diamonds represent a calculation step. The purple dashed square is the area in which an iterative process takes places. The arrow which leaves the purple dashed square happens after the iterative process. The (FIT*) red diamond represent fitting the data with an alternative model (either LC Model or RH Model). 83
68 LC Model parameters $\hat{Q}_x$ and $\hat{\beta}_x$ after the final fit correction method (LC Model) has been applied. The graphs show the relative differences (Equation (4.5)) in the parameters for ages 0-98 for men in Switzerland (calendar years 1970-2010). The blue lines show the relative differences between no correction and the final fit correction (LC Model). The orange lines show the relative differences between the single correction and the final fit correction (LC Model). The green lines show the relative differences between the stationary iterative correction and the final fit correction (LC Model). The red lines show the relative differences between the moving iterative correction and the final fit correction (LC Model). All correction methods use credibility weight $z = 1$. 85

69 LC Model parameter $\hat{\kappa}_t$ after the final fit correction method (LC Model) has been applied. The graphs show the relative difference (Equation (4.5)) in the parameter for ages 0-98 for men in Switzerland (calendar years 1970-2010). The blue line shows the relative difference between no correction and the final fit correction (LC Model). The orange line shows the relative difference between the single correction and the final fit correction (LC Model). The green line shows the relative difference between the stationary iterative correction and the final fit correction (LC Model). The red line shows the relative difference between the moving iterative correction and the final fit correction (LC Model). All correction methods use credibility weight $z = 1$. . . 86
70 Absolute improvements (shown in green) or deteriorations (shown in red) between no correction, the single correction, the stationary iterative correction, the moving iterative correction and the final fit correction for the LC Model. The improvement is defined by Equation (4.3). 87
71 Parameters of the RH Model for calendar years 1970-2010 and ages 0-98 for men in Switzerland. The top left graph shows the logarithmic mean mortality rate $\hat{\alpha}_x$. The top right graph shows the mean mortality rate $\hat{Q}_x = \exp(\hat{\alpha}_x)$. The middle left graph shows age sensitivity for the mortality trend $\hat{\beta}_x$. The middle right graph shows the mortality trend $\hat{\kappa}_t$. The bottom graph shows the cohort trend $\hat{\iota}_{(t-x)}$. 88
72 RH Model parameter $\hat{Q}_x$ after the final fit correction method (RH Model) has been applied. The blue line represents the difference between the RH Model without correction and the final fit correction (RH Model). The upper graph is cut off at age 70 allow for better visibility of the lower ages. 89
73 RH Model parameters $\hat{\beta}_x$ and $\hat{\kappa}_t$ after the final fit correction method (RH Model) has been applied. The blue lines represent the differences between the RH Model without correction and the final fit correction (RH Model). 90
74 RH Model parameter $\hat{\iota}_{(t-x)}$ after the final fit correction method (RH Model) has been applied. The blue line represents the difference between the RH Model without correction and the final fit correction (RH Model). 91
75 Absolute improvements (shown in green) or deteriorations (shown in red) between no correction and the final fit correction for the RH Model. The improvement is defined by Equation (4.3). . . . 92

76 Nolfi Model mortality rate estimation errors for calendar years 1895-1925 and ages 0-98 (French, male). The black box highlights the singular event as identified by the algorithm with parameters $\varepsilon = 0.3$, $\gamma^{(year)} = 1/3$, $\alpha^{(year)} = 0.5$, $\gamma^{(age)} = 2/3$ and $\alpha^{(year)} = 0.4$. 97
77 Nolfi Model mortality rate estimation errors before correction for calendar years 1895-1930 and ages 0-98 (French, male), the last five years were projected (above the black line). 98
78 Nolfi Model mortality rate estimation errors after correction with the moving iterative correction method for calendar years 1895-1930 and ages 0-98 (French, male), the last five years were projected (above the black line). 98
79 Nolfi Model mortality rate estimation improvements for calendar years 1895-1930 and ages 0-98 (French, male), the last five years were projected (above the black line). The graph compares no correction to the moving iterative correction. 99
80 Nolfi Model mortality rate correction steps for calendar years 1895-1930 and age 30 (French, male), the last five years were projected (left of the black line). 99
81 Lee-Carter Model mortality rate estimation errors before correction for calendar years 1895-1930 and ages 0-98 (French, male), the last five years were projected (above the black line). 100
82 Lee-Carter Model mortality rate estimation errors after correction with the final fit correction method for calendar years 1895-1930 and ages 0-98 (French, male), the last five years were projected (above the black line). 100
83 Lee-Carter Model mortality rate estimation improvements for calendar years 1895-1930 and ages 0-98 (French, male), the last five years were projected (above the black line). The graph compares no correction to the final fit correction. 101
84 Lee-Carter Model mortality rate correction steps for calendar years 1895-1930 and age 30 (French, male), the last five years were projected (left of the black line). 101
85 Renshaw-Haberman Model mortality rate estimation errors before correction for calendar years 1895-1930 and ages 0-98 (French, male), the last five years were projected (above the black line). . 102
86 Renshaw-Haberman Model mortality rate estimation errors after correction with the final fit correction method for calendar years 1895-1930 and ages 0-98 (French, male), the last five years were projected (above the black line). 102

87 Renshaw-Haberman Model mortality rate estimation improvements for calendar years 1895-1930 and ages 0-98 (French, male), the last five years were projected (above the black line). The graph compares no correction to the final fit correction. 103
88 Renshaw-Haberman Model mortality rate correction steps for calendar years 1895-1930 and age 30 (French, male), the last five years were projected (left of the black line). 103
89 Mortality rate estimation improvements for calendar years 1895-1930 and ages 0-98 (French, male), the last five years were projected (above the black line). The graph shows the Nolfi, Lee-Carter and Renshaw-Haberman Model estimation errors before correction. 104
90 Mortality rate estimation improvements for calendar years 1895-1930 and ages 0-98 (French, male), the last five years were projected (above the black line). The graph shows the Nolfi, Lee-Carter and Renshaw-Haberman model estimation errors after correction. 104
91 Mortality rate estimation improvements for calendar years 1895-1930 and ages 0-98 (French, male), the last five years were projected (above the black line). The graph compares the Nolfi, Lee-Carter and Renshaw-Haberman Models after correction. In the graphs the model before the"vs" is better when the colour is red, whereas the model after the "vs" is better when the colour is green. 105
92 Nolfi Model mortality rate estimation errors for calendar years 1925-1955 (French, male). The black box highlights the singular event as identified by the algorithm with parameters $\varepsilon = 0.3$, $\gamma^{(year)} = 1/3$, $\alpha^{(year)} = 0.5$, $\gamma^{(age)} = 2/3$ and $\alpha^{(year)} = 0.4$. 106
93 Nolfi Model mortality rate estimation errors before correction for calendar years 1925-1960 and ages 0-98 (French, male), the last five years were projected (above the black line). 107
94 Nolfi Model mortality rate estimation errors after correction with the moving iterative correction method for calendar years 1925-1960 and ages 0-98 (French, male), the last five years were projected (above the black line). 107
95 Nolfi Model mortality rate estimation improvements for calendar years 1925-1960 and ages 0-98 (French, male), the last five years were projected (above the black line).The graph compares no correction to the moving iterative correction method. 108
96 Nolfi Model mortality rate correction steps for calendar years 1925-1960 and age 30 (French, male), the last five years were projected (above the black line). 108

97 Lee-Carter Model mortality rate estimation errors before correction for calendar years 1925-1960 and ages 0-98 (French, male), the last five years were projected (above the black line). 109
98 Lee-Carter Model mortality rate estimation errors after correction with the final fit correction method for calendar years 1925-1960 and ages 0-98 (French, male), the last five years were projected (above the black line). 109
99 Lee-Carter Model mortality rate estimation improvements for calendar years 1925-1960 and ages 0-98 (French, male), the last five years were projected (above the black line). The graph compares no correction to the final fit correction method. 110
100 Lee-Carter Model mortality rate correction steps for calendar years 1925-1960 and age 30 (French, male), the last five years were projected (above the black line). 110
101 Renshaw-Haberman Model mortality rate estimation errors before correction for calendar years 1925-1960 and ages 0-98 (French, male), the last five years were projected (above the black line). . 111
102 Renshaw-Haberman Model mortality rate estimation errors after correction with the final fit correction method for calendar years 1925-1960 and ages 0-98 (French, male), the last five years were projected (above the black line). 111
103 Renshaw-Haberman Model mortality rate estimation improvements for calendar years 1925-1960 and ages 0-98 (French, male), the last five years were projected (above the black line).The graph compares no correction to the final fit correction method. 112
104 Renshaw-Haberman Model mortality rate correction steps for calendar years 1925-1960 and age 30 (French, male), the last five years were projected (above the black line). 112
105 Mortality rate estimation improvements for calendar years 1925-1960 and ages 0-98 (French, male), the last five years were projected (above the black line). The graph shows the Nolfi, Lee-Carter and Renshaw-Haberman Model estimation errors before correction. 113
106 Mortality rate estimation improvements for calendar years 1925-1960 and ages 0-98 (French, male), the last five years were projected (above the black line). The graph shows the Nolfi, Lee-Carter and Renshaw-Haberman Model estimation errors after correction. 113

107 Mortality rate estimation improvements for calendar years 1925-1960 and ages 0-98 (French, male), the last five years were projected (above the black line). The graph compares the Nolfi, Lee-Carter and Renshaw-Haberman Models after correction. In the graphs the model before the"vs" is better when the colour is red, whereas the model after the "vs" is better when the colour is green. 114
108 Nolfi Model mortality rate estimation errors for calendar years 1895-1925 (Swiss, male). The black box highlights the singular event as identified by the algorithm with parameters $\varepsilon = 0.3$, $\gamma^{(year)} = 1/3$, $\alpha^{(year)} = 0.5$, $\gamma^{(age)} = 2/3$ and $\alpha^{(year)} = 0.4$. 115
109 Nolfi Model mortality rate estimation errors before correction for calendar years 1895-1930 and ages 0-98 (Swiss, male), the last five years were projected (above the black line). 116
110 Nolfi Model mortality rate estimation errors after corretion with the moving iterative correction method for calendar years 1895-1930 and ages 0-98 (Swiss, male), the last five years were projected (above the black line). 116
111 Nolfi Model mortality rate estimation improvements for calendar years 1895-1930 and ages 0-98 (Swiss, male), the last five years were projected (above the black line). The graph compares no correction to the moving iterative correction method. . 117
112 Nolfi Model mortality rate correction steps for calendar years 1895-1930 and ages 30 (Swiss, male), the last five years were projected (left of the black line). 117
113 Lee-Carter Model mortality rate estimation errors before correction for calendar years 1895-1930 and ages 0-98 (Swiss, male), the last five years were projected (above the black line). 118
114 Lee-Carter Model mortality rate estimation errors after corretion with the final fit correction method for calendar years 1895-1930 and ages 0-98 (Swiss, male), the last five years were projected (above the black line). 118
115 Lee-Carter Model mortality rate estimation improvements for calendar years 1895-1930 and ages 0-98 (Swiss, male), the last five years were projected (above the black line). The graph compares no correction to the final fit correction method. 119
116 Lee-Carter Model mortality rate correction steps for calendar years 1895-1930 and ages 30 (Swiss, male), the last five years were projected (left of the black line). 119
117 Renshaw-Haberman Model mortality rate estimation errors before correction for calendar years 1895-1930 and ages 0-98 (Swiss, male), the last five years were projected (above the black line). . 120

118 Renshaw-Haberman Model mortality rate estimation errors after corretion with the final fit correction method for calendar years 1895-1930 and ages 0-98 (Swiss, male), the last five years were projected (above the black line). 120
119 Renshaw-Haberman Model mortality rate estimation improvements for calendar years 1895-1930 and ages 0-98 (Swiss, male), the last five years were projected (above the black line). The graph compares no correction to the final fit correction method. 121
120 Renshaw-Haberman Model mortality rate correction steps for calendar years 1895-1930 and ages 30 (Swiss, male), the last five years were projected (left of the black line). 121
121 Mortality rate estimation improvements for calendar years 1895-1930 and ages 0-98 (Swiss, male), the last five years were projected (above the black line). The graph shows the Nolfi, Lee-Carter and Renshaw-Haberman Model estimation errors before correction. 122
122 Mortality rate estimation improvements for calendar years 1895-1930 and ages 0-98 (Swiss, male), the last five years were projected (above the black line). The graph shows the Nolfi, Lee-Carter and Renshaw-Haberman Model estimation errors after correction. 122
123 Mortality rate estimation improvements for calendar years 1895-1930 and ages 0-98 (Swiss, male), the last five years were projected (above the black line). The graph compares the Nolfi, Lee-Carter and Renshaw-Haberman Models after correction. In the graphs the model before the“vs” is better when the colour is red, whereas the model after the “vs” is better when the colour is green. 123

List of Abbreviations

CDF Cumulative Distribution Function

BfS Bundesamt für Statistik of Switzerland

WW I World War I

WW II World War II

LS Method Least Squares Method

GLM Generalized Linear Model

LC Model Lee-Carter Model

ML Method Maximum-Likelihood Method

RH Model Renshaw-Haberman Model

1 Introduction

The rapid decrease of mortality rates is a well-documented phenomenon in the modern world. Barring a few exceptions, one can see that infant mortality has greatly decreased over the last century. Mortality rates of older ages have also decreased, although to a smaller degree (see Figure 1).

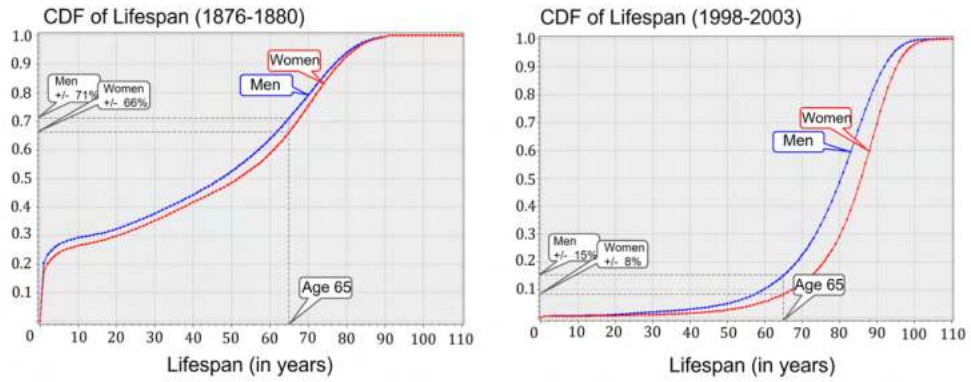

Figure 1: Lifespan cumulative distribution function (CDF) for Swiss people for years 1876-1880 and 1998-2003. The left graph shows an infant mortality rate (ages 0-1) of approximately 20%, whereas the right graph shows an infant mortality rate (ages 0-1) of less than 1%. Furthermore, the left graph shows that between 1876-1880 only approximately 30% of the population reached an age of 65 years or older. In the right graph, approximately 90% of people reach an age that is older than 65 years. Source: (cf. [1]).

Whether this downward trend will continue infinitely is still being debated amongst actuaries (and medical professionals). Nevertheless, in 2020 the Bundesamt für Statistik of Switzerland (BfS) published a report stating that COVID-19 has decreased the life expectancy (thus increasing the mortality rates) of men by approximately one year.[1] Women got a reduction of only half a year of life expectancy. Does this mean that the debate on ever-decreasing mortality rates is settled, or is something else going on?

Reading further in the BfS report gives clues as to what might be happening. Namely, the BfS report states that such a drastic decrease in life expectancy for men has not been observed since 1944. Moreover, the accompanying graph also shows other effects. For example, 1918 shows a significant drop in the life expectancy due to the Spanish Flu (see Figure 2). However, the overall increasing trend of life expectancy in Figure 2 is undeniable. Therefore, it is a fair question to ask whether these historic events are representative of

[1] cf. [2]

the overall mortality development. If not, they should be mitigated in the calculations.

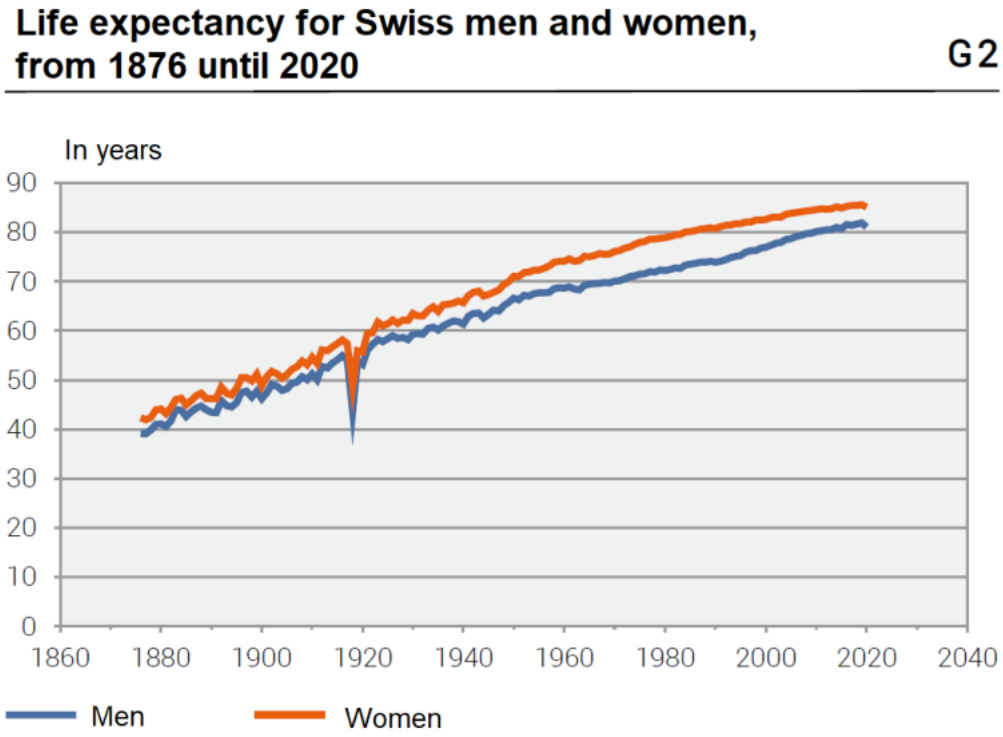

Figure 2: Life expectancy for Swiss men and women for generations 1876 until 2020. The graph shows a consistent higher life expectancy for women than for men. Additionally, the Spanish Flu from 1918 can clearly be recognized in the graph. Source: BfS (cf. [2]).

A life expectancy of 81 years in 2020 intuitively means that a newborn in calendar year 2020 is on average expected to die at the age of 81.[2] In 2019 this life expectancy was 81.9 years. Is it truly expected that there will still be a COVID-19 effect on the people born in the year 2020, impacting their average health condition enough to decrease their life expectancy by a full year? If the answer is no, then the life expectancy and the estimated mortality rates are distorted. These distortions can have negative consequences for life insurance companies and pension funds.

Life insurance companies and pension funds use mortality rates, which are collected in mortality tables. These mortality tables are then used to price life

[2]The BfS states (in German): "2020 betrug die Lebenserwartung bei Geburt 81.0 Jahre bei den Männern und 85.1 Jahre bei den Frauen. Ein Jahr zuvor hatten die Männer eine Lebenserwartung bei Geburt von 81.9 Jahren und die Frauen von 85.6 Jahren." Note, that this is calculated using a periodic mortality table, not a generation mortality table.

insurance products or to calculate the reserves needed to ensure that pensioners can receive their promised pensions. If the mortality rates are estimated too high, then not enough reserves are saved up, thereby leading to insufficient capital coverage. This is known as the longevity risk. It is therefore in the interest of a life insurance company to pay close attention to mortality rates and their development. Mortality forecasting models are used by life insurance companies to aid in this process. However, before going into more detail on mortality forecasting models, a short introduction to life insurance mathematics is required.

A Short Introduction to Life Insurance Mathematics

In life insurance mathematics there are a few key statistical components, which are introduced below:

- ${}_sp_x$ describes the probability that a person with an age of x years survives the coming s years (i.e. that the person reaches at least age $x+s$),
- $p_x := {}_1p_x$ describes the probability that a person with an age of x years survives the coming year and
- $q_x = 1 - p_x$ describes the probability that a person with an age of x years does not survive the coming year (i.e. the person dies within a year).[3]

Here, the age variable x is an element of the natural numbers including zero ($x \in \mathbb{N}_0$).

Note, that the statistical components described above are probabilities. These probabilities are generally unknown values that can only be estimated. This can be done by using mortality forecasting models. These models need empirical data to fit their model parameters. For mortality forecasting models, the following empirical data is generally used for the model fitting process:

- $l_x(t)$ describes the number of people with an age of x years who are alive in calendar year t,[4]
- $D_x(t)$ describes the number of people with an age of x years in calendar year t who were alive in the beginning of the year, but did not survive the year[5] and

[3] cf. [1]

[4] In this thesis, the variable t is described as a calendar year and a year interchangeably.

[5] In life insurance mathematics $D_x(t)$ mostly stands for the random variable which generates realizations for the number of people who died. We directly mean the number of people who died with $D_x(t)$, not the random variable.

- $E_x(t)$ is called the exposure[6] (from Farr) for age x in calendar year t:

$$E_x(t) = \frac{l_x(t) + l_x(t+1) + D_x(t)}{2}. \tag{1.1}$$

Here, the years variable t is an element of the natural numbers ($t \in \mathbb{N}$).

The aforementioned empirical data is obtained from mortality.org, which is a human mortality database. The retrieved empirical data is then used to calculate the observed mortality frequency:

$$\bar{q}_x(t) = \frac{D_x(t)}{E_x(t)}. \tag{1.2}$$

This observed mortality frequency is used as input for a mortality forecast model. This model is then fitted[7] using the input data, which returns an estimate for the mortality rate $\hat{q}_x(t)$.[8] Note, that the mortality rate is specifically calculated for a particular age x and calendar year t.

Testing the Accuracy of Mortality Forecasting Models

To test for the accuracy of the model, the deviation between the observed mortality frequency and the estimated mortality rate is calculated:

$$\varepsilon_x(t) = \frac{\bar{q}_x(t)}{\hat{q}_x(t)} - 1 = \frac{D_x(t)}{\hat{q}_x(t)E_x(t)} - 1. \tag{1.3}$$

This deviation is referred to as the error of the mortality forecasting model. If the error is positive, the estimated mortality rate is lower than the observed mortality frequency. If the error is negative, the estimated mortality rate is higher than the observed mortality frequency. One can plot these errors for multiple ages and calendar years.[9] Ideally, such a plot would look similar to Figure 3.

[6]The exposure takes into account the changing sizes of populations due to migration between years.

[7]Note, that in this thesis the words fitted and estimated are used interchangeably.

[8]The fitting and forecasting process will be explained in more detail for multiple mortality forecasting models in Chapter 2. For now, it suffices to know that these models produce a mortality rate estimate $\hat{q}_x(t)$.

[9]The combination of a certain age and a calendar year is sometimes referred to as a tuple (x, t) or data point.

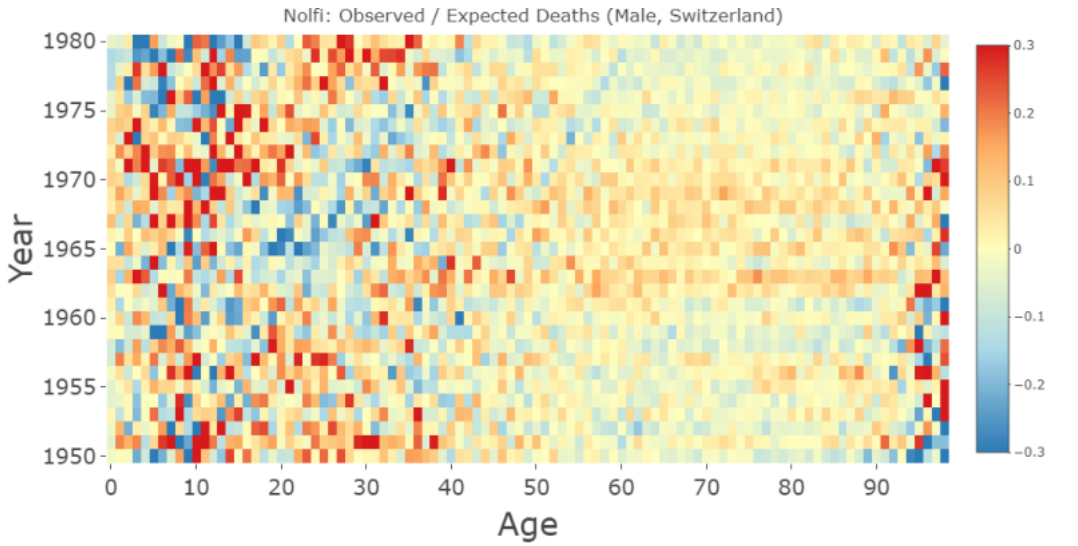

Figure 3: Errors as defined by Equation (1.3) for the Nolfi Model (introduced in Chapter 2) for Swiss data (Male, years 1950-1980, ages 0-98). Red colours show underestimations, blue colours show overestimations and yellow colours show a relatively accurate estimation.

In Figure 3, the estimated mortality rates which are lower than the observed mortality frequency are red, the estimated mortality rates which are higher than the observed mortality frequency are blue and the estimated mortality rates which are close to the observed mortality frequency are yellow. In Figure 3, it is visible that there are large areas of yellow, meaning that the overall estimation quality is satisfactory. In the areas where there are larger errors (for ages below 40 and ages above 95), the sign of the error is often changing. Concretely, this means that an underestimation is often followed by an overestimation and vice versa. This random mixture between overestimation and underestimation is generally seen as a good sign for the model quality.[10]

In a less ideal case, the error graph contains large neighbouring areas of either overestimation or underestimation. This tends to be the case if there is a historic event that has a large impact on mortality (see Figure 4).

[10]The larger errors for ages below 40 and above 95 are due to the lack of data. For the ages below 40 there is a low mortality rate, meaning that there are no high number of deaths observed for these ages. This leads to a higher variance in the estimation. For the ages above 95 there are not many people alive anymore (i.e. low exposure), which also leads to a higher variance of the estimation.

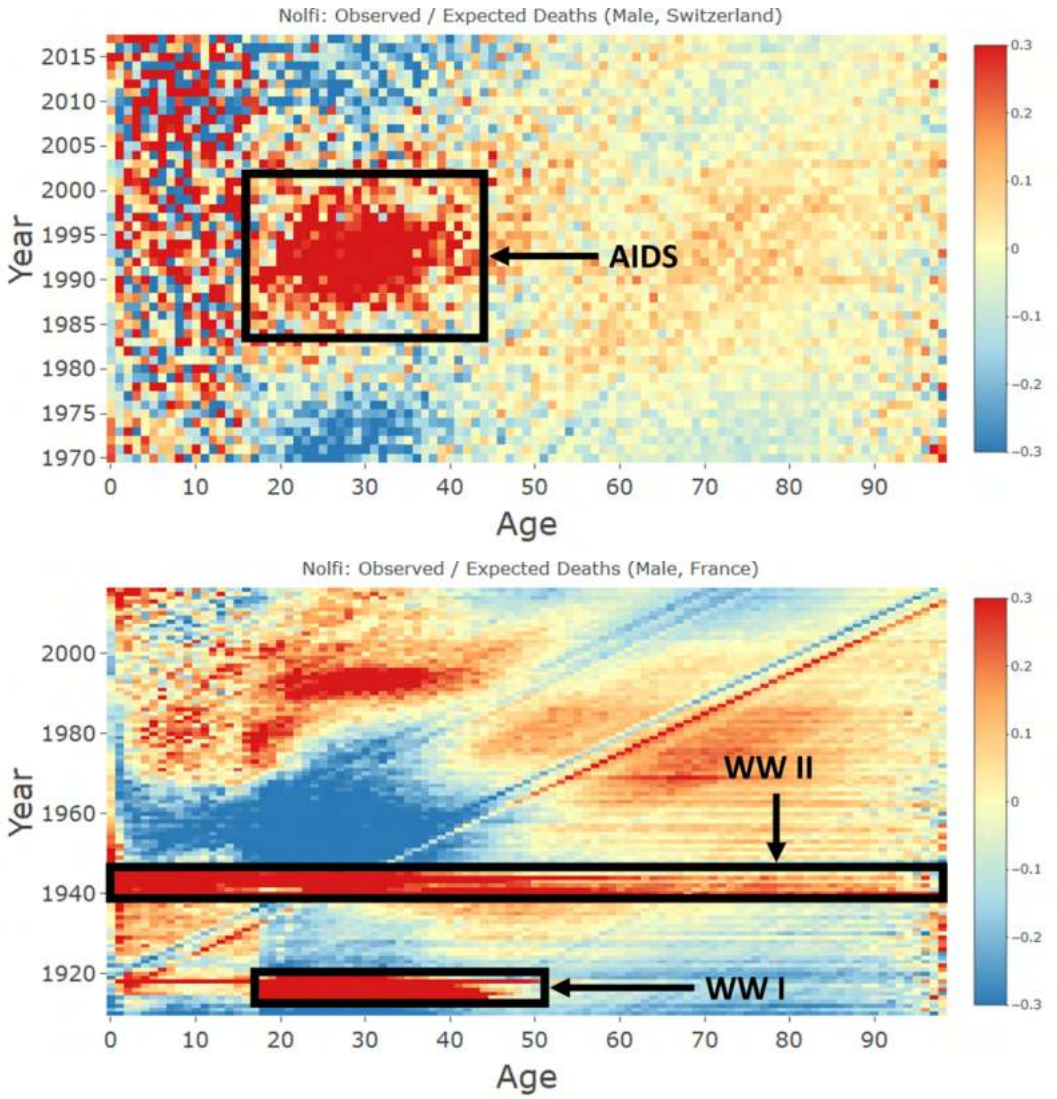

Figure 4: Estimated Nolfi Model errors in time periods where there are several historical events with a large impact on mortality. The upper graph shows the mortality model fitted on Swiss data from years 1970-2015 and ages 0-98. In this graph the AIDS effect is visible as a large area of underestimation (i.e. positive errors). The lower graph shows the mortality model fitted on French data from years 1910-2016 and ages 0-98. Here the two World Wars are visible as two large areas of underestimation. Additionally, in the year 1918 one can see the impact of the Spanish Flu, which overlaps with World War I and is therefore more difficult to recognize.

Singular Events

These historical events with a large impact on mortality are from now on

referred to as singular events.[11] In Figure 4, the singular events contain data points with large errors by definition. However, the large errors are not limited to the singular events. Areas above and below a singular event seem to have large overestimation errors. This is because singular events lead to parameter distortions.

A mortality forecasting model generally tries to fit to all the empirical data as well as possible. An event which causes a spike in the observed mortality frequency will cause the model to attempt to increase the estimated mortality rate in this area. However, most models do not allow for a large local increase of the mortality estimate. Instead, models tend to allow for a general increase in some parameter, which tends to increase the estimated mortality inside and outside the singular event. Given that the estimated mortality rate is increased in the areas outside of the singular event, the model now likely overestimates the mortality rate in the areas without a singular event.

These parameter distortions have multiple consequences:

1. First, the estimated mortality rates have large errors compared to the observed mortality frequencies. These deviations tend to be positive in areas of the singular event and negative in the areas outside of the singular event (i.e. they do not randomly fluctuate around the estimated mortality rate).

2. Second, the distorted parameters generally cause the projection quality of the model to deteriorate; the inaccurate pattern within the parameters is extrapolated into the future, also causing large errors.

3. Third, the distorted parameters and the inaccurate mortality rates lead to further inaccurate results when these estimates are used in calculations. A good example here is the BfS life expectancy data in Figure 2. The Spanish Flu in 1918 is not representative of the mortality development for the generation of 1918. However, due to a suboptimal model fit and no intervention, this data was assumed to be representative.

4. Lastly, distorted parameters also tend to be volatile. The model parameters from Figure 3 are likely not very distorted, given that the fitting period did not contain a singular event. When shifting the fitting period by 20 years (i.e. by fitting from 1970-2015 instead of 1950-1980), the fitting period now does contain a singular event (see Figure 4, upper graph). The parameters produced by this later time period, which contains the AIDS singular event, will be significantly different to the

[11] A more exact definition will follow in Chapter 3.

parameters of the model without AIDS. This also counts for the estimated mortality rates between the two models and their mortality rate projections. Hence, between these two fitting periods, one can expect large jumps between the two results. This is undesirable, as all jumps need to be thoroughly investigated.

One potential approach to solve the singular event distortion problem is to allow for complexer models which capture these events. However, increasing the complexity of the models mostly has a negative effect on its forecasting quality and risks overfitting.[12] Therefore, there needs to be a balance between model complexity and accuracy of the fitted mortality model.

Thesis Structure

This thesis attempts to pursue another approach, by defining a framework for dealing with singular events. In Chapter 2, the thesis will introduce three common mortality forecasting models: Nolfi, Lee-Carter and Renshaw-Haberman. For each of these models, the fitting and projection procedure will be explained. Additionally, the model parameters will be interpreted. In Chapter 3, the thesis covers how to consistently define and identify a singular event. In Chapter 4, several correction methods will attempt to correct for the identified singular event. The thesis will end with a short conclusion in Chapter 5, which will focus on the COVID-19 life expectancy case discussed in this Introduction. Chapters 2, 3 and 4 will each introduce a building block.[13] These will be combined in Chapter 4 to form diagrams for correction methods. These building block are shown in Figure 5.

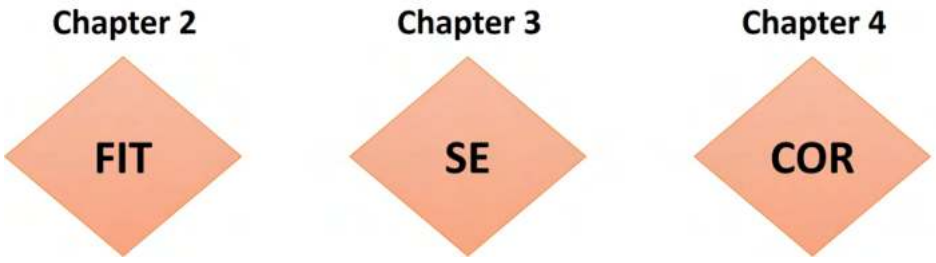

Figure 5: Overview of the diagram building blocks, which will be explained throughout the thesis. FIT stands for the mortality forecasting model fitting process. SE stands for the singular event detection process. COR stands for the singular event correction process.

[12] cf. [3]

[13] These building blocks could also be explained as data steps. Each building block takes some data as input, processes it and calculates something new with it.

2 Mortality Forecasting Models

As mentioned in the Introduction, mortality forecasting models are used to estimate mortality rates. All estimated mortality rates and the related estimated parameters will be characterized by a hat sign "∧". In this chapter, the Nolfi, Lee-Carter and Renshaw-Haberman Model will be described. The fitting process will be explained and the results will be discussed for each model.[14] This process of fitting is summarized by a red diamond in Figure 6. These red diamonds will be used in Chapter 4 to explain correction methods. Additionally, this chapter will cover the projection process for each model. In short, this projection process entails that the fitted parameters are extrapolated and then used to calculate estimated mortality rates outside of the fitting time period.

Figure 6: The diagram symbol for the fitting process described in this chapter is a red diamond with "FIT" written in it. This symbol will be relevant for the diagrams in Chapter 4.

2.1 Nolfi

The Nolfi Model is the simplest model discussed in this thesis and is described below:

$$q_x(t) = q_x(t_0)\exp(\alpha_x(t - t_0)), \tag{2.1}$$

where

... α_x is a fitting parameter described below:

$$\alpha_x = -\frac{\ln(2)}{\beta_x},$$

... β_x is the half-value period for age x and

... t_0 is the starting year for the fitting process.

The interpretation for the half-value period parameter β_x is the number of years it takes for the mortality rate of a person with age x to half. Hence,

[14] Part of these results were covered in a previously written seminar paper. (cf. [4])

if this parameter value is positive, then the mortality rate is estimated to decrease. If the parameter value is negative, the mortality rate is estimated to increase. Finally, if the parameter value equals 0, the mortality rate is estimated to remain stable.

Even though Equation (2.1) is good for interpretation, the equation is not optimal for parameter estimation. One can solve this by taking the logarithm of Equation (2.1) which will transform it to a linear function:

$$\ln(q_x(t)) = \gamma_x + \alpha_x(t - t_0),$$

where γ_x is the logarithm of the starting mortality rate:

$$\gamma_x = \ln(q_x(t_0)).$$

The parameters γ_x and α_x can then be estimated using the Least Squares Method (LS Method).

2.1.1 Fitting

Introducing the Least Squares Method

The LS Method is an estimation method used for regression problems.[15] It minimizes a loss function and is called the "Least" Squares Method because it minimizes the squared distance between all observations and their estimated value. The LS Method is used for classical linear regression models and for special cases of the Generalized Linear Models (GLM). In this case, the LS Method for a special GLM case is used:

$$\mathbf{y} = \mathbf{X}\boldsymbol{\beta} + \boldsymbol{\varepsilon},$$

where

- ... $\mathbf{y}$ is a vector (dimensions $n \times 1$) with the observed values for the dependent variable,
- ... $\mathbf{X}$ is a matrix (dimensions $n \times m$) with the observed values for the independent variables,[16]
- ... $\boldsymbol{\beta}$ is a vector (dimensions $m \times 1$) with the model parameters[17] and
- ... $\boldsymbol{\varepsilon}$ is a vector (dimensions $n \times 1$) with the errors of the model.

[15] This section uses slides from Michael Merz as a foundation. (cf. [5])
[16] Note, that the number of columns m must be smaller than the number of rows n.
[17] In the Nolfi model case, this vector contains the parameters α_x and γ_x.

The assumptions related to this method are described below:

1. $\mathbb{E}[\boldsymbol{\varepsilon}] = \mathbf{0}$,
2. $\text{Cov}(\boldsymbol{\varepsilon}, \boldsymbol{\varepsilon}) = \sigma^2 \mathbf{W}^{-1}$, where $\mathbf{W}^{-1} \in \mathbb{R}^{n \times n}$ is the inverse of a known positive definite matrix and
3. $\text{rank}(\mathbf{X}) = m$.

The positive definite matrix is defined below:

$$\mathbf{W} = \begin{pmatrix} w_1 & 0 & \cdots & 0 \\ 0 & w_2 & \cdots & 0 \\ \vdots & \vdots & \ddots & \vdots \\ 0 & 0 & \cdots & w_n \end{pmatrix},$$

where $w_1, ..., w_n$ are known weights. The introduced variables and parameters are then combined to form the loss function, which is minimized to obtain the estimated model parameters:

$$\underset{\beta_1,\ldots,\beta_m}{\text{argmin}} \sum_{i=1}^{n} w_i (y_i - (\mathbf{X}\boldsymbol{\beta})_i)^2, \tag{2.2}$$

where

... w_i is the i^{th} diagonal element of the weight matrix $\mathbf{W}$,

... y_i is the i^{th} element of the dependent variable vector $\mathbf{y}$ and

... $(\mathbf{X}\boldsymbol{\beta})_i$ is the i^{th} of the calculated vector $\mathbf{X}\boldsymbol{\beta}$.

The solution to Equation (2.2) is shown below:

$$\hat{\boldsymbol{\beta}} = (\mathbf{X}^T \mathbf{W} \mathbf{X})^{-1} \mathbf{X}^T \mathbf{W} \mathbf{y} \tag{2.3}$$

Applying the Least Squares Method

The LS method will now be applied to the Nolfi Model to obtain estimates for the parameters α_x and γ_x. This will be done for calendar years (t) until $(t+s)$ and for ages (x) until $(x+r)$. The vectors and matrices used in this fitting

process are shown below:

$$\mathbf{y}_x = \begin{pmatrix} \bar{q}_x(t) \\ \bar{q}_x(t+1) \\ \vdots \\ \bar{q}_x(t+s) \end{pmatrix}, \quad \mathbf{X} = \begin{pmatrix} 1 & t-t \\ 1 & t+1-t \\ \vdots & \vdots \\ 1 & t+s-t \end{pmatrix}, \quad \boldsymbol{\beta}_x = \begin{pmatrix} \gamma_x \\ \alpha_x \end{pmatrix} \text{ and}$$

$$\mathbf{W}_x = \begin{pmatrix} E_x(t) & 0 & \cdots & 0 \\ 0 & E_x(t+1) & \cdots & 0 \\ \vdots & \vdots & \ddots & \vdots \\ 0 & 0 & \cdots & E_x(t+s) \end{pmatrix}.$$

The vectors and matrices are then plugged into Equation (2.3) to obtain the fitted parameters. Note, that this must be done separately for each age x. Figure 7 shows the results for the parameter estimations for fitting years 1970 until 2010 and fitting ages 0 until 98. These results were obtained by applying the steps above in the programming language R.

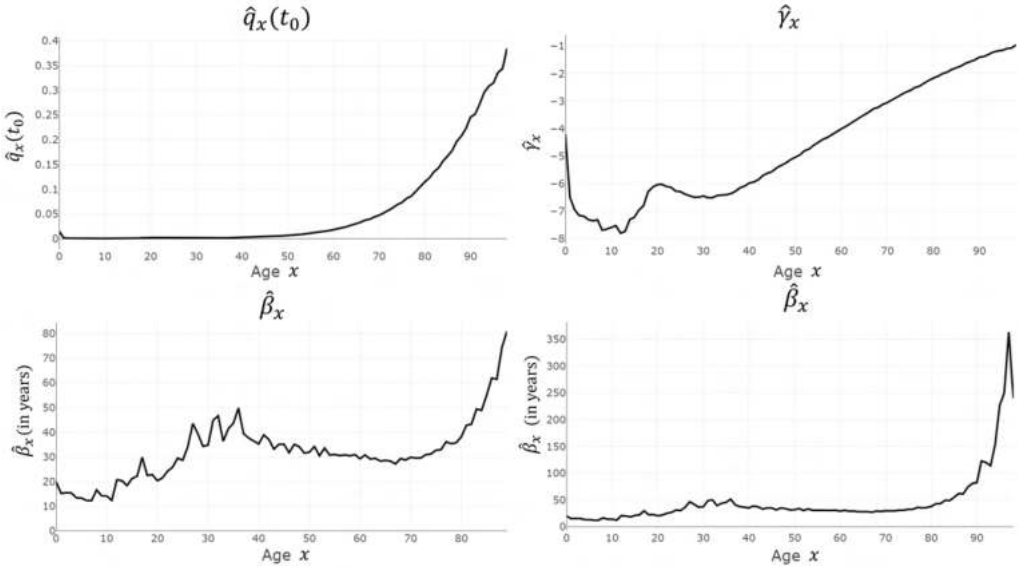

Figure 7: Parameters of the Nolfi Model for calendar years 1970-2010 and ages 0-98 for men in Switzerland. The top left graph shows the starting mortality rate $\hat{q}_x(t_0)$. Here, $t_0 = 1970$. The top right graph shows the logarithm of the starting mortality rate $\hat{\gamma}_x = \ln(\hat{q}_x(t_0))$. The bottom graphs show the half-value period $\hat{\beta}_x$, which is measured in years. The bottom left graph shows the ages 0-90, whereas the bottom right graph shows the ages 0-98.

The top left graph in Figure 7 shows the estimated starting mortality rate $(\hat{q}_x(t_0))$. It can be seen that there is a slight infant mortality effect at age

0. Additionally, it can be observed that the starting mortality rate begins increasing rapidly around the age of 50.

When taking the logarithm of this starting mortality rate, ($\hat{\gamma}_x$) is obtained. In the top right graph, the estimated values for this parameter are shown. It shows an overall linear increasing pattern for the higher ages, hence these starting mortality rates increase exponentially. Furthermore, one can recognize the infant mortality more clearly in this graph and a local maximum around the age of 20 is noticable. This local maximum is caused by the high accident rate among young men.

The bottom two graphs show the half-value period ($\hat{\beta}_x$), the left graph only shows the parameter values until the age of 90. The right graph shows the full span of the parameter. The half-value period parameter is the highest for the older ages, meaning that the mortality rate is estimated to decrease the slowest for older ages. Furthermore, there is a local maximum around the age of 30, which might be due to the AIDS pandemic.

The Nolfi Model parameter ($\hat{\alpha}_x$) was also obtained during the fitting process. However, no graph is shown for this parameter because it lacks intuitive explanatory value.

2.1.2 Projecting

The estimated parameters can now be used to estimate the mortality rate:

$$\hat{q}_x(t) = \hat{q}_x(t_0) \exp(\hat{\alpha}_x(t - t_0)). \tag{2.4}$$

In this example, the fitting period is from 1970 until 2010. A benefit of the Nolfi Model is that obtaining mortality rate estimates outside of the fitting period (i.e. projecting the mortality estimates) is not complicated. One must simply increase the value of t outside of the last fitted year in Equation (2.4). This will result in projected estimated mortality rates. In this example, the Nolfi model mortality rates will be projected for five years until calendar year 2015.

These fitted and projected mortality rate estimates can then be compared to observed mortality frequencies (see Equation (1.3)). Hereby, the errors of the mortality estimates are obtained. Note, that comparing projected mortality rates with observed mortality frequencies is known as backtesting. The mortality estimation errors for the fitting and projection period are shown in Figure 8.

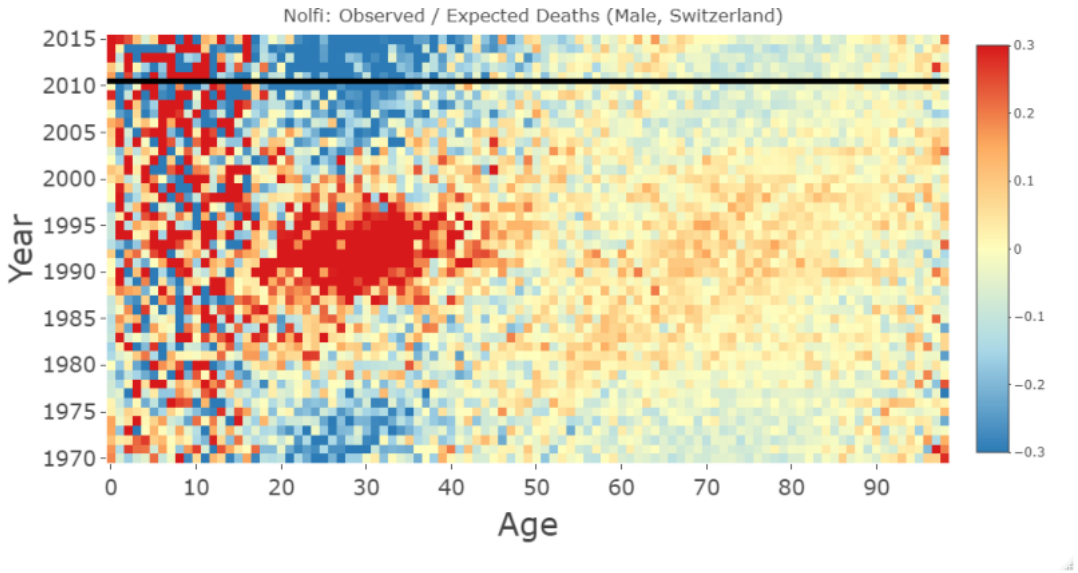

Figure 8: Mortality estimation errors of the Nolfi Model for calendar years 1970-2015 and ages 0-98 for men in Switzerland. The final five years were projected. The start of the projection point is shown by the black line in the Figure.

Figure 8 shows large errors in the fitted part of the graph (i.e. the part below the black line). The AIDS pandemic can clearly be observed as a large area of underestimation. Additionally, the years before and after the AIDS pandemic have large overestimation errors. The projection part of the graph (i.e. the part above the black line) are the worst in the age group that was affected by the AIDS pandemic.

2.2 Lee-Carter

The Lee-Carter Model (LC Model) adds a layer of complexity to the Nolfi Model by adding an interaction parameter for time t and age x.[18] This allows the LC Model to be more flexible when fitting the model to the data. Mathematically, the LC Model is described below:

$$q_x(t) = \exp(\alpha_x + \beta_x \kappa_t) = Q_x \exp(\beta_x \kappa_t), \tag{2.5}$$

where Q_x is the exponent of α_x:

$$Q_x = \exp(\alpha_x).$$

[18] cf. [6]

Similarly to the Nolfi Model, one often takes the logarithm of this function:

$$\ln(q_x(t)) = \alpha_x + \beta_x \kappa_t,$$

where

... α_x is the logarithm of the mean mortality rate for age x,

... Q_x is the mean of the mortality rate for age x,

... κ_t is the mortality trend throughout the years and

... β_x is the age sensitivity effect for the mortality trend (i.e. a higher β_x will give the mortality trend more effect for those ages).

To allow for a unique solution for the LC Model, the following assumptions are made:

1. $\sum_t \kappa_t = 0$ and
2. $\sum_x \beta_x = 1$.

The LC Model parameters will be estimated in R using the StMoMo lc() function, which utilizes the Maximum-Likelihood Method (ML Method).[19] Below, a mathematical explanation of this function will be given.

2.2.1 Fitting

Introducing the Maximum-Likelihood Method

For the estimation of the LC Model, it is assumed that the mortality rate is Poission distributed:

$$D_x^{(RV)}(t) \sim Poisson(E_x(t)q_x(t)),$$

where $q_x(t)$ is defined by Equation (2.5).[20]

By applying the ML Method one can estimate the unknown parameters α_x, β_x and κ_t. Combined, these will give an estimate for $q_x(t)$. These results will then be used to estimate the underlying distribution of the random variable $D_x^{(RV)}(t)$. The log-likelihood function that needs to be maximized is defined by:

$$L(\boldsymbol{\alpha}, \boldsymbol{\beta}, \boldsymbol{\kappa}) = \sum_{x,t} \{D_x(t)(\alpha_x + \beta_x \kappa_t) - E_x(t) \exp(\alpha_x + \beta_x \kappa_t)\} + \text{constant}. \quad (2.6)$$

[19] cf. [7]

[20] Note, that $D_x^{(RV)}(t)$ is a random variable. The realisations of this random variable are denoted by $D_x(t)$.

To find this maximum, the one-dimensional Newton method is used. For each iteration $(i+1)$ the parameter values are updated as described below:

$$\hat{\theta}^{(i+1)} = \hat{\theta}^{(i)} - \frac{\partial L^{(i)}/\partial\theta}{\partial^2 L^{(i)}/\partial\theta^2}, \tag{2.7}$$

where

... $\hat{\theta}^{(i)}$ is some model parameter value[21] in iteration $(i) \in \mathbb{N}_0$,

... $\hat{\theta}^{(0)}$ is the starting value for some parameter which is specified by the user or randomly generated and

... $L^{(i)}$ is the loss function which uses these model parameter values as input:

$$L^{(i)} = L^{(i)}(\hat{\theta}^{(i)}).$$

Applying the Maximum-Likelihood Method

The equations below are obtained by applying the Newton algorithm (see Equation (2.7)) to the LC Model parameters with the loss function defined by Equation (2.6).[22] The Newton algorithm starts with the values $\hat{\alpha}_x^{(0)} = 0$, $\hat{\beta}_x^{(0)} = 1$ and $\hat{k}_t^{(0)} = 0$. Note, that the iterative process for estimating the model parameters happens in sub-iterations of three iterations (see equations below). This is because the LC Model has three model parameters and not all parameters can be updated simultaneously.

In the equations below, $\hat{D}_x^{(i)}(t)$ represents the estimated number of deaths for age x in calendar year t for iteration (i):

$$\hat{D}_x^{(i)}(t) = E_x(t)\exp(\hat{\alpha}_x^{(i)} + \hat{\beta}_x^{(i)}\hat{k}_t^{(i)}).$$

1. The first sub-iteration calculates a new value for $\hat{\alpha}_x^{(i+1)}$, whereas the other parameters remain constant.

   (i) $\hat{\alpha}_x^{(i+1)} = \hat{\alpha}_x^{(i)} - \dfrac{\sum_t (D_x(t) - \hat{D}_x^{(i)}(t))}{-\sum_t \hat{D}_x^{(i)}(t)}$.

   (ii) $\hat{\beta}_x^{(i+1)} = \hat{\beta}_x^{(i)}, \quad \hat{\kappa}_t^{(i+1)} = \hat{\kappa}_t^{(i)}$.

[21] Note, that for the LC Model these are $\hat{\alpha}_x$, $\hat{\beta}_x$ and $\hat{\kappa}_t$.

[22] cf. [8]

2. The second sub-iteration calculates a new value for $\hat{\kappa}_t^{(i+2)}$, whereas the other parameters remain constant.

   (i) $\hat{\kappa}_t^{(i+2)} = \hat{\kappa}_t^{(i+1)} - \dfrac{\sum_x (D_x(t) - \hat{D}_x^{(i+1)}(t))\hat{\beta}_x^{(i+1)}}{-\sum_x \hat{D}_x^{(i+1)}(t)(\hat{\beta}_x^{(i+1)})^2}$.

   (ii) $\hat{\alpha}_x^{(i+2)} = \hat{\alpha}_x^{(i+1)}, \quad \hat{\beta}_x^{(i+2)} = \hat{\beta}_x^{(i+1)}$.

3. The third sub-iteration calculates a new value for $\hat{\beta}_x^{(i+3)}$, whereas the other parameters remain constant.

   (i) $\hat{\beta}_x^{(i+3)} = \hat{\beta}_x^{(i+2)} - \dfrac{\sum_t (D_x(t) - \hat{D}_x^{(i+2)}(t))\hat{\kappa}_t^{(i+2)}}{-\sum_t \hat{D}_x^{(i+2)}(t)(\hat{\kappa}_t^{(i+2)})^2}$.

   (ii) $\hat{\alpha}_x^{(i+3)} = \hat{\alpha}_x^{(i+2)}, \quad \hat{\kappa}_t^{(i+3)} = \hat{\kappa}_t^{(i+2)}$.

The Newton algorithm stops updating the values of the parameters once a certain incremental improvement is not reached. Generally, this is a very small value (e.g. 10^{-6}).

The results of this algorithm are discussed below in Figure 9.

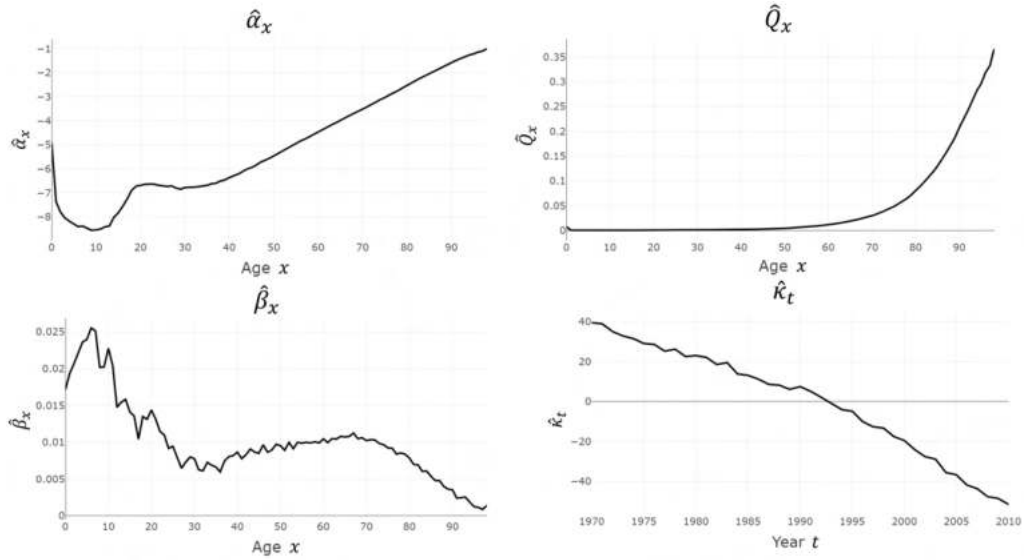

Figure 9: Parameters of the LC Model for calendar years 1970-2010 and ages 0-98 for men in Switzerland. The top left graph shows the estimated logarithmic mean mortality rate $\hat{\alpha}_x$. The top right graph shows the estimated mean mortality rate $\hat{Q}_x = \exp(\hat{\alpha}_x)$. The bottom left graph shows the estimated age sensitivity for the mortality trend $\hat{\beta}_x$. The bottom right graph shows the estimated mortality trend $\hat{\kappa}_t$.

The logarithmic mean mortality rate ($\hat{\alpha}_x$) shows an infant mortality (ages 0-1) effect. For older ages the logarithmic mean mortality rate trend is linear,

which matches the exponential increase in the older ages for the mean mortality rate. Furthermore, in the logarithmic mean mortality rate one can spot a local maximum around the age of 20. This is related to the higher mortality rate among young men due to accidents.

The age sensitivity to the mortality trend ($\hat{\beta}_x$) is the highest for ages below 20. This means that the mortality trend ($\hat{\kappa}_t$) has the largest effect for these younger ages. Given that the mortality trend is decreasing, this means that the decrease in mortality rate is the strongest for young ages. This is aligned with Figure 1, which was shown in the Introduction.

2.2.2 Projecting

These fitted parameters can now be used to project and estimate the mortality rate ($\hat{q}_x(t)$). However, since the LC Model includes a time dependent parameter ($\hat{\kappa}_t$), this parameter must first be extrapolated.

The projection of the mortality trend is approximated by a random walk with a drift which equals the average slope of ($\hat{\kappa}_t$). To simplify the random walk, the noise parameter of the random walk will be set to 0 (i.e. the mean slope of (κ_t) is simply extrapolated). This ensures that each time the same mortality rates are projected, the outcomes are the same. Formally, assuming the fitting time period is from $t, t+1, ..., t+s$, $\hat{\kappa}_t$ is extrapolated as shown in Equation (2.8).

$$\hat{\kappa}_{t+s+p} = \hat{\kappa}_{t+s} + p\hat{\kappa^*}, \tag{2.8}$$

where

... p represents the number of years which are projected into the future and

... $\hat{\kappa}^*$ is the mean slope of $\hat{\kappa}_t$ in the fitting time period $t, t+1, ..., t+s$:

$$\hat{\kappa}^* = \frac{\sum_{j=t}^{t+s} \hat{\kappa}_j}{(t+s-t+1)}.$$

Note, that this extrapolation method is strongly dependent on the fitting time period. These extrapolated and fitted parameters can then be plugged into the LC Model formula to obtain the estimated mortality rates:

$$\hat{q}_x(t) = \exp(\hat{\alpha}_x + \hat{\beta}_x\hat{\kappa}_t).$$

These fitted and projected mortality rate estimates can then be compared to observed mortality frequencies (see Equation (1.3)). Hereby, the errors of the mortality rate estimates are obtained. The errors for the projected (above

the black line) and fitted mortality rates (below the black line) are shown in Figure 10.

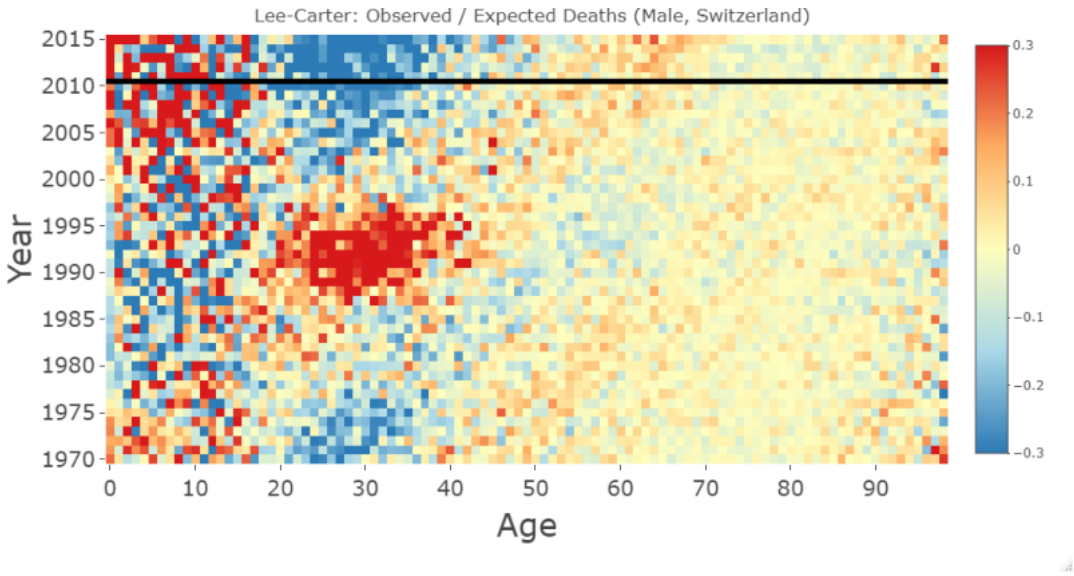

Figure 10: Mortality estimation errors of the LC Model for calendar years 1970-2015 and ages 0-98 for men in Switzerland. The last five years were projected. The start of the projection point is shown by the black line in the Figure.

Similarly to the Nolfi Model errors, Figure 10 also shows a large area of underestimation for the affected ages during the AIDS period. The years before and after the AIDS event show large overestimations. The projected years for the ages affected by the AIDS pandemic also show large underestimations.

2.3 Renshaw-Haberman

The Renshaw-Haberman Model (RH Model) adds a cohort parameter to the LC Model.[23] This allows the model to adapt to the data more precisely. The model is mathematically described below:

$$q_x(t) = \exp(\alpha_x + \beta_x \kappa_t + \beta^*_x \iota_{(t-x)}), \tag{2.9}$$

where:

... α_x is the logarithm of the mean mortality rate of age x,

... κ_t is the mortality trend for time,

... β_x is the age sensitivity for the time mortality trend,

[23] cf. [9]

... $\iota_{(t-x)}$ is the mortality trend for the cohorts and

... β_x^* is the age sensitivity for the cohort mortality trend (i.e. a larger β_x^* will give ι_{t-x} more impact).

Similar to the LC Model, the RH Model makes additional assumptions to allow for a unique solution:

1. $\sum_t \kappa_t = 0$,
2. $\sum_x \beta_x = 1$,
3. $\beta_x^* = 1$, the model makes this stricter assumption because fitting this parameter increases the computational cost of the fitting process significantly[24] and
4. $\sum_c \iota_c = 0$, where c is the set of all generations within the fitting period:

$$c = [\, min_{x,t}\{t-x\}, max_{x,t}\{t-x\}].$$

The RH Model parameters will be estimated in R using the StMoMo rh() function, which utilizes the ML Method.[25] Below, a mathematical explanation of this function will be given.

2.3.1 Fitting

Introducing the Maximum-Likelihood Method

Similarly to the LC Model, the RH Model also assumes a Poisson distribution:

$$D_x^{(RV)}(t) \sim Poisson(E_x(t)q_x(t)),$$

where $q_x(t)$ is defined by Equation (2.9).[26] With the addition of the cohort parameter, the RH Model log-likelihood function is slightly different from the LC Model log-likelihood function:

$$L(\boldsymbol{\alpha}, \boldsymbol{\beta}, \boldsymbol{\kappa}, \boldsymbol{\iota}) = \sum_{x,t} \{D_x(t)(\alpha_x + \beta_x\kappa_t + \iota_{(t-x)}) - E_x(t)\exp(\alpha_x + \beta_x\kappa_t + \iota_{(t-x)})\} + \text{constant}. \quad (2.10)$$

[24] Furthermore, research has shown that this assumption also makes the model more stable. (cf. [10])

[25] cf. [7]

[26] Note, that $D_x^{(RV)}(t)$ is a random variable. The realizations of this random variable are denoted by $D_x(t)$.

Applying the Maximum-Likelihood Method

Similarly to the LC Model, the Newton algorithm is used to find the RH Model parameter values. Contrary to the LC Model, the RH Model maximizes another log-likelihood function (see Equation (2.10)).[27] Furthermore, the Newton algorithm starts with randomly generated starting values instead of pre-specified values:

$$\hat{\alpha}_x^{(0)}, \hat{\beta}_x^{(0)}, \hat{\kappa}_t^{(0)}, \hat{\iota}_{(t-x)}^{(0)} \sim Uniform(-0.1, 0.1),$$

which are then used to start the iterative process shown in Equation (2.7).[28] Note, that each iteration consists of four sub-iterations. This is because the four parameters cannot be updated simultaneously.

In the equations below, $\hat{D}_x^{(i)}(t)$ represents the estimated number of deaths for calendar year t and age x in iteration (i):

$$\hat{D}_x^{(i)}(t) = E_x(t) \exp(\hat{\alpha}_x^{(i)} + \hat{\beta}_x^{(i)} \hat{\kappa}_t^{(i)} + \hat{\iota}_{(t-x)}^{(i)}).$$

1. The first sub-iteration calculates a new value for $\hat{\alpha}_x^{(i+1)}$, whereas the other parameters remain constant.

   (i) $\hat{\alpha}_x^{(i+1)} = \hat{\alpha}_x^{(i)} - \dfrac{\sum_t (D_x(t) - \hat{D}_x^{(i)}(t))}{-\sum_t \hat{D}_x^{(i)}(t)}.$

   (ii) $\hat{\beta}_x^{(i+1)} = \hat{\beta}_x^{(i)}, \quad \hat{\kappa}_t^{(i+1)} = \hat{\kappa}_t^{(i)}, \quad \hat{\iota}_{(t-x)}^{(i+1)} = \hat{\iota}_{(t-x)}^{(i)}.$

2. The second sub-iteration calculates a new value for $\hat{\kappa}_t^{(i+2)}$, whereas the other parameters remain constant.

   (i) $\hat{\kappa}_t^{(i+2)} = \hat{\kappa}_t^{(i+1)} - \dfrac{\sum_x (D_x(t) - \hat{D}_x^{(i+1)}(t)) \hat{\beta}_x^{(i+1)}}{-\sum_x \hat{D}_x^{(i+1)}(t) (\hat{\beta}_x^{(i+1)})^2}.$

   (ii) $\hat{\alpha}_x^{(i+2)} = \hat{\alpha}_x^{(i+1)}, \quad \hat{\beta}_x^{(i+2)} = \hat{\beta}_x^{(i+1)}, \quad \hat{\iota}_{(t-x)}^{(i+2)} = \hat{\iota}_{(t-x)}^{(i+1)}.$

3. The third sub-iteration calculates a new value for $\hat{\beta}_x^{(i+3)}$, whereas the other parameters remain constant.

   (i) $\hat{\beta}_x^{(i+3)} = \hat{\beta}_x^{(i+2)} - \dfrac{\sum_t (D_x(t) - \hat{D}_x^{(i+2)}(t)) \hat{\kappa}_t^{(i+2)}}{-\sum_t \hat{D}_x^{(i+2)}(t) (\hat{\kappa}_t^{(i+2)})^2}.$

   (ii) $\hat{\alpha}_x^{(i+3)} = \hat{\alpha}_x^{(i+2)}, \quad \hat{\kappa}_t^{(i+3)} = \hat{\kappa}_t^{(i+2)}, \quad \hat{\iota}_{(t-x)}^{(i+3)} = \hat{\iota}_{(t-x)}^{(i+2)}.$

[27] cf. [10]
[28] cf. [11]

4. The fourth sub-iteration calculates a new value for $\hat{\iota}_{(t-x)}^{(i+4)}$, whereas the other parameters remain constant.

   (i) $\hat{\iota}_{(t-x)}^{(i+4)} = \hat{\iota}_{(t-x)}^{(i+3)} - \dfrac{\sum_{x,t}(D_x(t) - \hat{D}_x^{(i+3)}(t))}{-\sum_{x,t}\hat{D}_x^{(i+3)}(t)}$.

   (ii) $\hat{\alpha}_x^{(i+4)} = \hat{\alpha}_x^{(i+3)}, \quad \hat{\beta}_x^{(i+4)} = \hat{\beta}_x^{(i+3)}, \quad \hat{\kappa}_t^{(i+4)} = \hat{\kappa}_t^{(i+3)}$.

The algorithm stops when the incremental improvements are smaller than a very small number (e.g. 10^{-6}).[29] Figure 11 shows the results of this fitting process.

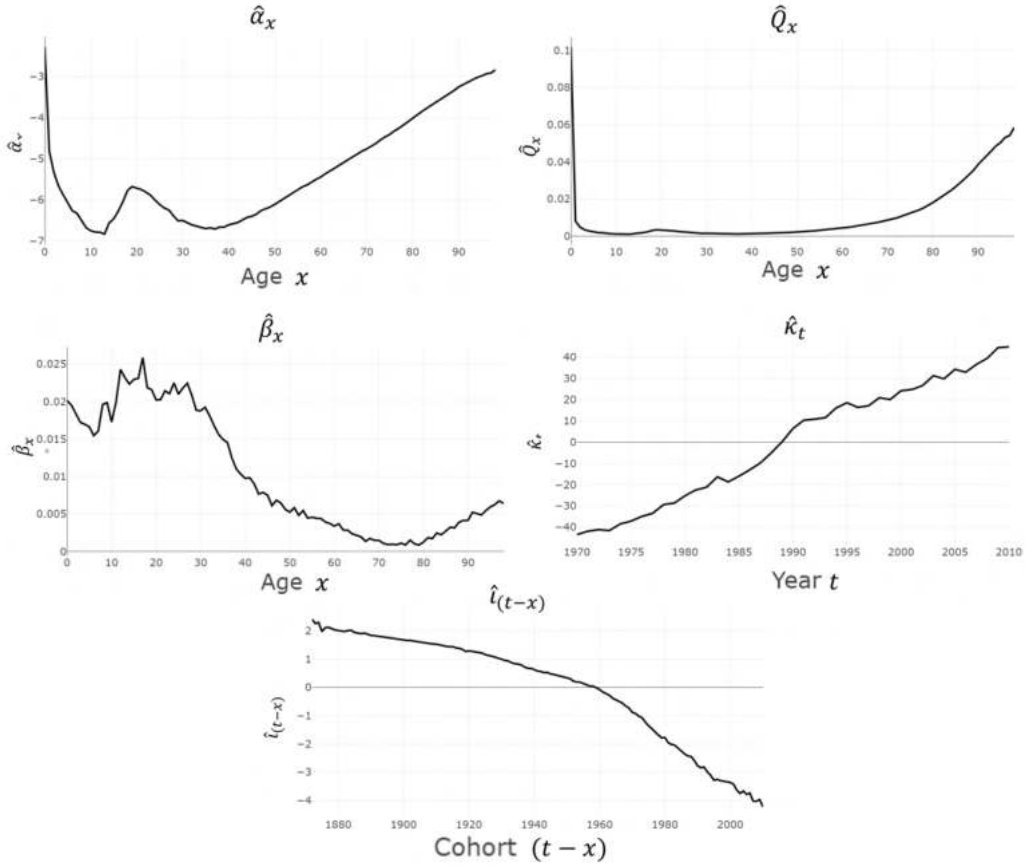

Figure 11: Parameters of the RH Model for calendar years 1970-2010 and ages 0-98 for men in Switzerland. The top left graph shows the logarithmic mean mortality rate $\hat{\alpha}_x$. The top right graph shows the mean mortality rate $\hat{Q}_x = \exp(\hat{\alpha}_x)$. The middle left graph shows age sensitivity for the mortality trend $\hat{\beta}_x$. The middle right graph shows the mortality trend $\hat{\kappa}_t$. The bottom graph shows the cohort trend $\hat{\iota}_{(t-x)}$.

In Figure 11 the logarithmic mean mortality rate ($\hat{\alpha}_x$) shows a similar shape

[29] cf. [10]

to the equivalent LC Model parameters. However, in the RH Model the infant mortality effect is bigger (this can also be seen in the mean mortality rate parameter ($\hat{Q}_x$)). The age sensitivity parameter for the mortality trend ($\hat{\beta}_x$) also shows a similar pattern to the LC Model parameter. The younger ages tend to have a higher sensitivity to the mortality trend than older ages.

The mortality trend ($\hat{\kappa}_t$) shows different behavior. Instead of having a decreasing mortality trend, the RH Model parameter shows an increasing mortality trend. This increasing mortality trend is mitigated by the decreasing cohort trend ($\hat{\iota}_{(t-x)}$). The decreasing effect in the cohort parameter has an exponential shape instead of a linear shape.

2.3.2 Projecting

These parameters can now be used for projecting the mortality rate estimates. Note, that the RH Model has two time dependent parameters ($\hat{\kappa}_t$ and $\hat{\iota}_{(t-x)}$). Before projecting the estimated mortality rates, both of these parameters must first be extrapolated. The extrapolation for the mortality trend ($\hat{\kappa}_t$) is the same as described for the LC Model (see Equation (2.8)).

Formally, assuming the fitting time period is from $t, t+1, ..., t+s$, the cohort trend parameter ($\hat{\iota}_{(t-x)}$) extrapolation is described below:

$$\hat{\iota}_{n+g} = \hat{\iota}_n + g\hat{\iota}^*, \tag{2.11}$$

where

... n is the newest cohort in the time fitting period:

$$n = (t+s) - \min(x),$$

... $\hat{\iota}^*$ is the mean cohort trend from the last quarter of cohorts:

$$\hat{\iota}^* = \frac{\sum_{j=d}^{n} \hat{\iota}_j}{n-d+1},$$

... o is the oldest cohort in the time fitting period:

$$o = t - \max(x),$$

... g is the number of cohorts that will be extrapolated and

... d is the starting point of the last quarter of cohorts within the fitting

period:

$$d = \text{int}\left(\frac{3(n-o)}{4}\right) + o,$$

where int() is the integer function which rounds down a decimal number to an integer.

The mean of the last quarter is taken, given that the extrapolation is linear, whereas the parameter development is exponential. If one does not extrapolate far into the future, this linear continuation of the cohort trend from the last quarter approximates the further exponential development. Note, that this extrapolation method is therefore dependent on the fitting time period.

The extrapolated and fitted parameters can then be plugged into the RH Model formula to obtain the estimated mortality rates:

$$\hat{q}_x(t) = \exp(\hat{\alpha}_x + \hat{\beta}_x\hat{\kappa}_t + \hat{\iota}_{(t-x)})$$

These fitted and projected mortality rate estimates can then be compared to observed mortality frequencies (see Equation (1.3)). Hereby, the errors of the mortality estimates are obtained. The errors for the projected (above the black line) and fitted mortality rates (below the black line) are shown in Figure 12.

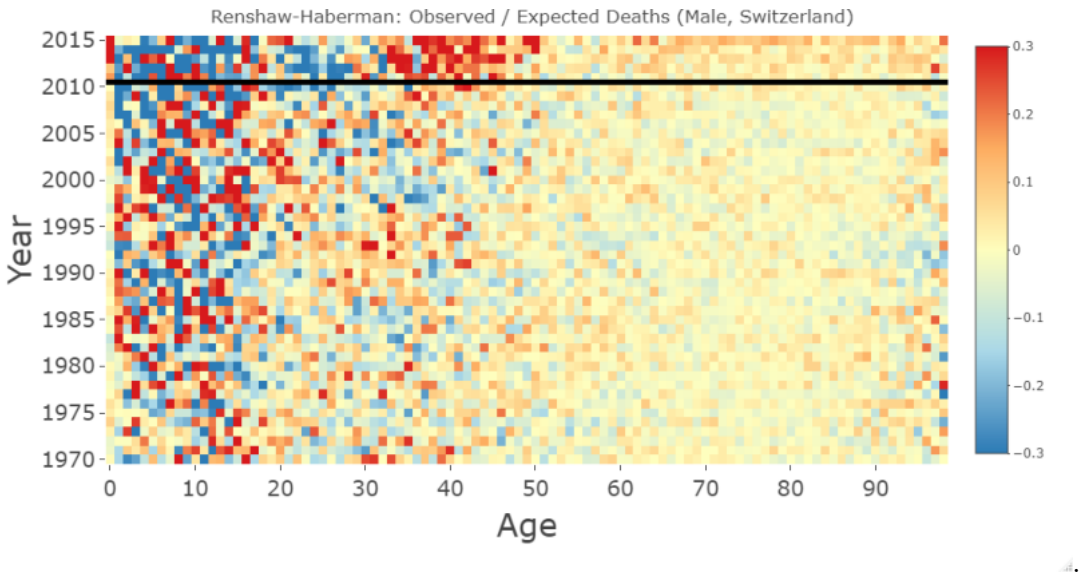

Figure 12: Mortality estimation errors of the RH Model for calendar years 1970-2015 and ages 0-98 for men in Switzerland. The last five years were projected. The start of the projection point is shown by the black line in the Figure.

Contrary to the LC Model and the Nolfi Model, the AIDS effect is not visible

in this error plot. Moreover, the errors are generally lower for ages 20 until 40. Additionally, the projected mortality rates have lower errors, except for the year 2015 for ages from 60 and above and the ages 30 until 35. Note, that this does not mean that the RH Model is always better at projecting the mortality rates.[30] In some cases, the RH Model overfits to the data and leads to large errors in projection, whereas the LC Model and the Nolfi Model have a lower risk of overfitting.

[30] cf. [3]

3 Defining and Identifying Singular Events

Remedies for singular events can only be proposed once the term singular event has been consistently defined. For this definition, two main questions come to mind:

1. Which calendar years are affected by the singular event?
2. Which ages are affected by the singular event?

For each of these questions[31], there are multiple ways of answering them.

Consider the example of the AIDS pandemic. From a medical perspective, one could say that AIDS started when the first person was diagnosed with AIDS within a certain country. From an actuarial perspective, this starting point of the AIDS pandemic is not of interest. An actuary will more likely define the start of the AIDS pandemic as the point in which the mortality rate of certain subgroups are significantly affected. Given that this is an actuarial thesis, we will only focus on the actuarial perspective.

The search for the singular events, from the actuarial perspective, will be aided by the aforementioned mortality forecasting models Nolfi, Lee-Carter and Renshaw-Haberman. These models will be used to fit a mortality curve during a timeperiod in which we expect a singular event. For the AIDS example, this timeperiod could be from calendar year 1960 until 2010. This timeperiod is long[32] because it will allow the singular event to stand out against normal mortality development outside of the singular event. Given that these singular events distort the underlying mortality development, it is expected that the singular events will produce large deviations between the observed mortality frequencies and the fitted mortality rates. One can then spot these deviations in a graph, as shown in Figure 13.

[31]Note, that the generational dimension is ignored in this case. There are a few cases where generational singular events are present. However, these are mostly constricted to one year only, leading to a small impact on model fitting. Therefore, the generational effect is not taken into account.

[32]Note, that the timeperiod should always be long when identifying a singular event, not just for the AIDS example.

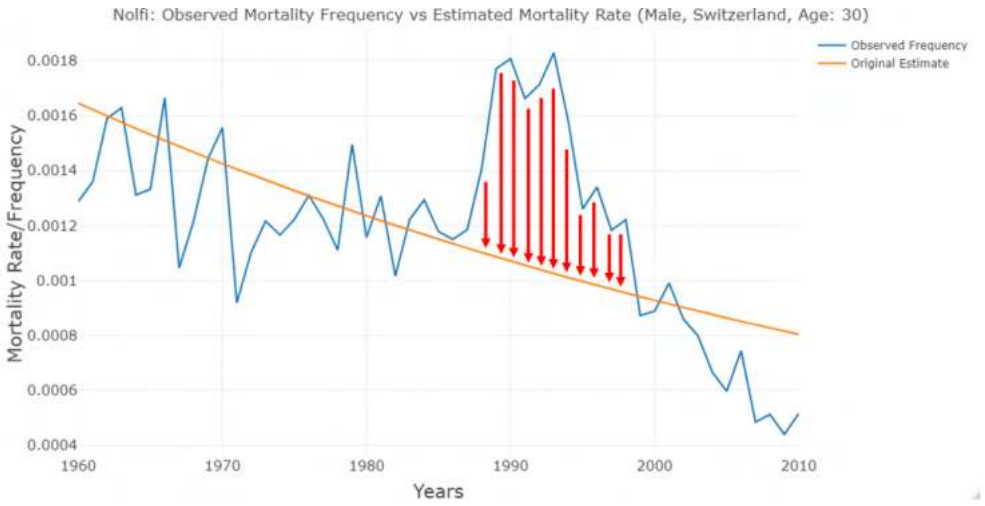

Figure 13: Observed mortality frequencies (in blue) versus the estimated mortality rates by the Nolfi Model (in orange). The red arrows depict the location of a consistent area of underestimation by the Nolfi Model.

The blue line in Figure 13 shows the observed mortality frequencies for a 30 year-old man. The orange line shows the fitted Nolfi mortality rate based on the blue line. The red arrows highlight an area in which there is a consistent underestimation of the mortality rate by the Nolfi Model. Note, that the starting years and final years of the fitting process (i.e. the far left and far right of Figure 13) show exactly the opposite effect. Here, the fitted Nolfi Model line seems to overestimate the mortality rate.

The change from underestimation to overestimation is logical, given that it is caused by the distorted parameters of the Nolfi Model. The AIDS peak in Figure 13 leads to the distortion of the Nolfi Model parameters during the fitting process. Without the AIDS peak, one would expect a lower half-value period for the mortality rate (i.e. the line would decrease with a steeper slope). Given the extremity of the AIDS peak, the Nolfi Model parameters fail to adapt enough to match the observed frequencies during the AIDS pandemic, leading to underestimation. However, due to the attempt of the model parameters to fit to this extreme peak, the model overestimates the mortality rates in areas outside of the AIDS peak. Besides large fitting errors, parameter distortion can also lead to a worse projection quality and to more jumps in estimated mortality rates between fitting sessions with different fitting years.

One can imagine expanding Figure 13 into the third dimension (i.e. showing Figure 13 for all ages). If one were to only focus on the relative errors of this three-dimensional graph, then it results in the familiar error graphs shown

throughout the thesis (see Figure 14). If one focuses on the age 30 in Figure 14, it can be observed that it matches to Figure 13. This can mathematically be shown, as we defined the error as follows:

$$\varepsilon_x(t) = \frac{D_x(t)}{\hat{q}_x(t)E_x(t)} - 1 = \frac{\bar{q}_x(t)}{\hat{q}_x(t)} - 1. \tag{3.1}$$

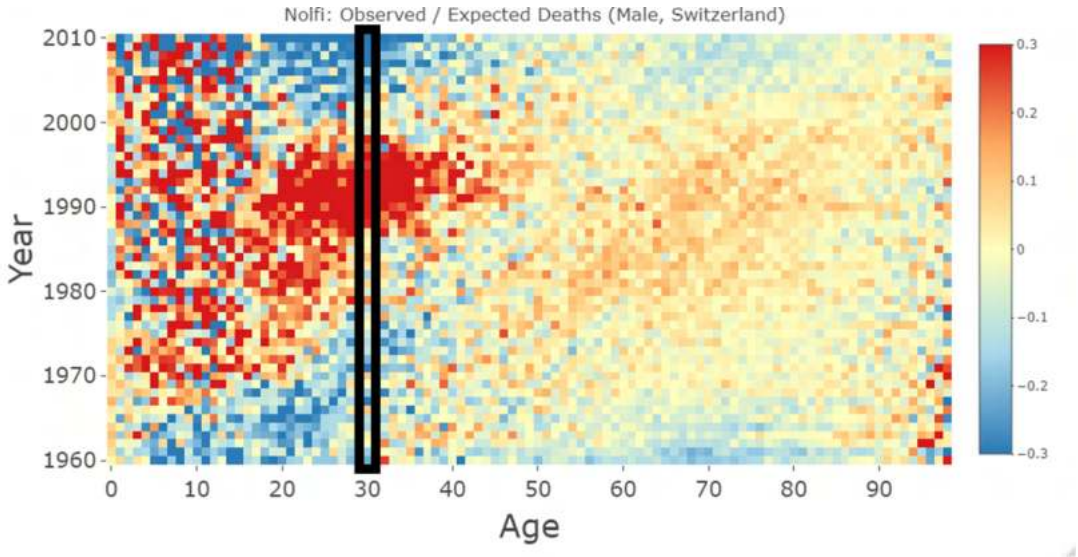

Figure 14: Nolfi Model effects of singular historic events. Switzerland (Male, 1960-2010) on the right. The black rectangle highlights the age 30, which is shown individually in Figure 13.

Fitting the mortality frequencies with the LC Model and the RH Model gives different results (see Figure 15 and Figure 16). The LC Model estimation adapts more to the singular event than the Nolfi Model. This is because it has multiple parameters which makes it more flexible for adaption. In this particular graph it does not create a problem, given that the singular event is still visible due to the higher errors. However, if one were to use the LC Model for singular event detection during World War I (WW I) or World War II (WW II), then it would fail (see Appendix). The added flexibility from the LC Model makes the event detection impossible in time periods in which the mortality data is even more distorted than during the AIDS pandemic.[33]

[33]In this case the singular events get more weight because the observed mortality frequencies deviate more from the overall mortality trend. Hence, the LC Model adapts more to the singular event, making it impossible to see it in an error graph.

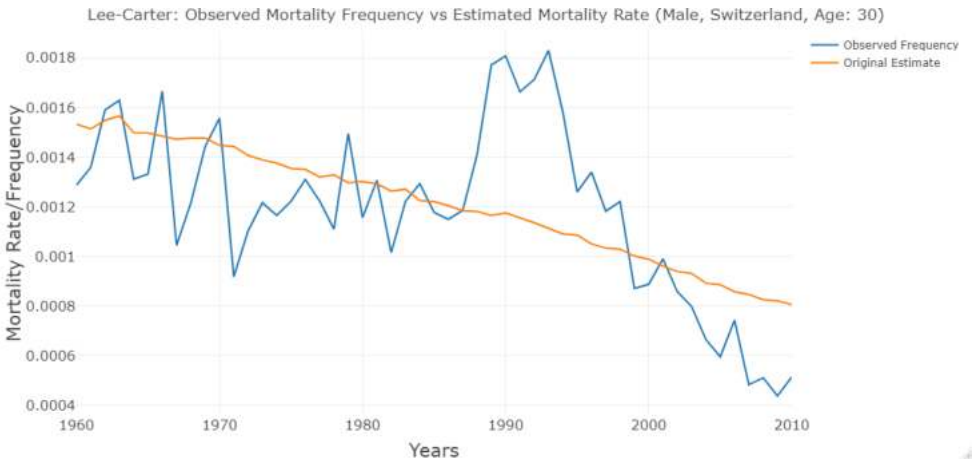

Figure 15: Raw observed mortality frequencies (in blue) versus the estimated mortality rates by the LC Model (in orange).

The RH Model estimation adapts more than the LC Model estimation (see Figure 16). The added flexibility of the RH Model estimation is so effective, that the singular event would not be visible in the error graphs. This is also the case when the RH Model is used for fitting WW II mortality data. Moreover, during the WW II timeperiod there appear to be singular events that do not exist in the data, because the RH Model tries to fit the existing singular event so well that other non-existent large underestimation error areas start to appear (see Appendix). Note, that this added flexibility is also not necessarily a positive sign for the model fitting or projection process outside of singular event detection. The added flexibility increases the risk of overfitting the model, leading to a worse performance when the model is used outside of the training data (i.e. when forecasting mortality development).

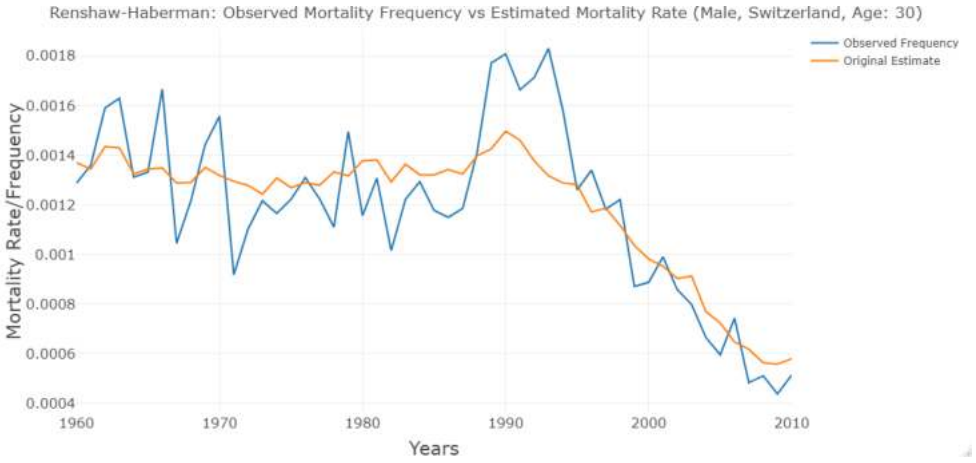

Figure 16: Raw observed mortality frequencies (in blue) versus the estimated mortality rates by RH Model (in orange).

Given the differences in model performance for visualizing singular events, this thesis will only use the Nolfi Model and LC Model for locating the singular events. In time periods where the LC Model is unsuccesful, only the Nolfi Model will be used. Now that the models are selected, there is still no clear definition of a singular event. In the following sections, the thesis will cover two methods that take the visualized output from the models and use it to define the singular event. The first method is the "expert judgement" method and the second method is the "algorithm" method. The process of identifiying the singular event by one of the methods will be represented by Figure 17 in the diagrams in Chapter 4.

Figure 17: The diagram symbol for the singular event identification process described in this chapter is a red diamond with "SE" written in it. This symbol will be relevant for the diagrams in Chapter 4.

3.1 Expert Judgement

The first method for identifying singular events is the expert judgement method. This method relies solely on the perception of the expert. Initially, the expert

receives a graph containing errors of either the Nolfi Model or the LC Model (see Figure 14). Based on this error graph, the expert is then asked to visually judge how many singular events can be seen within this graph. Afterwards, the expert must state the affected calendar years and the affected ages for each event. Thereby, the expert answered the two questions which were mentioned in the beginning of this chapter. Below in Figure 18 and Figure 19, an overview of the message pop-ups within R and the results of one expert judgment singular event classification can be found.

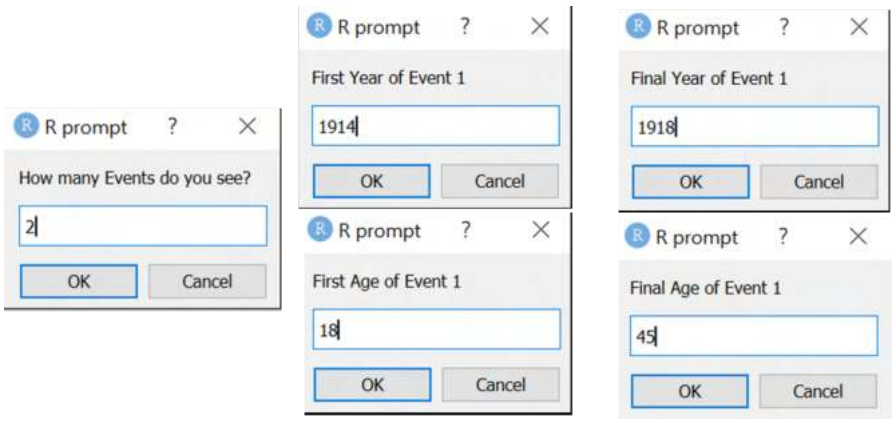

Figure 18: Pop-up questions in R which are consecutively shown when the expert judgement method is used.

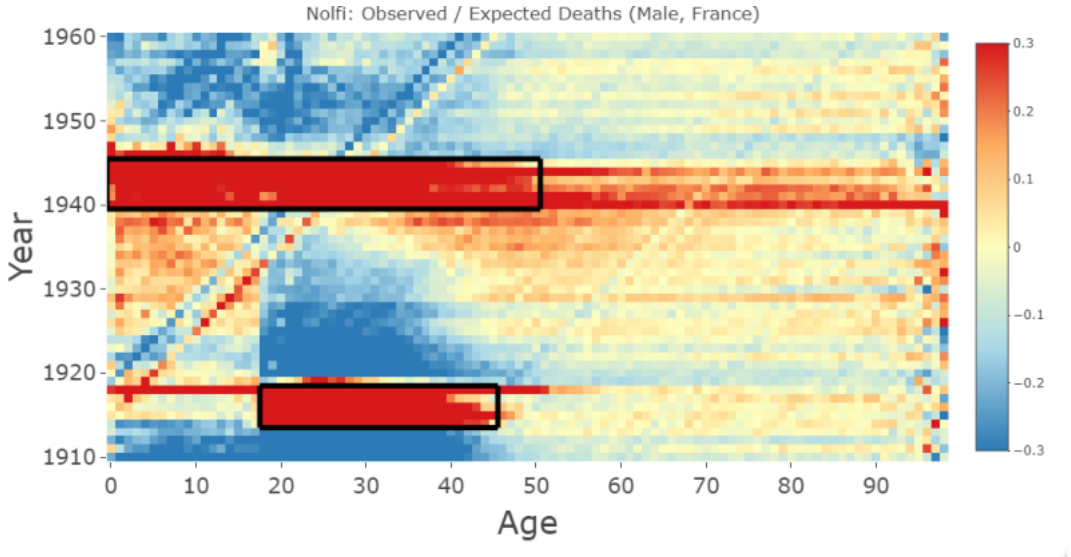

Figure 19: Results from the expert judgement pop-up questions. The singular events are now highlighted by black rectangles. Note how event 1 (WW I) matches with the answers given in Figure 18.

The advantages of this method are its simple implementation and the possibility of being as conservative with the size of the singular event as preferred. Given the rectangular nature of the singular event detection method, an expert might deliberately choose a bigger rectangle so that the event is likely to be fully contained within the rectangle. The downside of this method comes with the required manual input. If the future correction of the singular event has an iterative nature, then with each iteration new boundaries for the event would have to be chosen. Alternatively, the event boundaries could remain constant throughout the iteration, although this might impact the correction quality.[34] Moreover, the expert judgement method also risks inconsistencies between the opinion of experts. For example, one expert might identify a singular event to be 10% larger compared to the identification of another expert.

3.2 Algorithm

The second method for identifying singular events is the algorithm method. This method uses a prespecified set of parameters, which are then used to algorithmically search the error graphs (e.g. Figure 14) for singular events. This algorithm will be explained in two parts, given that this allows for a more natural explanation of the algorithm. The first part focuses on finding the affected calendar years. The second part focuses on finding the affected ages. In each of these parts, the parameters used in that part will be verbally and graphically introduced. Furthermore, a pseudocode will be shown to explain both parts of the algorithm. For the graphical explanations the following graph will be used throughout the section:

[34] This will be covered in more detail in Chapter 4 about the singular event correction, when discussing the stationary and moving iterative correction methods.

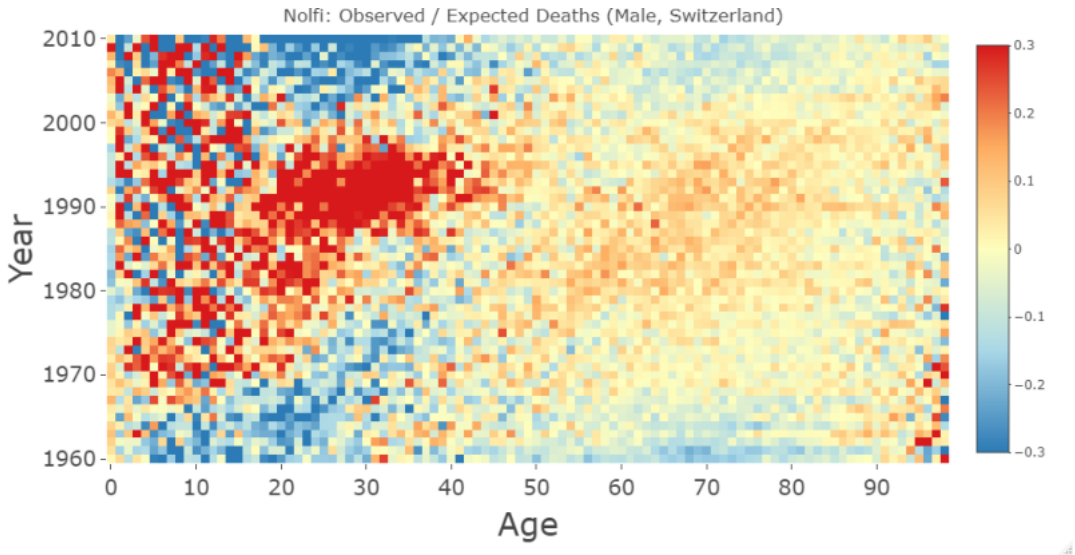

Figure 20: Fitting errors for the Nolfi Model in time period 1960-2010 for men in Switzerland. The AIDS effect is clearly visible and will be used to explain the algorithm.

3.2.1 Part One: Finding the Affected Calendar Years

For the first part of the algorithm, the following parameters are used:

- ε : This parameter works on a data point[35] level and serves as a threshold for counting a data point as a large error or not. If the error in the data point is larger than ε, it is counted as a large error. Increasing the ε parameter will increase the threshold for large errors. Hence, it will decrease the size and number of singular events found. In this algorithm, the error per data point is defined below:

$$\varepsilon_x(t) = \frac{D_x(t)}{\hat{q}_x(t)E_x(t)} - 1, \tag{3.2}$$

  where

  ... $D_x(t)$ is the observed number of people at age x, who were alive at the beginning of year t, but did not surive until the end of year t,

  ... $\hat{q}_x(t)$ is the estimated mortality rate by the Nolfi or LC Model and

  ... $E_x(t)$ is the exposure for people alive in year t with age x.

  For example, focusing on the ages 18 until 28 and calendar year 1989, the parameter ε could be set to 0.3 (i.e. the darkest colour red in the

[35] A data point represents a combination of a calendar year t and an age x. Together they form the tuple (x, t). In the error graphs (e.g. Figure 14), a data point is a single error observation wihtin that graph (i.e. a single rectangle with a blue, yellow or red colour).

error graph, see Figure 20). In this case, only the data points with $\varepsilon_x(t) \geq \varepsilon = 0.3$ would count as a large error. Visually, this means that only the dark red colours count as large events (see Figure 21).

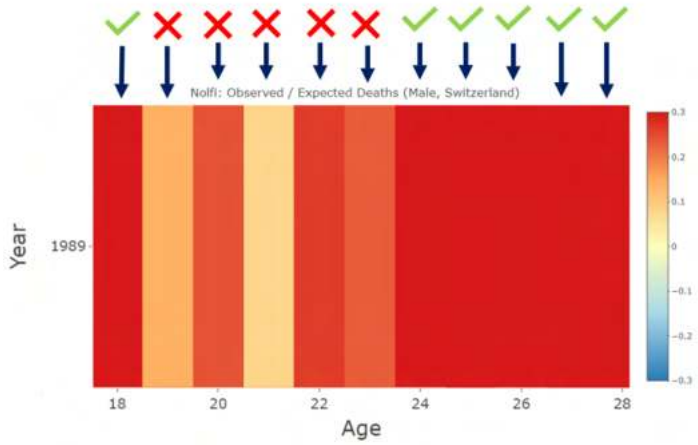

Figure 21: Fitting errors for the Nolfi Model in calendar year 1989, ages 18 until 28 for men in Switzerland. The green check marks identify the data points which contain errors $\geq \varepsilon = 0.3$, thereby counting as large errors. The red crosses indicate the data points which are $< \varepsilon = 0.3$, thereby not counting as large errors.

Note, that only the positive errors are considered for being a large error (i.e. not the blue errors). This is done because an area of underestimation (red) is often followed by overestimation (blue), as explained in the Introduction of this chapter. If one were to focus on both positive and negative errors, one would firstly find more singular events spread across multiple years for certain age groups. This would not be an accurate representation of the singular event in historic terms. Secondly, one would have trouble correcting for the event, given that fixing the overestimation will worsen the underestimation and vice versa. Hence, it is necessary to focus on only one side of the error, positive or negative. Furthermore, only the positive errors are considered because so far in history most, if not all, singular events have been events where more people died than expected from the previous mortality trend.

These large error data points are then used to calculate a score for each data point:

$$Score^{(year)}(x,t) =$$

$$= \begin{cases} \chi_{\{\varepsilon_x(t) \geq \varepsilon\}} + 0.5\chi_{\{\varepsilon_{x+1}(t) \geq \varepsilon\}} & \text{if } x - 1 < \min(\mathbf{x}), \\ \chi_{\{\varepsilon_x(t) \geq \varepsilon\}} + 0.5\chi_{\{\varepsilon_{x-1}(t) \geq \varepsilon\}} & \text{if } x + 1 > \max(\mathbf{x}), \\ \chi_{\{\varepsilon_x(t) \geq \varepsilon\}} + 0.5\chi_{\{\varepsilon_{x+1}(t) \geq \varepsilon\}} + 0.5\chi_{\{\varepsilon_{x-1}(t) \geq \varepsilon\}} & \text{otherwise,} \end{cases} \tag{3.3}$$

where

... χ is the indicator function,

... $\min(\mathbf{x})$ is the lowest fitting age used and

... $\max(\mathbf{x})$ is the highest fitting age used.

In words, Equation (3.3) describes that a data point gets one score point if its own error $\varepsilon_x(t)$ is greater than the threshold ε. Furthermore, a data point gets an additional half score point per horizontal neighbour (i.e. left and right) that has an error above the threshold. Hence, the maximum score per data point is 2. This is graphically shown in Figure 22.

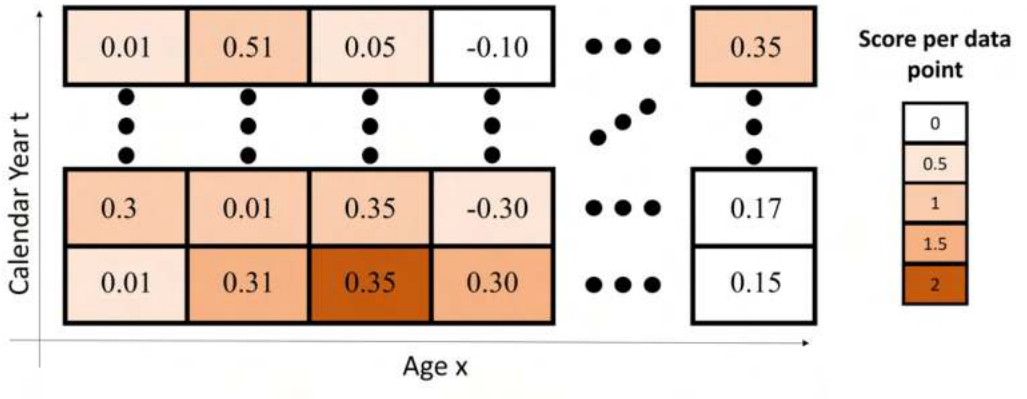

Figure 22: Graphical overview of the score calculation. Each data point is represented by a rectangle, the number within the rectangle is the error which is calculated as shown in Equation (3.2). If the data point has an error $\geq \varepsilon = 0.3$ it receives a point. For each of its lateral neighbours that has an error $\geq \varepsilon = 0.3$ it receives half a point. If the score is calculated for finding the affected ages, the upper and lower neighbours are used (not shown in this figure). For each calendar year, the points are summed. This is then divided by the number of data points in calendar year t (i.e. the number of ages), see Equation (3.4).

These data point scores are then combined to form a score per calendar year:

$$Score(t) = \frac{\sum_{x \in Ages} Score^{(year)}(x,t)}{\sum_{x \in Ages} 1}, \tag{3.4}$$

where $Ages$ is the set containing all ages which are used in the fitting process. Note, that the score can be larger than 1.

- γ^{year}: This parameter works on a calendar year level and checks whether a calendar year has a high enough score to classify as a singular event year. This is done using the score calculations in Equation (3.3) and Equation (3.4). In other words, the γ^{year} will set the threshold which the score must exceed for it to be considered a singular event year. Increasing

γ^{year} will require a higher score (i.e. more large errors to be found within a calendar year) per calendar year to be classified as a singular event year, hence it will decrease the size and number of singular events.

For instance, for the following example we will focus on all ages and calendar years from 1987 until 1989. The parameter γ^{year} (in this example $\gamma^{year} = 0.33$) might be set in such a way that the calendar year 1989 contains enough large error data points (i.e. check marks in Figure 21), so that the calendar year 1989 is classified as a singular event year. In this example, the calendar years 1987 and 1988 do not have enough large error data points (i.e. not a high enough score) to be classified as a singular event year (see Figure 23).

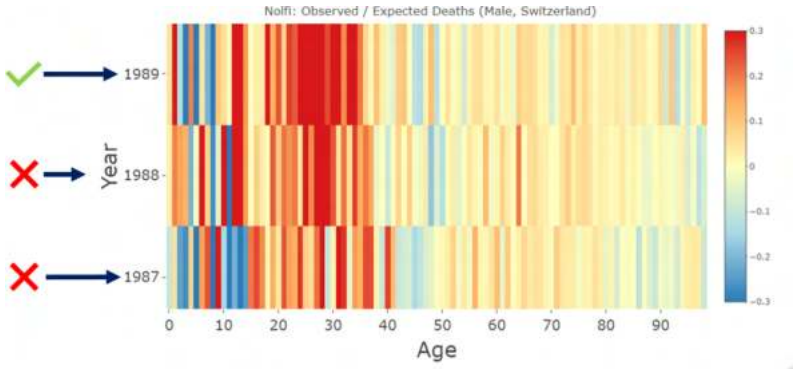

Figure 23: Fitting errors for the Nolfi Model in calendar year 1987-1989, ages 0-98 for men in Switzerland. The green check marks identify the calendar years which have a score $\geq \gamma^{year} = 0.33$, thereby counting as a singular event year. The red crosses indicate the calendar years with scores $< \gamma^{year} = 0.33$, thereby not counting as singular event years.

- $\alpha^{year} \in [0, 1]$: This parameter works on a calendar year level and allows calendar years, which are adjacent to a singular event calendar year, to merge with the singular event if they have a high enough score. This is checked by lowering the γ^{year} threshold by multiplying it with α^{year} (i.e. $\alpha^{year}\gamma^{year}$).

  For example, assume that calendar years 1989 until 1995 have high enough scores and are identified as singular event years (shown as the area within the dashed lines in Figure 24). The adjacent years to these dashed boundaries are then checked. If one of these adjacent years (or both) have a score $\geq \alpha^{year}\gamma^{year}$ (with $\alpha^{year} = 0.5$), then it is added to the singular event years. In Figure 24, calendar years 1987, 1988 and 1996 passed this less strict criterion $\alpha^{year}\gamma^{year}$ and were added to the singular event years. The final singular event years are shown within the filled black lines. Note, that it is possible for multiple adjacent years to

be added to the singular event, as long as the final subset of years is one continuous area.

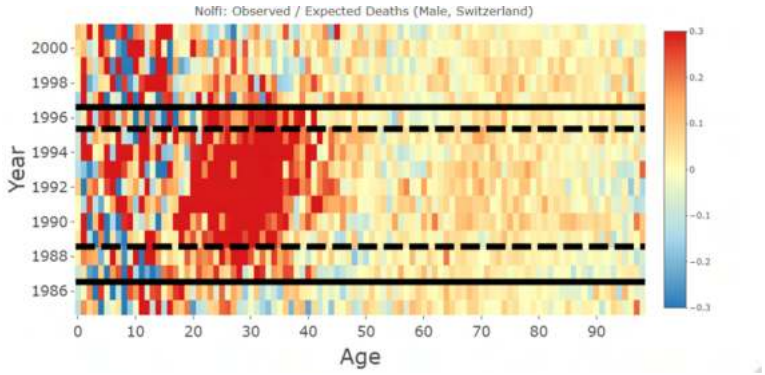

Figure 24: Fitting errors for the Nolfi Model in calendar year 1985-2001, ages 0-98 for men in Switzerland. Within the dashed lines are the years that exceeded some level γ^{year}, thereby counting as a singular event years. The years between the dashed and filled lines, were lines that passed the easier threshold $\alpha^{year}\gamma^{year}$ and were therefore added to the singular event years (with $\alpha^{year} = 0.5$).

The pseudocode below shows how these parameters are combined to obtain the affected calendar years of the singular event. In the code below γ^{year} is depicted as gamma_year and α^{year} is depicted as alpha_year. Furthermore, the score_year is calculated as shown in Equation (3.3) and Equation (3.4).

```
for(year in calendar_years){
  if (score_year > gamma_year){
     add year to list singular_event_years
  }
  else if (score_year > alpha_year*gamma_year){
    add year to list maybe_singular_event_years
  }
}
for(year in singular_event_years){
  if((year-1) is in maybe_singular_event_years) {
    add (year-1) to list singular_event_years
  }
  else if((year+1) is in maybe_singular_event_years){
    add (year+1) to list singular_event_years
  }
  remove possible duplicates in singular_event_years
}
```

Listing 1: Finding the affected calendar years for the singular event.

After this part of the algorithm is done, the calendar years that belong to the singular event have been identified.The final result for the calendar year part of the algorithm is depicted in Figure 25. The years between the black lines show the singular event years.

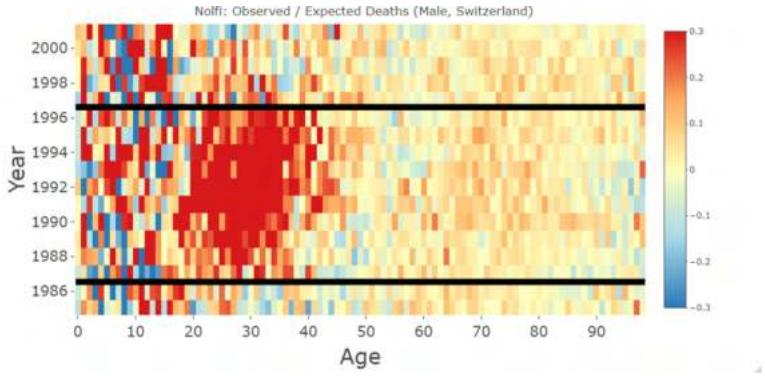

Figure 25: Fitting errors for the Nolfi Model in calendar year 1985-2001, ages 0-98 for men in Switzerland. The calendar years within the black filled line show the calendar years which are affected by the singular event. This information is used by the second part of the algorithm to calculate the affected ages.

3.2.2 Part Two: Finding the Affected Ages

The second part of the algorithm focuses on the results of the first part of the algorithm, which are the calendar years included in the singular event (see Figure 25). To find the affected ages within these calendar years, the following parameters are used:

- ε: This parameter works on a data point level and is the same parameter as used in the first part of the algorithm (i.e. always has the same value). This is graphically explained in Figure 21. The score for the age dimension is then calculated by using these large error data points:

$$Score^{(age)}(x,t) =$$

$$= \begin{cases} \chi_{\{\varepsilon_x(t)\geq\varepsilon\}} + 0.5\chi_{\{\varepsilon_x(t+1)\geq\varepsilon\}} & \text{if } t-1 < \min(\mathbf{t}), \\ \chi_{\{\varepsilon_x(t)\geq\varepsilon\}} + 0.5\chi_{\{\varepsilon_x(t-1)\geq\varepsilon\}} & \text{if } t+1 > \max(\mathbf{t}), \\ \chi_{\{\varepsilon_x(t)\geq\varepsilon\}} + 0.5\chi_{\{\varepsilon_x(t+1)\geq\varepsilon\}} + 0.5\chi_{\{\varepsilon_x(t-1)\geq\varepsilon\}} & \text{otherwise,} \end{cases} \tag{3.5}$$

  where

  ... χ is the indicator function,

  ... $\min(\mathbf{t})$ is the lowest fitting year used and

  ... $\max(\mathbf{t})$ is the highest fitting year used.

  In words, the score for a data point is calculated by checking if the data point itself has a large error as defined by ε. If this is the case, then the data points get one score point. Furthermore, the data point receives half a score point for each of the vertical neighbours (i.e. up and down)

that has a large error as defined by ε. These scores are then summed for each age and divided through the number of calendar years in the fitting process which are also singular event years:

$$Score(x) = \frac{\sum_{t \in Years^*} Score^{(age)}(x,t)}{\sum_{t \in Years^*} 1}, \tag{3.6}$$

where $Years^*$ is the set containing all the calendar years which are used in the fitting process and are also defined as singular event years.

- γ^{age}: This parameter works on an age level and determines whether the score for a certain age is high enough to be classified as a singular event age.

  This is achieved by using a similar scoring calculation as with the γ^{year} parameter (see Equation (3.5) and Equation (3.6)). In this case, only the year neighbours are considered for the score calculation and only the calendar years which are within the singular event are summed.

  Increasing γ^{age} will require more large errors to be found within an age for it to classify as a singular event age. This leads to smaller singular events.

  For example, let's focus on the ages from 36 to 39. The parameter γ^{age} can be set in a way, such that ages 36 until 38 pass as a singular event age and age 39 does not (see Figure 26). Note, that only the calendar years which are classified as singular event years are considered in this part of the algorithm. In Figure 26 , these calendar years are the years within the black lines.

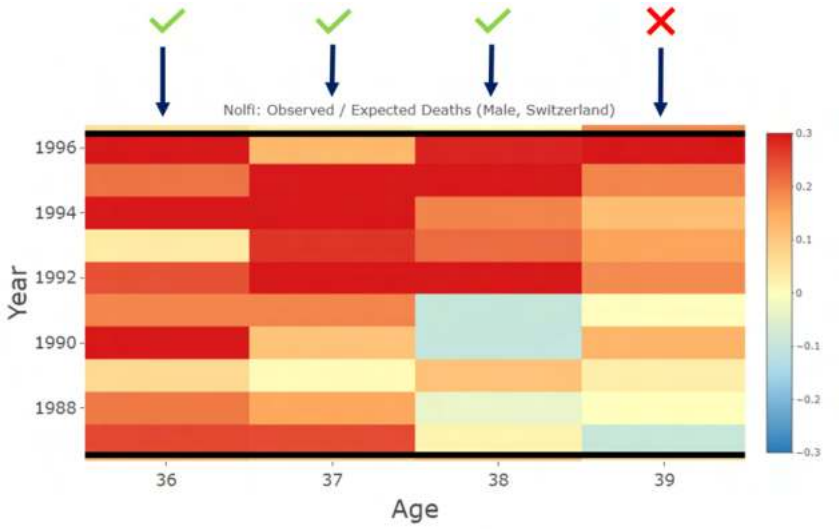

Figure 26: Fitting errors for the Nolfi Model in calendar year 1987-1996, ages 36-39 for men in Switzerland. The green check marks identify the ages which have a score $\geq \gamma^{age} = 0.66$, thereby counting as a singular event age. The red cross indicates the age with a score $< \gamma^{age}$, thereby not counting as a singular event age. Note, that only the singular event years are considered for defining which ages are affected. These years are contained within the black lines in this figure.

- $\alpha^{age} \in [0, 1]$: This parameter works on an age level and allows ages, which are adjacent to a singular event age, to merge with the singular event if they have a high enough score. This is achieved by lowering the γ^{age} threshold by multiplying it with α^{age} (i.e. $\alpha^{age}\gamma^{age}$).

  For example, assume that ages 20 until 38 have a high enough score to classify as singular event ages (shown as dashed lines in Figure 27). The ages adjacent to these dashed lines are then checked. If one of those ages has a score$\geq \alpha^{age}\gamma^{age}$ (with $\alpha^{age} = 0.4$), then it is added to the singular event ages. In Figure 27, the ages 18 and 19 are added to the singular event. The final ages are shown by the black filled vertical lines. Note, that it is possible for multiple adjacent ages to be added to the singular event (similar to the year case).

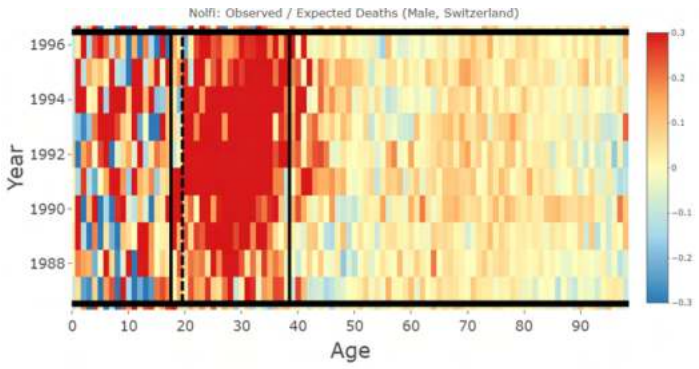

Figure 27: Fitting errors for the Nolfi Model in calendar year 1987-1996, ages 0-98 for men in Switzerland. Within the dashed vertical lines are the ages with a score $\geq \gamma^{age}$, thereby counting as a singular event years (the right dashed line overlaps with the filled line). The ages between the dashed and filled lines, were the adjacent ages with a score $\geq \alpha^{age}\gamma^{age}$ and were therefore added to the singular event years (with $\alpha^{age} = 0.4$).

The pseudocode below shows how these parameters are combined to obtain the affected calendar years of the singular event. In the code below γ^{age} is depicted as gamma_age and α^{age} is depicted as alpha_age. Furthermore, the score_age is calculated as shown in Equation (3.5) and Equation (3.6).

```
for(age in ages){
  if (score_age > gamma_age){
     add age to list singular_event_ages
  }
  else if (score_age > alpha_age*gamma_age){
    add age to list maybe_singular_event_ages
  }
}
for(age in singular_event_ages){
  if((age-1) is in maybe_singular_event_ages) {
    add (age-1) to list singular_event_ages
  }
  else if((age+1) is in maybe_singular_event_ages){
    add (age+1) to list singular_event_ages
  }
  remove possible duplicates in singular_event_ages
}
```

Listing 2: Finding the affected ages for the singular event.

Now, the algorithm is done finding singular events. The results are shown in Figure 28.

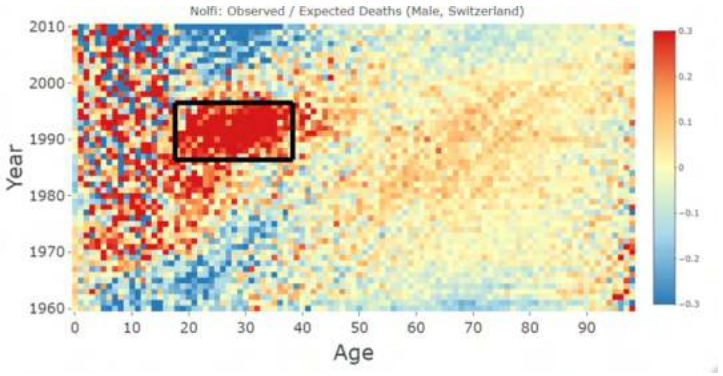

Figure 28: Fitting errors for the Nolfi Model in calendar year 1960-2010, ages 0-98 for men in Switzerland. The black rectangular box now shows the singular event as detected by the aforementioned algorithm.

4 Singular Event Corrections

With the singular event now defined and identified, it is possible to find a remedy. Before introducing the foundation of this remedy, it is useful to repeat the reasons for correcting for the singular event.

1. Singular events distorting the model parameters in the fitting process. These distorted parameters lead to

   ... large areas of overestimation (i.e. negative errors as defined in Equation 3.2) in areas outside of the singular event and

   ... a distorted projection, given that the parameters are not representative of the future.

2. Singular events cause bigger jumps in parameters as fitting periods change. One can imagine that certain time periods fully contain singular events (thereby leading to distorted parameters), whereas other time periods only partially contain singular events (leading to less distortion) or contain no singular events. The difference in parameters between two such fitting periods would be larger, than if there were no singular event in both of the fitting periods.

Below, a general correction method is explained. This correction method can be viewed as a building block. The methods that are discussed further in this chapter, will utilize this building block in varying ways.

Once a mortality model is fitted, the estimated number of deaths of the fitted model ($\hat{D}_x(t)$) can be compared to the observed number of deaths ($D_x(t)$). Within singular events, the difference between these two numbers can be large. This is due to the fact that the singular event does not follow the general underlying mortality development. The model therefore struggles to adapt to the singular event, where it tends to underestimate the mortality rate. However, the attempt to adapt to the singular event leads to the model overestimating the mortality rate in areas outside of the singular event. To fit the model properly to the areas outside of the singular event, the general correction method removes the singular event from the observed number of deaths data ($D_x(t)$).

The general correction method does so by assigning the estimated number of deaths ($\hat{D}_x(t)$) some credibility weight z.[36] The number of deaths matrix within the singular event is then updated by taking a convex combination of the observed number of deaths and the estimated number of deaths. The

[36]The term credibility weight in this thesis does not have the same meaning as in credibility theory.

number of deaths matrix outside of the singular event is not changed. This is mathematically described below:

$$\tilde{D}_x(t) = \begin{cases} z\hat{D}_x(t) + (1-z)D_x(t) & \text{if } (x,t) \in \Omega^{(se)}, \\ D_x(t) & \text{if } (x,t) \notin \Omega^{(se)}, \end{cases} \tag{4.1}$$

where

... $\Omega^{(se)}$ is the set containing the combination of ages and calendar years (tuples (x,t)) which are within a singular event,

... $\hat{D}_x(t)$ is the estimated number of deaths for age x and calendar year t,

... $D_x(t)$ is the observed number of deaths for age x and calendar year t and

... $z \in [0,1]$ is the credibility weight which quantifies how much the estimated number of deaths is trusted.

Figure 29 shows the symbol that summarizes the process of obtaining $\tilde{D}_x(t)$ using Equation (4.1).

Figure 29: Diagram symbol for the correction building block, which corrects the number of deaths data $\tilde{D}_x(t)$.

Each upcoming section in this chapter covers a correction method. The covered correction methods are the "single" correction method, the "stationary iterative" correction method, the "moving iterative" correction method and the "final fit" correction method. Each of these correction methods combines the correction building block (see Figure 29) with the other introduced building blocks in different ways. Each section will start of with a diagram showing the overall structure of the correction and its building blocks.

4.1 Single Model Correction

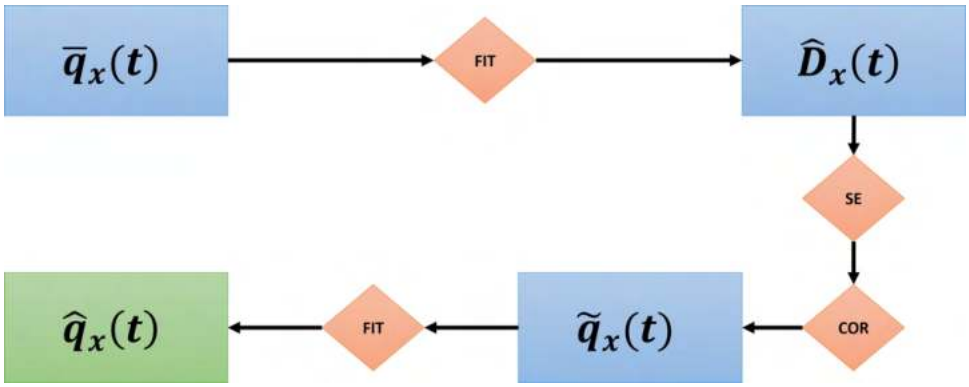

Figure 30: Diagram overview of the single model correction. Blue boxes represent obtained data, red diamonds represent different building blocks. The final result is represented by the green box.

The single model correction is the only correction which utilizes the correction building block (COR) once. This is shown in the diagram in Figure 30. Besides the correction building block, Figure 30 contains two fitting building blocks (FIT) and a singular event detection building block (SE). These building blocks are explained in Chapter 2 and Chapter 3 respectively. Below, an example will clarify how the single correction process works in more detail. The credibility weight used in the upcoming example is $z = 1$.

Figure 31: Overview of the single correction steps. The blue line represents the observed mortality frequency. The yellow line shows the estimated Nolfi mortality rate based on the blue line. The red line shows the altered observed mortality frequency. The green line shows the estimated mortality rate based on the red line. The AIDS singular event is within the black lines.

1. The observed number of deaths are taken $D_x(t)$ and divided by the observed exposures $E_x(t)$. This division results in the observed mortality frequency $\bar{q}_x(t)$:

$$\bar{q}_x(t) = \frac{D_x(t)}{E_x(t)}.$$

   In Figure 31, the observed mortality frequency is shown by the blue line (which overlaps with the red line outside of the black lines). This first step is represented by the "$\bar{q}_x(t)$" blue box in Figure 30.

2. The observed mortality frequency $\bar{q}_x(t)$ is then used to fit a mortality model. This model can be the Nolfi Model or the LC Model. This process is shown by the "FIT" red diamond in Figure 30.

3. The results of this fitting process are the estimated mortality rates $\hat{q}_x(t)$. In Figure 31 these are shown by the yellow line (which overlaps with the red line within the black lines). Furthermore, the estimated number of deaths are now retrieved by multiplying the estimated mortality rates by the observed exposures:

$$\hat{D}_x(t) = \hat{q}_x(t)E_x(t).$$

   This step is represented by the "$\hat{D}_x(t)$" blue box in Figure 30.

4. The estimated mortality rate $\hat{q}_x(t)$ is now compared with the observed mortality frequency $\bar{q}_x(t)$. The relative difference between these two will be defined as the error of the estimated mortality rate $\hat{q}_x(t)$:

$$\varepsilon_x(t) = \frac{\bar{q}_x(t)}{\hat{q}_x(t)} - 1. \tag{4.2}$$

   Based on these errors, the singular event will be defined by the expert judgment method or by the algorithm method. This is shown by the "SE" red diamond in Figure 30. In Figure 31, the singular event is marked by the two black lines.

5. As described in the beginning of this chapter, the number of deaths matrix is now corrected by creating a convex combination between the estimated and the observed number of deaths matrices (see Equation (4.1)). This step is represented by the "COR" red diamond in Figure 30.

6. The results of this correction are the new number of deaths $\tilde{D}_x(t)$ data points. This is then divided by the observed exposures to get the corrected mortality frequency $\tilde{q}_x(t)$:

$$\tilde{q}_x(t) = \frac{\tilde{D}_x(t)}{E_x(t)}.$$

This corrected mortality frequency is shown by the red line in Figure 31. Note, that given that the credibility weight was set to one in this example ($z = 1$), the corrected frequency now fully overlaps with the estimated model mortality rates $\hat{q}_x(t)$ (i.e. the yellow line) within the singular event. This step is represented by the "$\tilde{q}_x(t)$" blue box in Figure 30.

7. The corrected mortality frequency $\tilde{q}_x(t)$ is then used to fit the mortality model a second time. This process is shown by the second "FIT" red diamond in Figure 30.

8. The end result is a new mortality rate estimate $\hat{q}_x(t)$. The second estimate is shown by the green line in Figure 31. This step is shown by the last "$\hat{q}_x(t)$" green box in Figure 30.

If Figure 31 is extended into the third dimension (i.e. viewing the single model correction for all ages and calendar years), one can see what happens within the usual error graphs (see Figure 32).

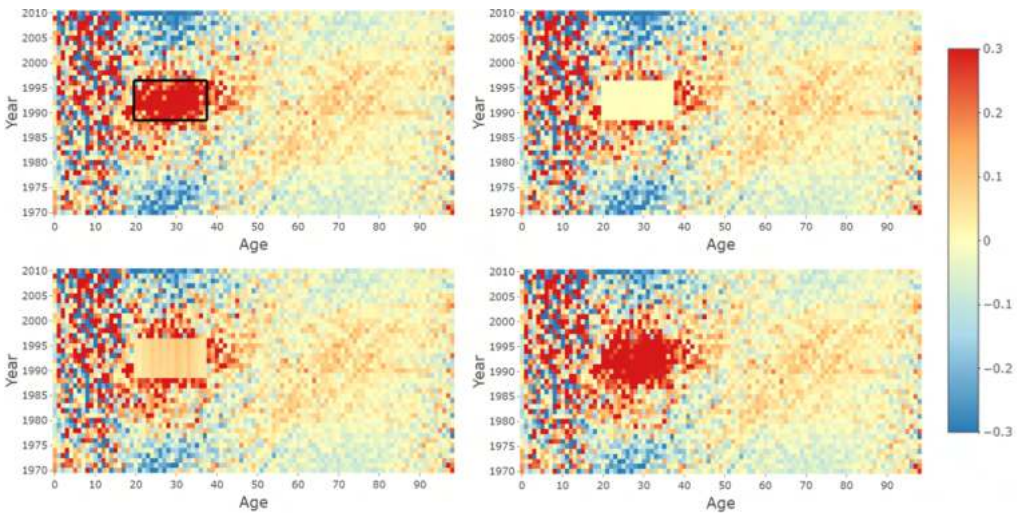

Figure 32: The error graphs above show the single correction method step-by-step.

In Figure 32, the top left graph shows the error (as defined by Equation (4.2)) after the first fitting with the identified singular event (black rectangle). In terms of Figure 31 this represent the error between the blue line and the yellow line. The top right graphs shows the effect of correcting within the singular event with credibility weight $z = 1$. Note, that the area within the singular event therefore has an error of zero. In Figure 31, this represent the error between the red line and the yellow line. The bottom left graphs show the new fitted model, in Figure 31 this shows the error between the red line

and the green line. The bottom right graph shows the final result, which in Figure 31 is the error between the blue line and the green line.

In Figure 32 it can be observed that the upper two graphs have areas with larger errors above and below the singular event. These errors are smaller in the lower graphs. Additionally, the singular event is bigger in the lower graphs. Summarized, the areas that are removed from the singular event by some years seem to improve whereas the areas in and closely around the singular event deteriorate.

Note, that it can be hard to clearly observe which areas improve and deteriorate after the correction in Figure 32. In Figure 33, one can see the absolute improvement (green) or deterioration (red) when comparing the model estimation before and after correction. This improvement is calculated as follows:

$$\zeta_x(t) = |\varepsilon_x^{(2)}(t)| - |\varepsilon_x^{(1)}(t)|, \tag{4.3}$$

where

... $|\varepsilon_x^{(1)}(t)|$ is the absolute value of the error of the first (corrected) model fit as defined by Equation (3.2) and

... $|\varepsilon_x^{(2)}(t)|$ is the absolute value of the error of the second (corrected) model fit as defined by Equation (3.2).

Note, that Equation (4.3) implies that negative values for $\zeta_x(t)$ are improvements between the first and second fit, whereas positive values are deteriorations between the first and the second fit. For Figure 33, $|\varepsilon_x^{(1)}(t)|$ represents the original fitting error and $|\varepsilon_x^{(2)}(t)|$ represents the fitting error after the single correction has been applied. In later sections of this chapter $|\varepsilon_x^{(1)}(t)|$ can also represent a simpler correction method error, whereas $|\varepsilon_x^{(2)}(t)|$ can represent a more complicated correction method error. This then allows us to compare the correction methods in terms of improvement (i.e. to see what the incremental benefit of the more complicated correction is).

In Figure 33, the absolute improvement between the top left graph and the bottom right graph of Figure 32 is shown. Note, how the estimation quality within and closely around the singular event decreases. This is to be expected, given that the singular event was taken out of the observed mortality frequency. Hence, the estimated mortality rate did not attempt to capture this spike in the observed mortality frequency. As a result, this leads to improvements in the areas further outside of the singular event. Given that the estimated mortality rate are now not distorted, they represent the normal mortality development better.

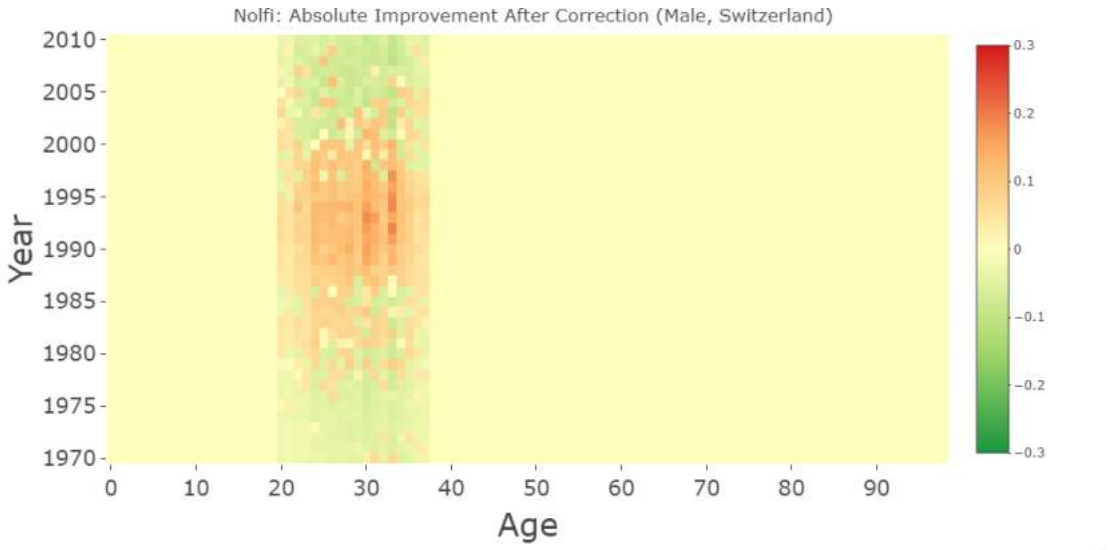

Figure 33: This error graph shows the absolute improvement (shown in green) or deteriorations (shown in red) when correcting for the singular event. The improvement is defined by Equation (4.3).

With the mechanism behind the single correction method explained, the thesis will now focus on the effects of the single correction method. In the subsections below, the effects of the single correction method will be investigated for credibility weights $z = 0.25$, $z = 0.5$, $z = 0.75$ and $z = 1$. These credibility weights will be applied to the Nolfi Model and the LC Model. For each of these models, an overview of the parameter changes due to the single correction method will be given. Furthermore, the improvement or deterioration of the estimation quality will be investigated for each model and credibility weight.

4.1.1 Nolfi

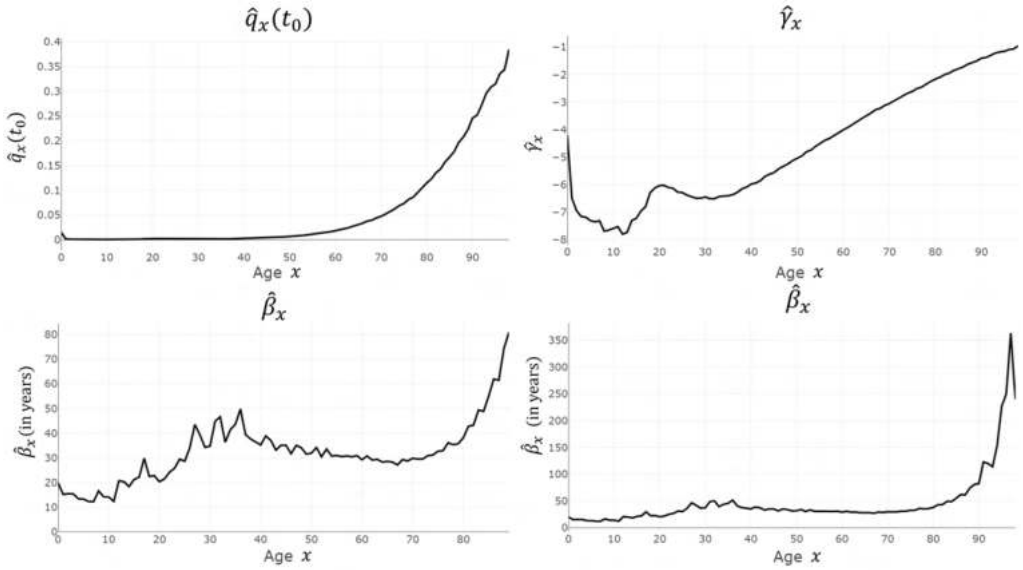

Figure 34: Parameters of the Nolfi Model for calendar years 1970-2010 and ages 0-98 for men in Switzerland. The top left graph shows the starting mortality rate $\hat{q}_x(t_0)$. Here, $t_0 = 1970$. The top right graph shows the logarithm of the starting mortality rate $\hat{\gamma}_x = \ln(\hat{q}_x(t_0))$. The bottom graphs show the half-value period $\hat{\beta}_x$, which is measured in years. The bottom left graph shows the ages 0-90, whereas the bottom right graph shows the ages 0-98.

Before discussing the changes in parameters due to correction methods, it is useful to first glance the parameters after they were fitted for the first time. In Figure 34 the relevant Nolfi Model parameters are shown. In the top left, one can see how the starting mortality rate is generally low for ages up until 50. One can spot a minor decrease between ages 0 and 1, which represents the infant mortality. Beyond age 50, the starting mortality rate increases rapidly into the double digit percentages.

The overall exponential trend of the starting mortality rate is captured by the parameter in the top right graph, which is the logarithm of the starting mortality rate. Here, one can clearly see the infant mortality rate. Additionally, between the ages 20 and 25, one can see a local maximum. This local maximum is explained by the fact that young men tend to have high mortality due to accidents. All in all, it can be observed that the remaining areas in the top right graph are a straight line, showing the exponential pattern of the starting mortality rate.

The speed at which the starting mortality rate halves is measured by the

parameter shown in the two bottom graphs of Figure 34. This parameter is known as the half-value period and is measured in years. It can be observed that half-value period is increasing as the age increases. This means that the lower ages generally have a quicker reduction in mortality rate across the years than older ages. Futhermore, one can see a slight local increase between ages 25 and 35. This might be due to the AIDS pandemic.

With the first fit of the parameters now discussed, the effects of the single correction will be investigated. For some parameters, the difference is calculated for credibility weights $z = 0.25$, $z = 0.5$, $z = 0.75$ and $z = 1$. In the upcoming graphs $z = 0.25$ is represented by the blue line, $z = 0.5$ is represented by the yellow line, $z = 0.75$ is represented by the green line and $z = 1$ is represented by the red line. Depending on the parameter, this difference will be in absolute terms or in relative terms. Below, the absolute and relative difference calculations are shown:

$$\Delta\hat{\rho} = \hat{\rho}^{(2)} - \hat{\rho}^{(1)}, \tag{4.4}$$

$$\Delta^{(\%)}\hat{\rho} = \frac{\hat{\rho}^{(2)}}{\hat{\rho}^{(1)}} - 1, \tag{4.5}$$

where

... $\hat{\rho}^{(1)}$ is some estimated parameter obtained from the first (corrected) model fit,

... $\hat{\rho}^{(2)}$ is some estimated parameter obtained from the second (corrected) model fit,

... $\Delta\hat{\rho}$ is the absolute estimated parameter difference and

... $\Delta^{(\%)}\hat{\rho}$ is the relative estimated parameter difference.

Note, that this means that a decrease in parameter values (from parameter (1) to (2)) will result in a negative $\Delta\hat{\rho}$ or $\Delta^{(\%)}\hat{\rho}$, whereas parameter increases result in positive values. For the upcoming graphs, $\hat{\rho}^{(1)}$ represents the parameter of the original fit, whereas $\hat{\rho}^{(2)}$ represents the parameter of the second fit after the single correction has been applied. Note, that in later parts of the thesis, $\hat{\rho}^{(1)}$ must not always be a parameter from the first fit, but can also be a parameter from a corrected model. This is done so that multiple correction methods can be compared.

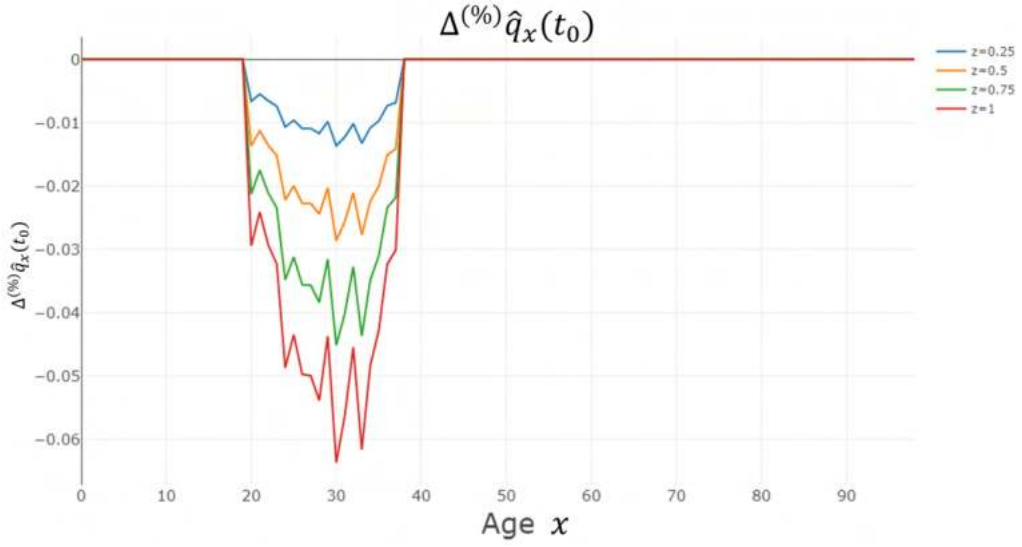

Figure 35: Nolfi Model parameter difference for $\hat{q}_x(t_0)$ after the single correction method has been applied. The graph shows the relative difference in the parameter for ages 0-98 for men in Switzerland (calendar years 1970-2010). The relative difference calculation is shown in Equation (4.5). The credibility weight z is shown for values 0.25, 0.5, 0.75 and 1.

Figure 35 shows the relative parameter difference for the starting mortality rate. The impact on this parameter, along with the impact on the upcoming parameters, is only between the ages of 20 and 37. This is within the age groups that are affected by the singular event as defined by the algorithm. Given that the Nolfi Model fits each age separately, this contained impact on the parameters is logical. Furthermore, it can be observed that the impacts on the starting mortality rate become larger as the credibility weight increases. Hence, when viewing a two-dimensional fitting graph (such as Figure 31), one would expect the corrected fitted Nolfi Model line to start lower than the first fitted Nolfi Model line and that this effect increases as the credibility weight increases.

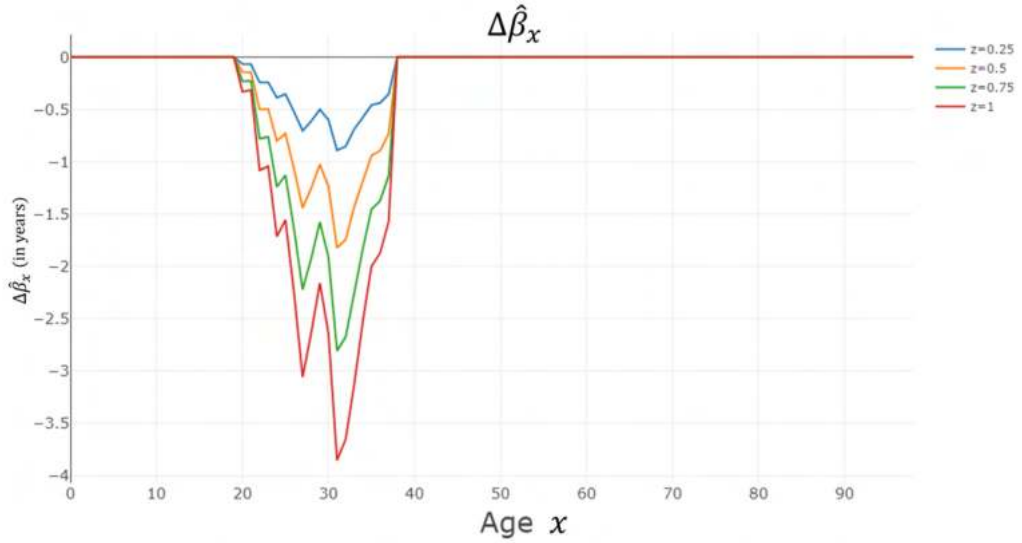

Figure 36: Nolfi Model parameter difference for $\hat{\beta}_x$ after the single correction method has been applied. The graph shows the absolute difference in the parameter for ages 0-98 for men in Switzerland (calendar years 1970-2010). The absolute difference calculation is shown in Equation (4.4). The credibility weight z is shown for values 0.25, 0.5, 0.75 and 1.

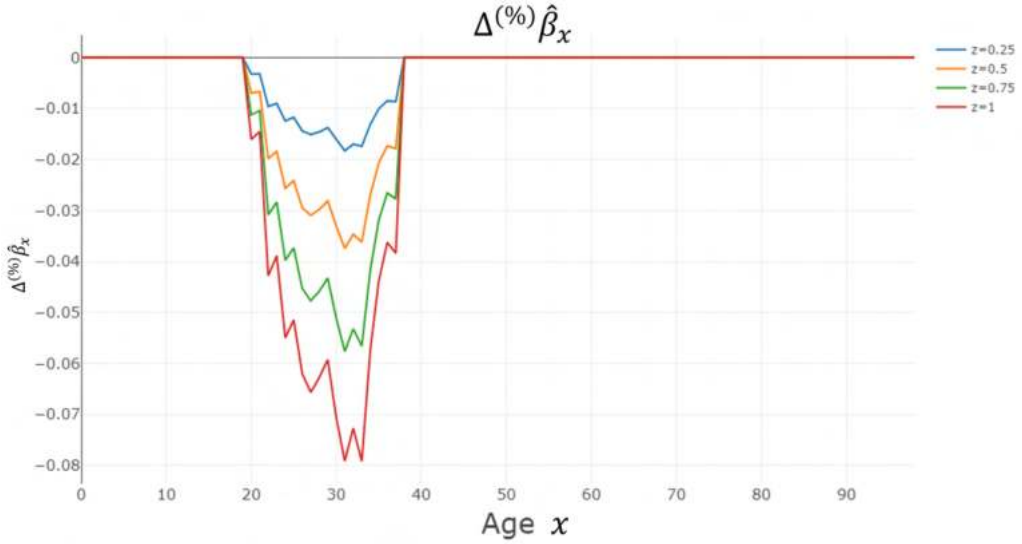

Figure 37: Nolfi Model parameter difference for $\hat{\beta}_x$ after the single correction method has been applied. The graph shows the relative difference in the parameter for ages 0-98 for men in Switzerland (calendar years 1970-2010). The percentage difference calculation is shown in Equation (4.5). The credibility weight z is shown for values 0.25, 0.5, 0.75 and 1.

Figure 36 and Figure 37 show the absolute and relative effects on the half-value period parameter respectively. The effects on the parameter increase as the

credibility weight increases. Similarly to the effects on the starting mortality rate, the effects are only visible between ages 20 and 37. Furthermore, the effects are all negative, sometimes decreasing the half-value period by up to approximately 4 years. Intuitively, this means that the mortality rate takes 4 years less to half in time, which in the long run will have a large influence on the mortality development.

Summarized, one would expected that in a two-dimensional fitting graph, the relative decline of the corrected fitted Nolfi Model mortality rate is faster compared to its starting mortality rate than for the first fitted Nolfi Model mortality rate. Given that in this case the starting mortality rate also decreases, this does not mean that the slope has to be steeper. On the contrary, one might expect the lines to look as though they run parallel with these results.

Below, a two-dimensional fitting graph will be shown for each of the credibility weights. To check whether the single correction method was succesful, the final parameters were used to project the data into the future for five years. This projected data is compared with the observed mortality frequencies. This approach is known as backtesting. Additionally, an error improvement graph will be shown for each of the credibility weights, also for the projected time period. The boundary between fitted and projected data is represented by a black line within the graphs. The singular event is now not highlighted by black lines anymore.

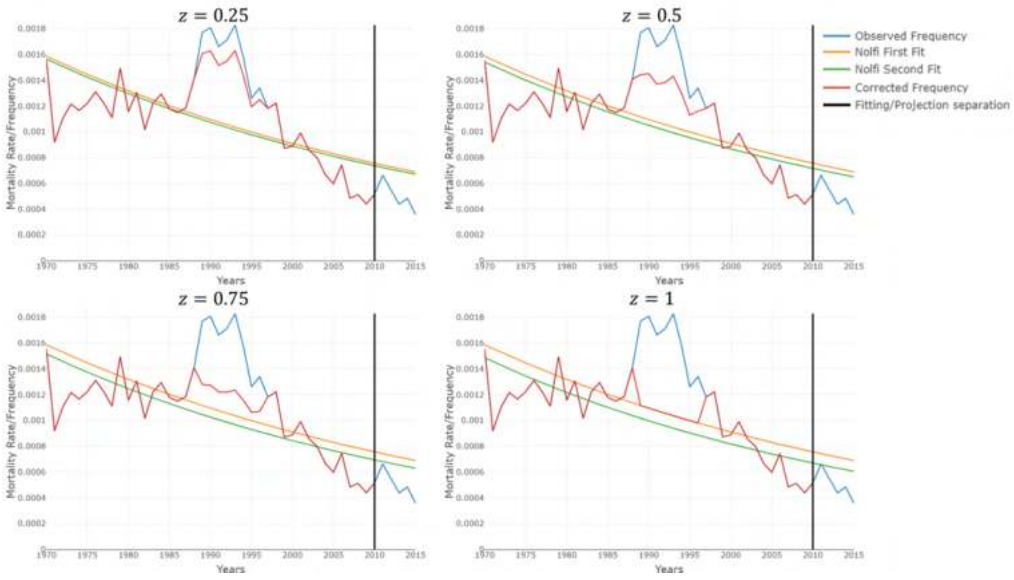

Figure 38: Overview of single correction steps for credibility weights z 0.25, 0.5, 0.75 and 1. Explanation similar to Figure 31. The black line represents the boundary between fitted and projected data. The data viewed is from Swiss males aged 30, between calendar years 1970 and 2010. The data is projected until 2015.

Figure 38 shows the two-dimensional fitting graphs, which are similar to the example in the beginning of the single correction model section. The higher the credibility weight gets, the lower the starting mortality rate becomes. Furthermore, one can observe that the lines seem to run parallel, which is in line with the negative differences for the half-value time parameter. As the credibility weights increase, the difference between the corrected fitted line and the observed frequencies outside of the singular event (ages 20 until 37) is getting smaller on average. To get a better understanding of the improvements and deteriorations, see Figure 39.

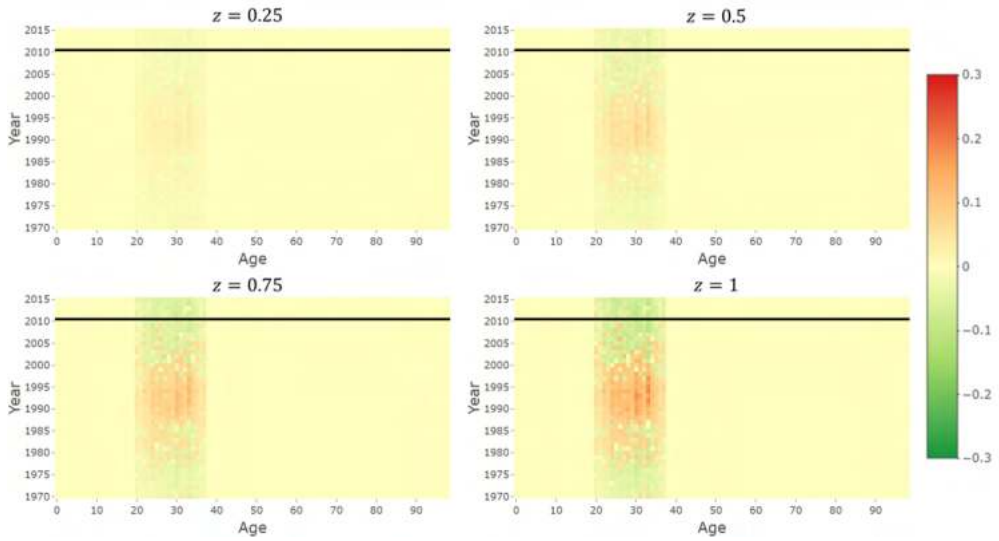

Figure 39: This error graph shows the absolute improvement (shown in green) or deteriorations (shown in red) when correcting for the singular event for different credibility weights z 0.25, 0.5, 0.75 and 1. The improvement is defined by Equation (4.3). The data viewed is from Swiss males aged 30, between calendar years 1970 and 2010. The data is projected until 2015.

From Figure 39 it becomes clear that an increase in credibility weight worsens the area within and closely around the singular event. At the same time, it can be observed that the areas which are further removed from the singular event improve. This also holds true for the projected data.

Below, a similar analysis will be done for the LC Model.

4.1.2 Lee-Carter

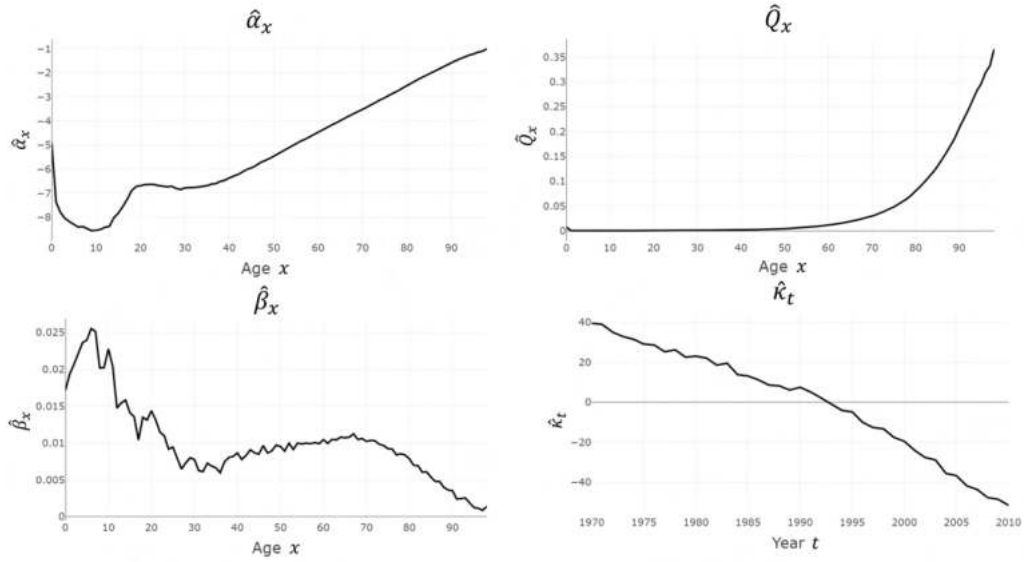

Figure 40: Parameters of the LC Model for calendar years 1970-2010 and ages 0-98 for men in Switzerland. The top left graph shows the logarithmic mean mortality rate $\hat{\alpha}_x$. The top right graph shows the mean mortality rate $\hat{Q}_x = \exp(\hat{\alpha}_x)$. The bottom left graph shows age sensitivity for the mortality trend $\hat{\beta}_x$. The bottom right graph shows the mortality trend $\hat{\kappa}_t$.

Figure 40 shows the parameters when fitting the LC Model for the first time. Note, that even though certain parameters have similar notations to other model parameters, the parameters are not the same. The top left graphs show the logarithmic mean mortality rate. It shows a similar shape as the starting mortality rate from the Nolfi Model. In the early ages, a clear decrease can be observed, which is linked to the infant mortality. Additionally, the local accelerated increase between ages 20 and 30 is linked to the increase in mortality rate for young men due to accidents.

The top right graph shows the mean mortality rate, which is obtained by taking the exponent of $\hat{\alpha}_x$. The mortality rate is low for ages up until 50, after which it increases rapidly.

The bottom left graph shows the age sensitivity to the mortality trend, not to be confused with the Nolfi Model half-value period parameter. The higher values for the young ages mean that the younger ages have larger changes in mortality rates across time than older ages. Note, this parameter is fitted so that the sum of the parameter values for all ages equals 1. This is good to keep in mind when looking at the parameter difference graphs.

The bottom right graph shows the mortality trend, which is decreasing at a stable rate. Intuitively, this means that the overall mortality rate decreases over time. Note, that this parameter is fitted so that the sum of parameter values for all calendar years equals 0. This is good to keep in mind when looking at the parameter difference graphs.

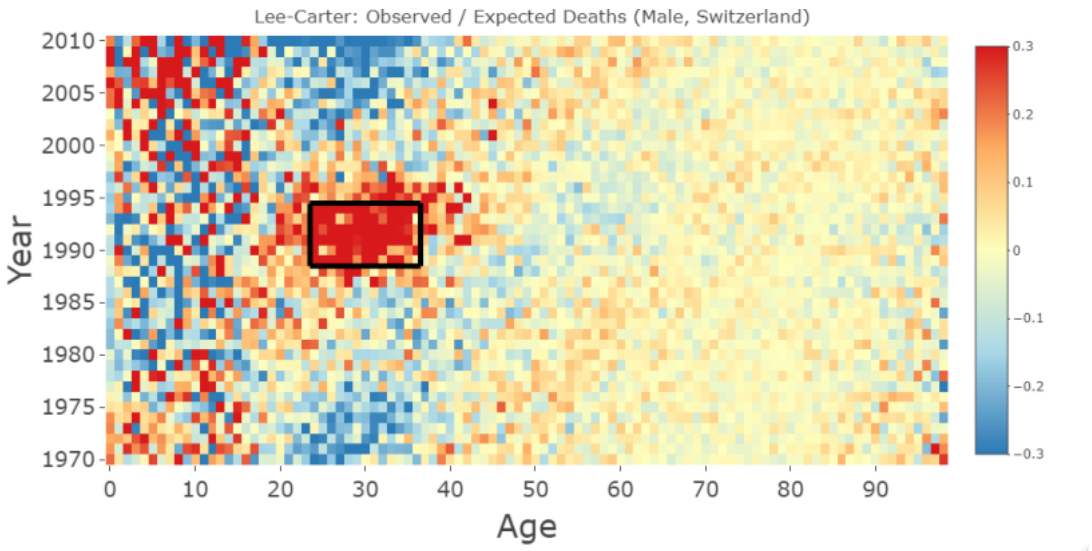

Figure 41: Fitting errors for the LC Model in calendar year 1970-2010, ages 0-98 for men in Switzerland. The black rectangular box now shows the singular event as detected by the algorithm. The ages 20-37 and calendar years 1989-1994 belong to the singular event.

Before analyzing the parameter differences before and after the correction, it is important to note that the singular event detection algorithm is now applied to LC Model errors (see Figure 41). Given that the errors per data point tend to be smaller in the LC Model (due to more fitting parameters), the singular events turned out smaller. This will have an impact on which ages and calendar years are affected by the single correction method.

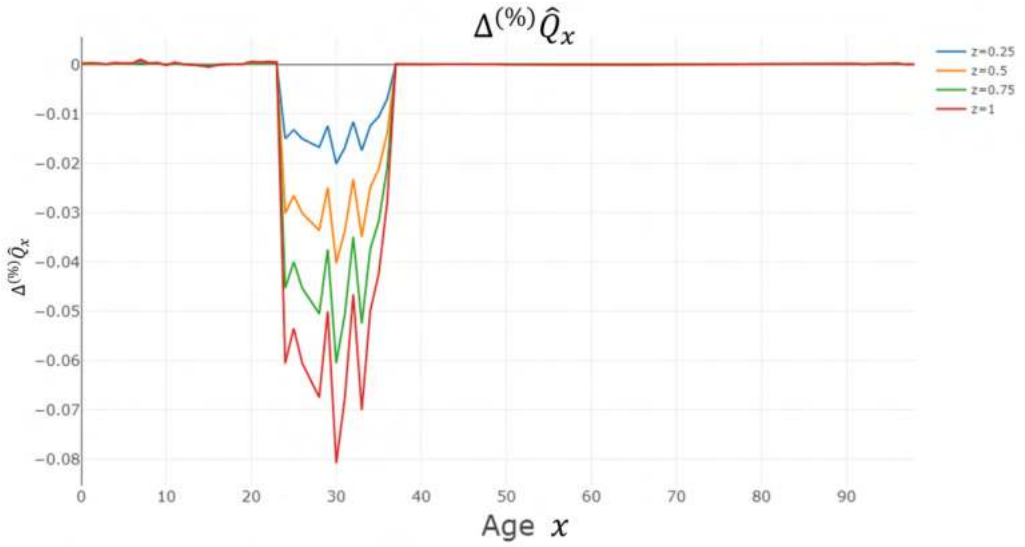

Figure 42: LC Model parameter $\hat{Q}_x$ difference after the single correction method has been applied. The graph shows the relative difference in the parameter for ages 0-98 for men in Switzerland (calendar years 1970-2010). The relative difference calculation is shown in Equation (4.5). The credibility weight z is shown for values 0.25, 0.5, 0.75 and 1.

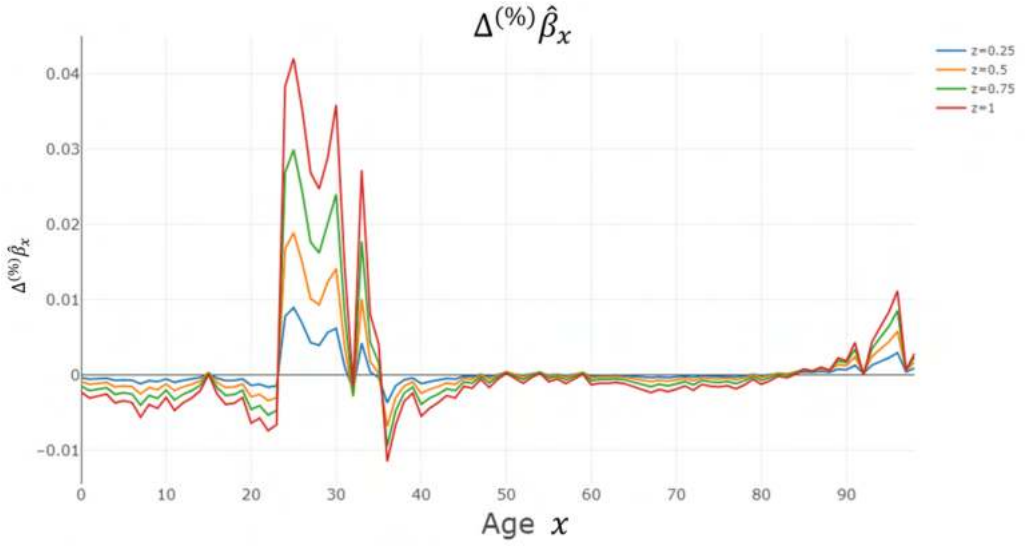

Figure 43: LC Model parameter $\hat{\beta}_x$ difference after the single correction method has been applied. The graph shows the relative difference in the parameter for ages 0-98 for men in Switzerland (calendar years 1970-2010). The relative difference calculation is shown in Equation (4.5). The credibility weight z is shown for values 0.25, 0.5, 0.75 and 1.

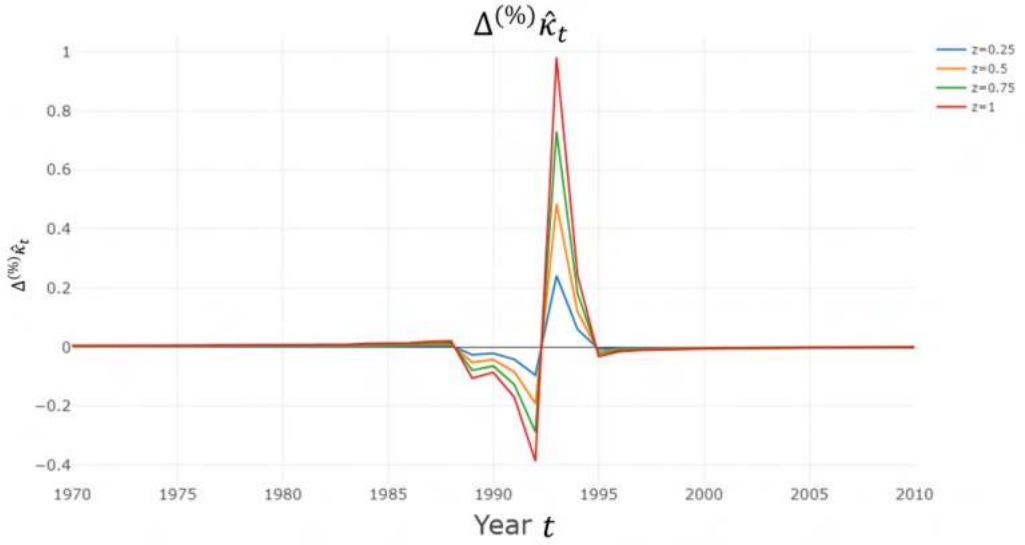

Figure 44: LC Model parameter $\hat{\kappa}_t$ difference after the single correction method has been applied. The graph shows the relative difference in the parameter for ages 0-98 for men in Switzerland (calendar years 1970-2010). The relative difference calculation is shown in Equation (4.5). The credibility weight z is shown for values 0.25, 0.5, 0.75 and 1.

After the single correction method is applied, the mean mortality rate decreases (see Figure 42). This effect is the largest for ages that belong to the singular event (ages 24-36). Note, that there are also small effects outside of the singular event ages. This is due to the fact that the LC Model, unlike the Nolfi Model, does not fit a model per age. Instead, the LC Model fits to the data as a whole, meaning that all ages and calendar years will be affected by data changes within the singular event. Furthermore, the decrease in the mortality rate is larger as the credibility weight increases. Based on all of this, one would expect that the new mortality rate estimate to be consistently lower than the original estimate, with bigger differences as the credibility weight increases.

Figure 43 shows a small increase in the age sensitivity within the ages of the singular event. The ages not contained within singular event mostly show a decrease in age sensitivity. This is due to the fitting contraint, which states that the sum of the parameter values for all ages must equal 1. Hence, an increase somewhere must be countered by a decrease elsewhere to satisfy this constraint. Similarly to the mean mortality rate, the effect sizes become larger as the credbility weight increases. This counts for both positive and negative differences.

Lastly, Figure 44 shows a large decrease of the mortality trend around the singular event years (calendar years 1989-1994). The last two years of the

singular event have a large compensating positive impact. This is logical, because the fitting constraint states that the sum of the parameter values of all ages must equal 0. Intuitively, this means that an increase somewhere must be countered by a decrease elsewhere. As with the other parameters, the effect sizes grow larger as the credibility weight increases.

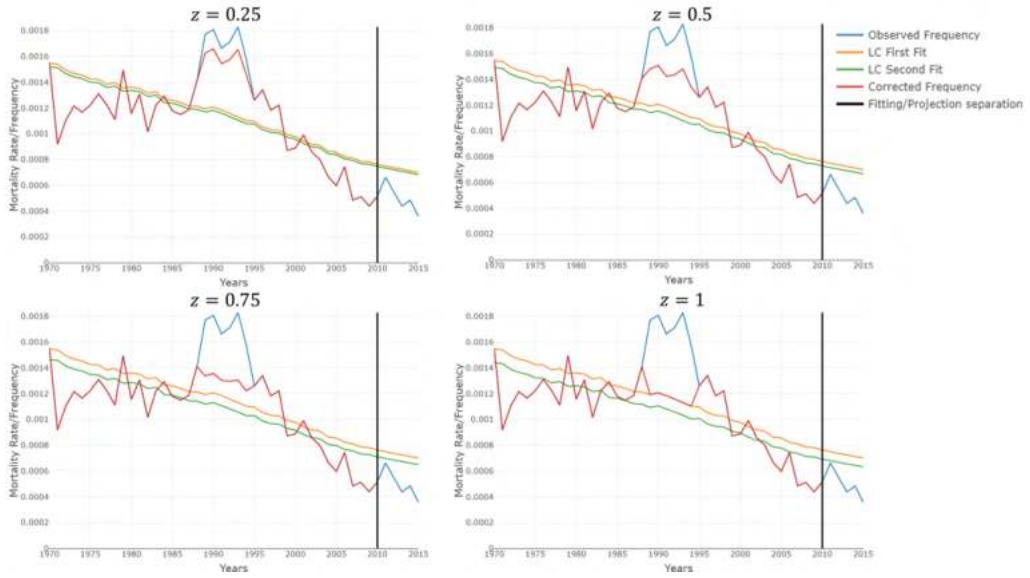

Figure 45: Overview of single correction steps for the LC Model for credibility weights z equal to 0.25, 0.5, 0.75 and 1. Explanation similar to Figure 31. The black line represents the boundary between fitted and projected data.

Figure 45 shows how all the discussed parameter differences lead to a different fitted mortality rate by the LC Model. The effects of the parameter changes are similar to the mortality rate changes for the Nolfi Model. The higher the credibility weight, the lower the corrected mortality rate line is compared to the original fit. Contrary to the effects of the Nolfi Model, the corrected frequency line does not become a smooth line when the credibility weight equals 1. This is because the LC Model mortality rate estimates are not smooth lines. With a crediblity weight of 1, this LC Model mortality rate is fully copied into the number of deaths matrix. Hence, the corrected frequency is not a smooth line for this credibility weight value. Another difference to the correction in the Nolfi Model is that the singular event is visibly smaller in Figure 45 (compared to Figure 38).

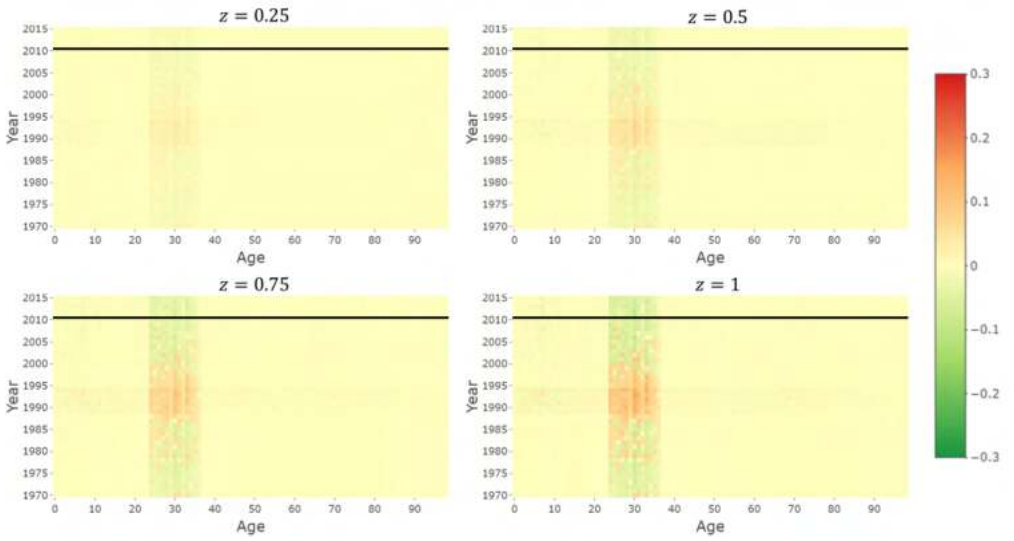

Figure 46: Absolute improvements (shown in green) or deteriorations (shown in red) when correcting for the singular event with different credibility weights $z \in \{0.25, 0.5, 0.75, 1\}$. The improvement is defined by Equation (4.3).

When extending the fitting improvements of Figure 45 into the third dimension, the smaller singular event is even more visible (see Figure 46). Similarly to the correction with the Nolfi Model, the calendar years within and closely around the singular event deteriorate. The calendar years further removed from the singular event improve, this includes the projected data. The deteriorations and improvements both become larger as the credibility weight increases. Contrary the the correction with the Nolfi Model, the improvement and deteriorations are now not restricted to the ages of the singular event. When looking closely, there are also effects happening in other data points. This is mostly visible for credibility weight $z = 1$, in the calendar years of the singular event (1989-1994).

When comparing the improvements resulting from the LC Model (Figure 46) and the Nolfi Model corrections (Figure 39), it is difficult to see which improvements are the largest. After close inspection, the LC Model improvements are slightly smaller than the Nolfi improvements. However, given that the LC Model estimate has a lower error before correcting, one cannot say which model has the more accurate mortality rate estimate after the correction. Hence, the comparison between the two corrections and their corrected mortality rate estimates will be discussed in the upcoming subsection.

4.1.3 Nolfi vs Lee-Carter

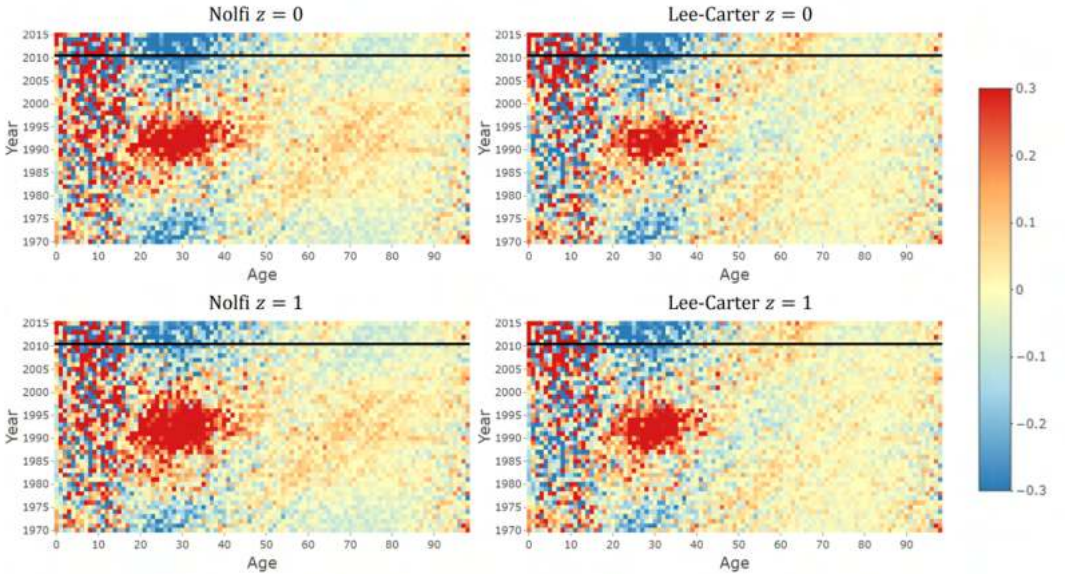

Figure 47: Fitting errors for the Nolfi Model and the LC Model in calendar year 1970-2010, ages 0-98 for men in Switzerland for credibility weight z values 0 and 1.

Figure 47 shows the fitting errors (Equation (3.2)) for the Nolfi Model and the LC Model before correction ($z = 0$) and after correction with the maximum credibility weight ($z = 1$). Comparing the top two graphs, it is clearly visible that the area of mortality rate underestimation during the AIDS pandemic is smaller in the LC Model. However, the projection quality between the two seems to be equally bad. After correction, the AIDS pandemic is even worse in the Nolfi Model, whereas the LC Model still has a moderately sized area of underestimation. However, the Nolfi model now shows a slightly better mortality rate estimate for the calendar years before and after (including projection) the singular event.

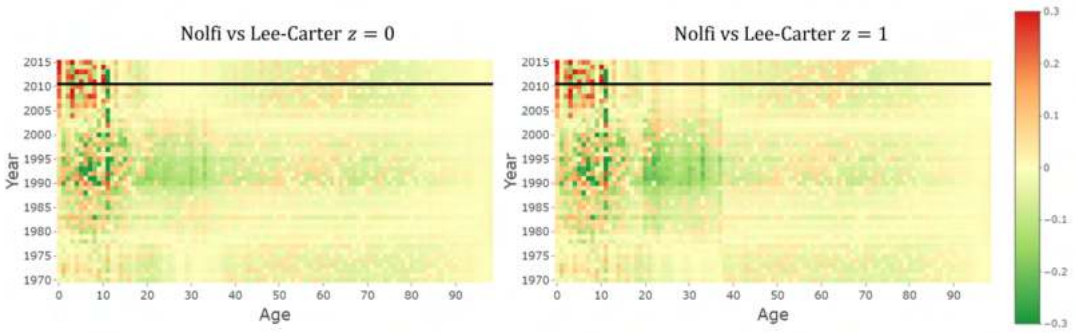

Figure 48: Absolute improvements (shown in green) or deteriorations (shown in red) between Nolfi Model and the LC Model for credibility weight z values 0 and 1. The improvement is defined by Equation.

The differences between the models before and after the corrections are more easily summarized by Figure 48. This is done by applying Equation (4.3) to the LC Model and the Nolfi Model. In Figure 48, $|\varepsilon_x^{(2)}(t)|$ is the LC Model fitting error and $|\varepsilon_x^{(1)}(t)|$ is the Nolfi Model fitting error. Hence, the areas where the LC Model is better are shown in green, whereas the areas where the Nolfi Model is better are shown in red. Note, that for the affected singular event ages, the Nolfi Model has lower errors in the projection area after the correction method has been applied.

4.2 Iterative Model Corrections

With the single model correction showing promising results, especially with credibility weight $z = 1$, it is interesting to investigate whether applying the single model correction multiple times increases these improvements even more. The application of the single model correction will be done in an iterative way, with each iteration the number of deaths matrix and the estimated mortality rate are updated. For each of these iterations, the correction will be applied with the credibility weight $z = 1$. In this section, two types of iterations correction will be discussed. The first one keeps the singular event constant, the second one updates the singular event in each iteration.

Due to its iterative nature, this new correction method needs certain stopping criteria to prevent the correction from running infinitely long. This thesis utilizes two stopping criteria, which are introduced below:

1. Starting with iteration 1, after each iteration a weighted error is calcu-

lated within the singular event:

$$\xi^{(i)} = \frac{\sum_{(x,t)\in\Omega^{(se)}} \tilde{\varepsilon}_x^{(i)}(t)\tilde{D}_x^{(i)}(t)}{\sum_{(x,t)\in\Omega^{(se)}} \tilde{D}_x^{(i)}(t)} \quad \text{for } (i) \geq 2, \tag{4.6}$$

where

... $\Omega^{(se)}$ is the set containing the combination of ages and calendar years (tuples (x,t)) which belong to a singular event,

... $(i) \in \mathbb{N}$ is the current iteration,

... $\tilde{D}_x^{(i)}(t)$ is the adjusted number of deaths for age x, calendar year t and iteration (i) as defined by Equation (4.1) and

... $\tilde{\varepsilon}_x^{(i)}(t)$ is the adjusted fitting error for age x, calendar year t and iteration (i):

$$\tilde{\varepsilon}_x^{(i)}(t) = \frac{\tilde{D}_x^{(i)}(t)}{\hat{q}_x^{(i)}(t)E_x(t)} - 1.$$

Note, that for the error calculation $(\tilde{\varepsilon}_x^{(i)}(t))$ the mortality rate $(\hat{q}_x^{(i)}(t))$ is estimated using the adjusted number of deahts $(\tilde{D}_x^{(i)}(t))$ data. Hence, the errors considered would be the bottom left errors in Figure 32. The first iteration is calculated using the usual fitting errors (Equation (3.2)) from the first fitted model:

$$\xi^{(1)} = \frac{\sum_{(x,t)\in\Omega^{(se)}} \varepsilon_x(t)D_x(t)}{\sum_{(x,t)\in\Omega^{(se)}} D_x(t)}.$$

The second iteration is then excecuted without a check, whereby $\xi^{(2)}$ is obtained by Equation (4.6). These weighted errors $\xi^{(i)}$ are then used to check two conditions:

(a) $\xi^{(i)} \geq \xi^{(i-1)}$ and

(b) $\xi^{(i)} \leq 10^{-4}$.

If one or more of these conditions are true, the iterative process is stopped. Otherwise, the next iteration $(i+1)$ is initiated. This first stopping criterion will be represented by Figure 49 in the upcoming diagrams.

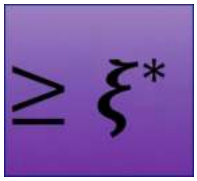

Figure 49: Symbol for the first stopping criterion.

2. For the second stopping criterion, the number of iterations are counted and represented by (i). A prespecified number is then used to specify the maximum number of iterations allowed. In this thesis the prespecified number is 10. If $(i) \geq 10$, then the iterative process is stopped. Otherwise, the iterative process will proceed with iteration $(i+1)$. This second stopping criterion will be represented by Figure 50 in the upcoming diagrams.

Figure 50: Symbol for the second stopping criterion.

4.2.1 Stationary Singular Event

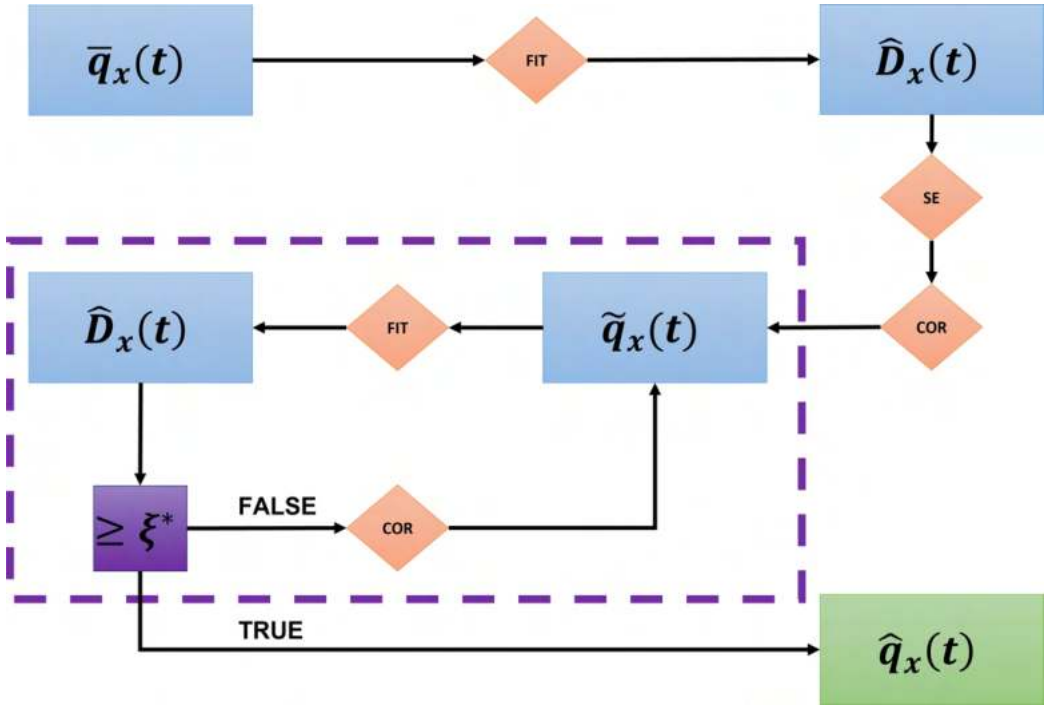

Figure 51: Diagram overview of the single model correction. Blue boxes represent obtained data, red diamonds represent a calculation step. The purple dashed area is the area in which the iterative process takes places. The purple square represents the stopping criterion for the iterative process. The final estimated mortality rate is shown by the green box.

For the stationary iterative model correction, the first eight steps are exactly the same as the single model correction (see Figure 51). The two fitting steps within these first eight steps are counted as the first two iterations, even though these happen before the first stopping criteria check. Afterwards, it is checked whether the stopping criteria are met or not. If they are not met, the iteration continues, meaning that the model is fitted again with the newly updated number of deaths $\tilde{D}_x(t)$. If one of the stopping criteria is met, the iteration ends, meaning that the last produced estimated mortality rate $\hat{q}_x(t)$ is the final result.

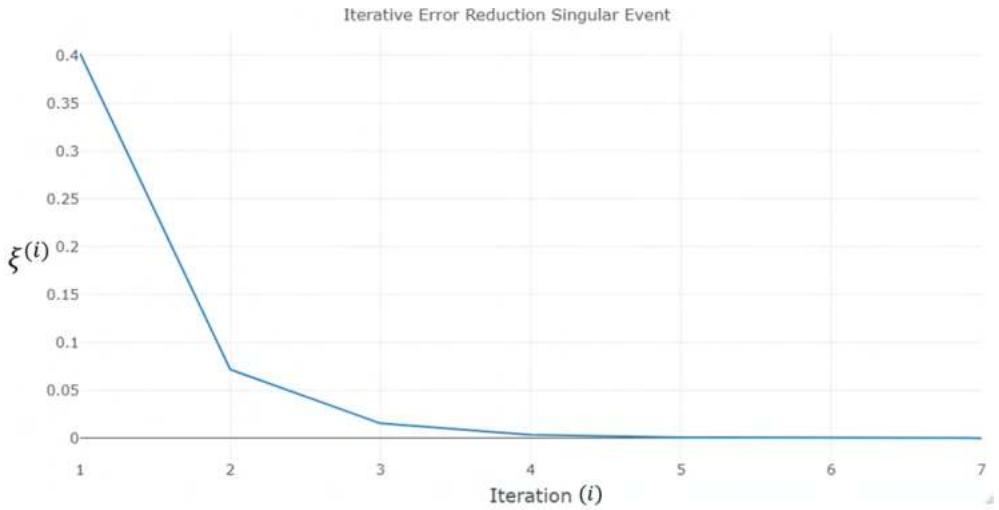

Figure 52: Development of the error $\xi^{(i)}$ (Equation (4.6)) as iterations go by. The iteration process is stopped by the stopping criteria at iteration 7.

Figure 52 shows how each iteration reduces the error ($\xi^{(i)}$) within the singular event. It is notable how quickly the error reduces between the first and the second iteration (i.e. still before the first stopping criteria check) . This is the reduction that is achieved by the single model correction. Each further iteration only happens within the iterative model correction. Looking at Figure 52, the added effect of these additonal iteration is small, leaving only approximately 20% for the remaining iterations to improve. Hence, the expectation is that the added value of these iteration is relatively small compared to the single model correction. After the 7^{th} iteration, the iteration process is stopped given that the error $\xi^{(7)}$ is smaller than 10^{-4}.

In the two subsections below, the incremental parameter differences and the overall estimation improvement for these correction methods will be discussed for the Nolfi Model and the LC Model. In the incremental parameter difference graphs, the difference between no correction and the stationary iterative correction method is represented by the blue line. The difference between the single correction method and the stationary iterative correction method is represented by the orange line.

4.2.1.1 Nolfi

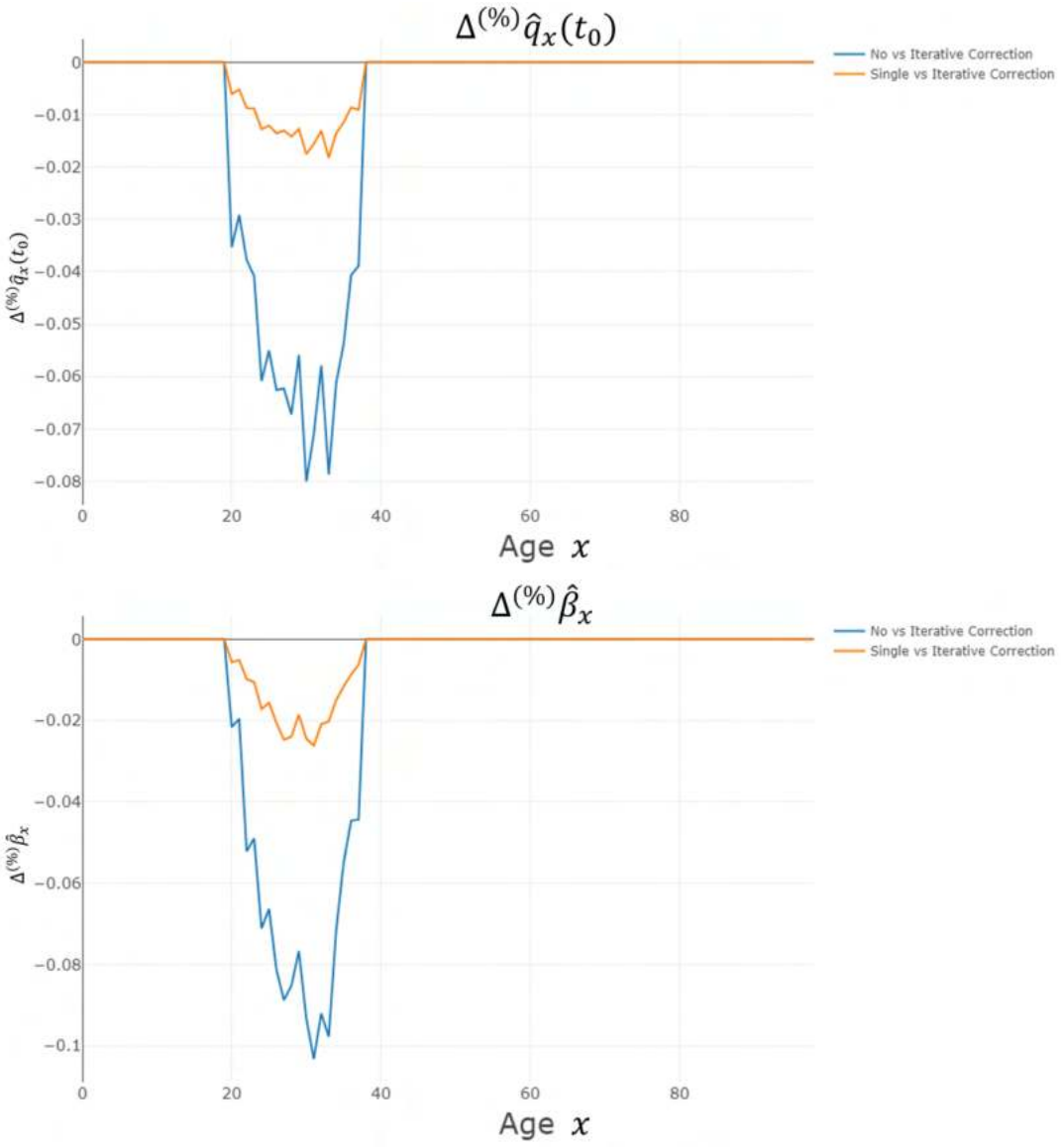

Figure 53: Nolfi Model parameters $\hat{q}_x(t_0)$ and $\hat{\beta}_x$ after the stationary iterative correction method has been applied. The graphs show the relative difference (Equation (4.5)) in the parameters for ages 0-98 for men in Switzerland (calendar years 1970-2010). The blue lines show the difference between no correction and the iterative correction. The orange lines show the difference between the single correction and the stationary iterative correction. The stationary iterative and the single correction method use credibility weight $z = 1$.

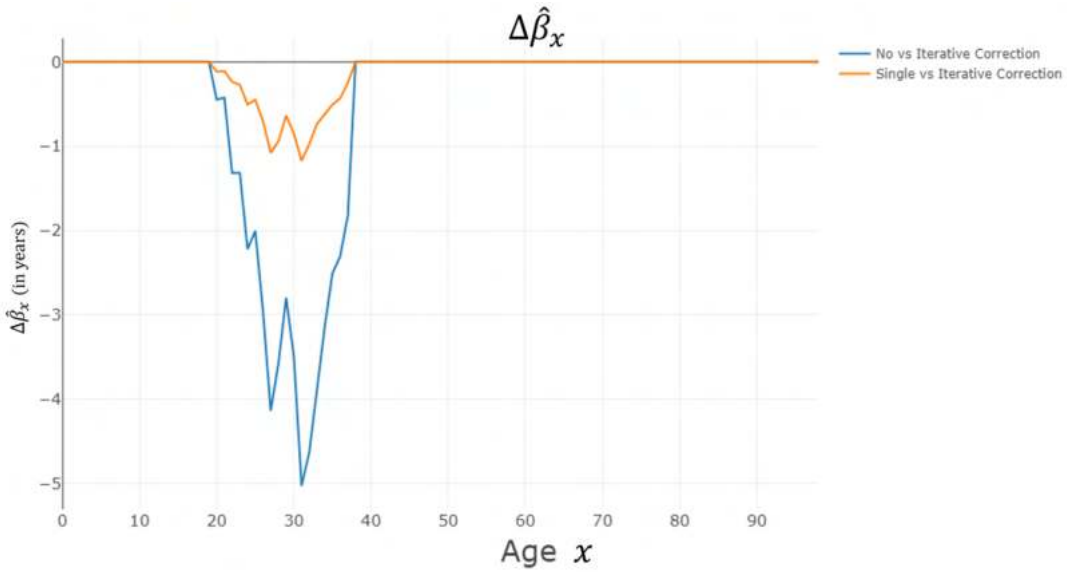

Figure 54: Nolfi Model parameter $\hat{\beta}_x$ after the stationary iterative correction method has been applied. The graph shows the relative difference (Equation (4.5)) in the parameter for ages 0-98 for men in Switzerland (calendar years 1970-2010). The blue line shows the difference between no correction and the iterative correction. The orange line shows the difference between the single correction and the iterative correction. The stationary iterative and the single correction method use credibility weight $z = 1$.

Figure 53 and Figure 54 show the parameter differences for the stationary iterative correction method. The blue line represents the full effect of the stationary iterative correction method, since it is compared to the no correction state. The orange line shows the incremental improvement compared to the single correction method. It can be observed, that the overall shape and effect size of the stationary iterative correction method is similar to that of the single correction method. The added value of introducing iterations is approximately 20% compared to the single correction model. Hence, it is expected that the estimation and projection quality increases slightly, but that the single correction method leads to the biggest part of the improvement.

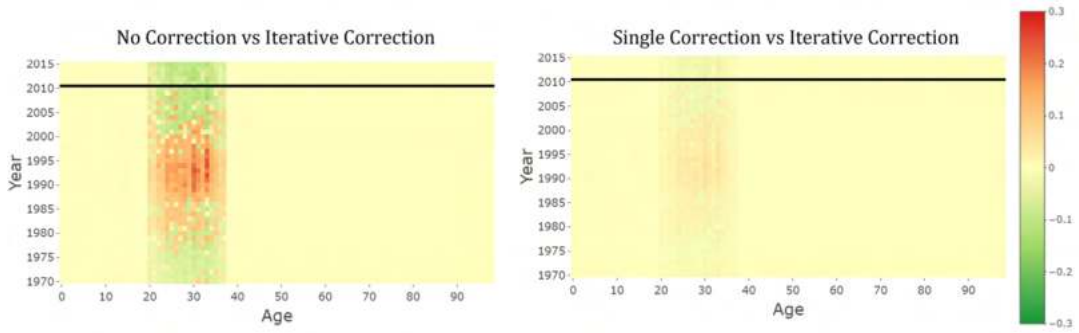

Figure 55: Absolute improvements (shown in green) or deteriorations (shown in red) between no correction, the single correction and the stationary iterative correction for the Nolfi Model. The improvement is defined by Equation (4.3).

The overall impact on the improvement is as expected from the parameter difference graphs. Figure 55 shows quite a significant change when comparing the iterative correction method to no correction. However, when comparing the single correction method with the stationary iterative correction method, the improvements and deteriorations only change marginally.

Below, the same analysis is done for the LC Model.

4.2.1.2 Lee-Carter

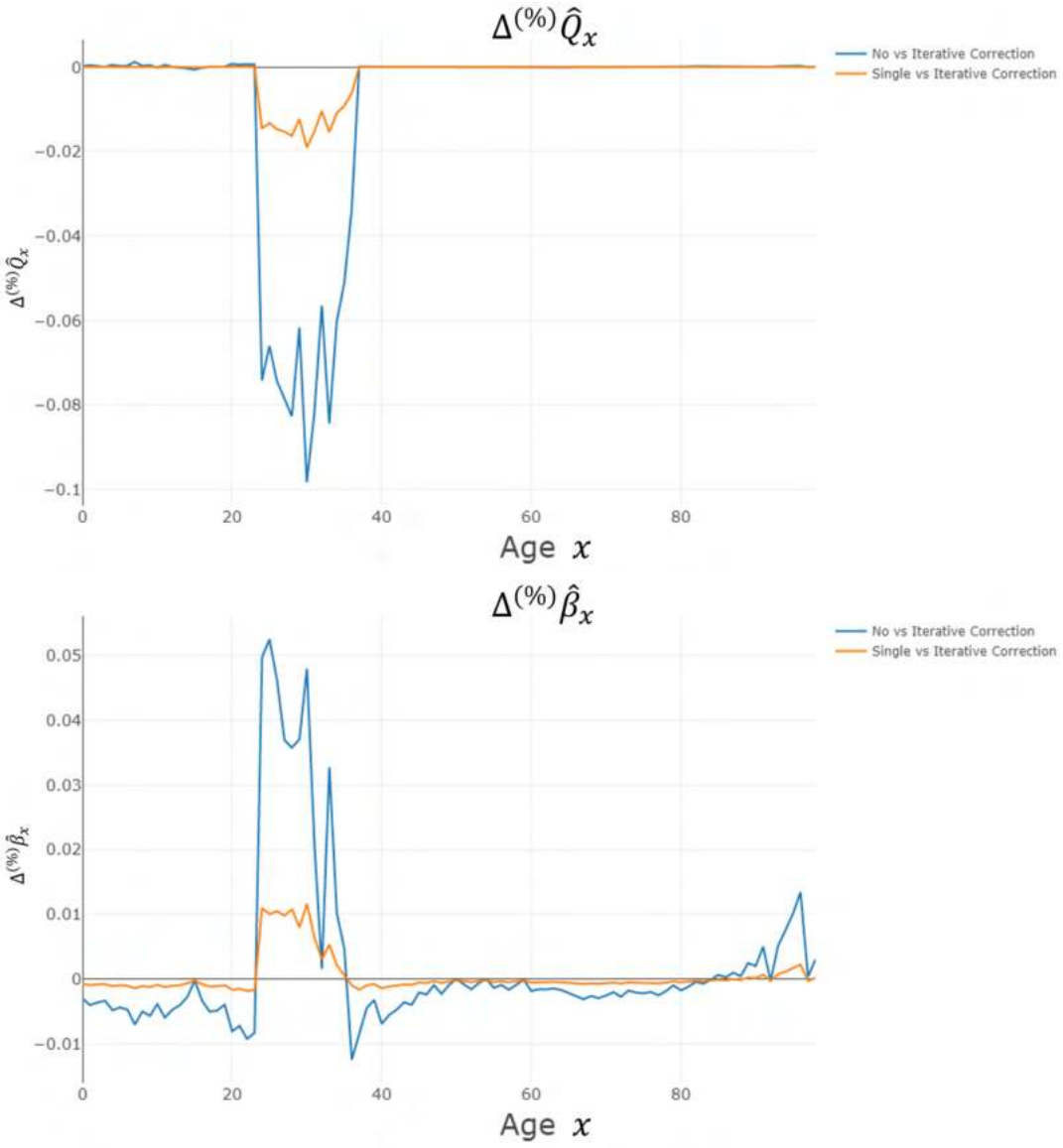

Figure 56: LC Model parametesr $\hat{Q}_x$ and $\hat{\beta}_x$ after the stationary iterative correction method has been applied. The graphs show the relative difference (Equation (4.5)) in the parameters for ages 0-98 for men in Switzerland (calendar years 1970-2010). The blue lines show the difference between no correction and the stationary iterative correction. The orange lines show the difference between the single correction and the stationary iterative correction. The stationary iterative and the single correction method use credibility weight $z = 1$.

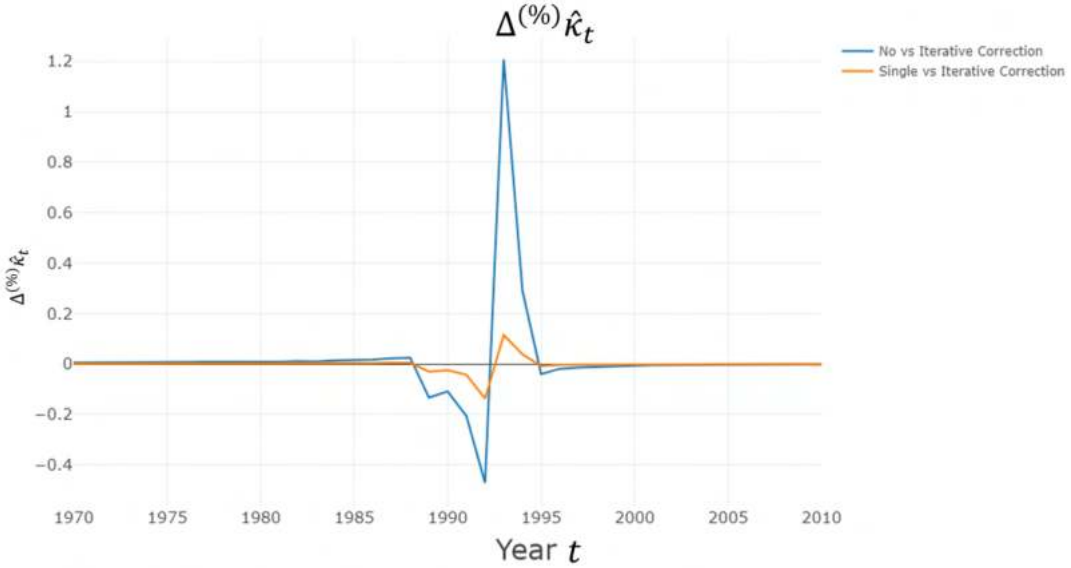

Figure 57: LC Model parameter $\hat{\kappa}_t$ after the stationary iterative correction method has been applied. The graph shows the relative difference (Equation (4.5)) in the parameter for ages 0-98 for men in Switzerland (calendar years 1970-2010). The blue line shows the difference between no correction and the stationary iterative correction. The orange line shows the difference between the single correction and the stationary iterative correction. The stationary iterative and the single correction method use credibility weight $z = 1$.

Figure 56 and Figure 57 show a similar pattern to the Nolfi Model iterative correction graphs. The added effect from the iterative process is approximately 20%. Hence, it is expected that the improvements and deteriorations will also increase by approximately 20%. Contrary to the Nolfi Model, one can spot an area where the orange graphs is higher in the positive value area of the graph for the $\hat{\beta}_x$ parameter (around age 32). This means that the single model correction makes a negative adjustment, whereas the stationary iterative correction method makes a positive adjustment to the parameter value for that age.

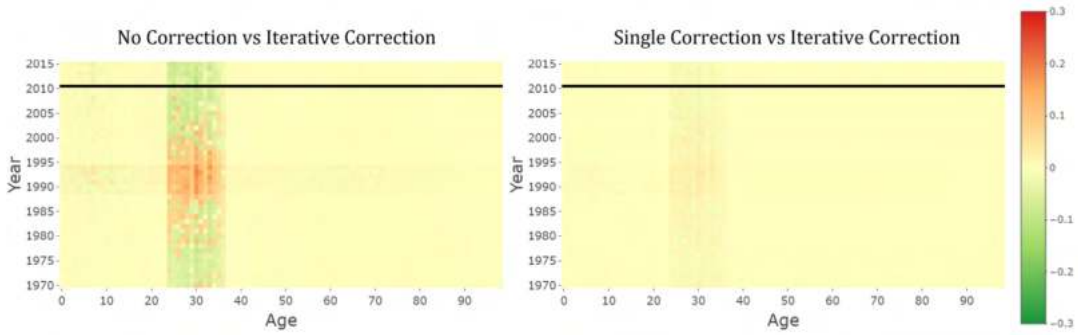

Figure 58: Absolute improvements (shown in green) or deteriorations (shown in red) between no correction, the single correction and the stationary iterative correction for the LC Model. The improvement is defined by Equation (4.3).

The improvements and deteriorations change as expected in Figure 58. Similarly to the Nolfi Model stationary iterative correction, the biggest improvement still comes from the single correction method. The difference between the two correction methods is so small, that the calendar year effects are not visible anymore in the right graph of Figure 58.

To attempt to improve the iterative process, a slight adjustment can be made to the overall structure of the iterative correction method. The adjustment and its effects are discussed in the upcoming subsection.

4.2.2 Moving Singular Event

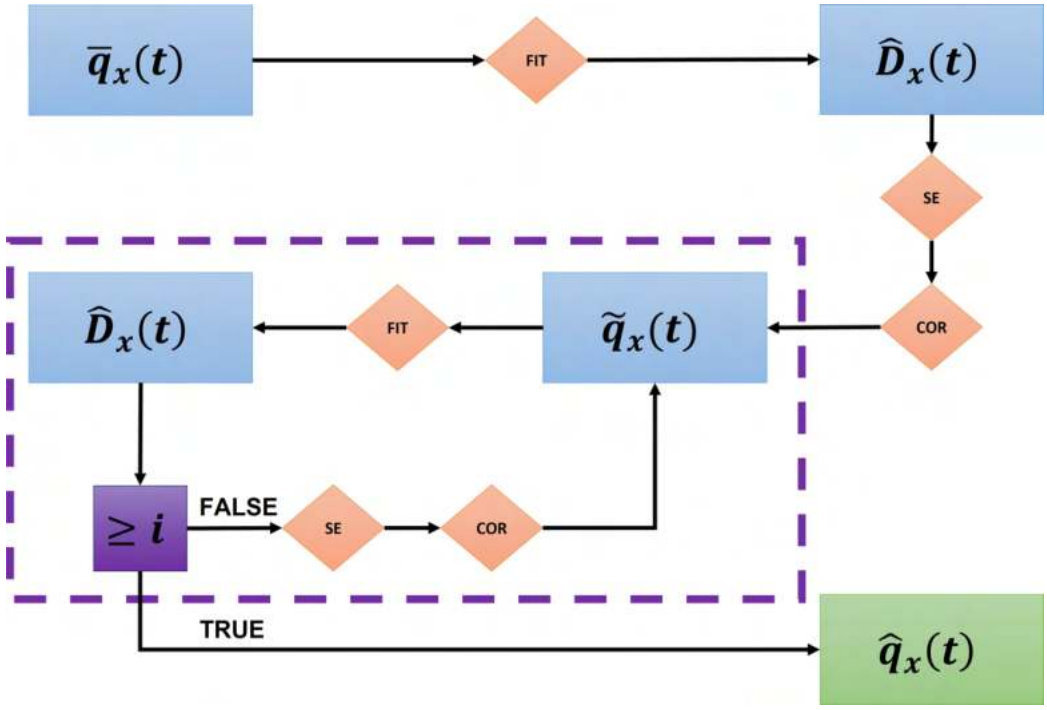

Figure 59: Diagram overview of the single model correction. Blue boxes represent obtained data, red diamonds represent a calculation step. The purple dashed area is the area in which the iterative process takes places. The purple square represents the stopping criterion for the iterative process. The final estimated mortality rate is shown by the green box. The differences with the stationary iterative correction diagram are the added (SE) red diamond before the (COR) red diamond and the different stopping criteria.

To improve the iterative correction method, the singular event detection algorithm will be activated in each iteration to re-evaluate the location of the singular event (see Figure 59). This variation of the method will be called the moving iterative correction method. Given that the errors within and closely around the singular event tend to increase as the corrections are made, this can lead to the singular event increasing in size over multiple iterations.

Additionally, the stopping criteria is changed for this variation of the iterative correction method. This is because the error $\xi^{(i)}$ tends not to decrease monotonically, due to the growing singular event between iterations. Hence, the stopping criterion that the error $\xi^{(i)}$ must decrease with each iteration cannot be used. Leaving this criterion out leaves the risk of the errors increasing and of the iteration process not converging. To avoid this, the stopping criterion type is changed. The stopping criteria used for this moving iterative correction

method is essentially a for-loop with a certain number of allowed iterations. For the upcoming graphs, the number of iterations was set to 10.

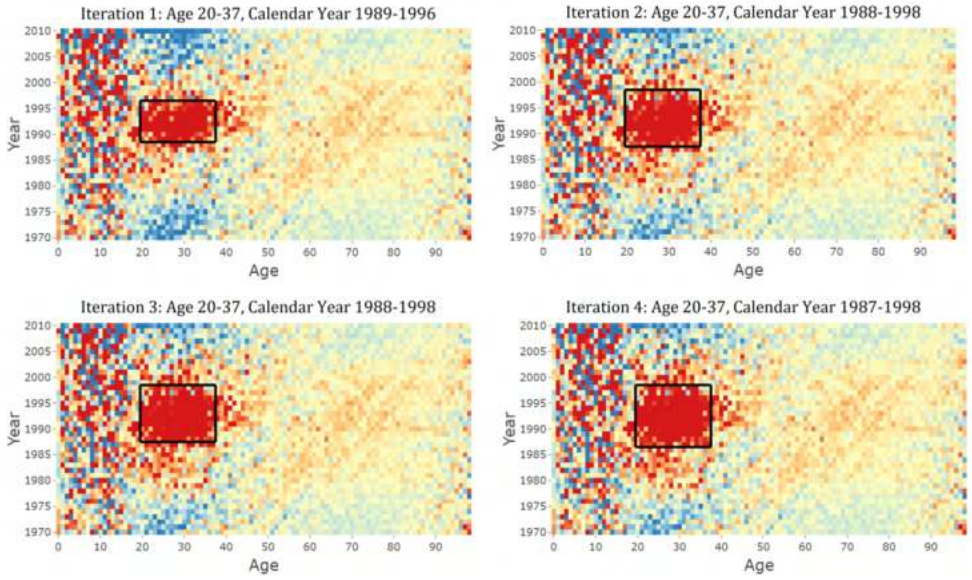

Figure 60: Overview of the changing size of the singular event per iteration. Above each graph, the ages and calendar years which belong to the singular event as defined by the algorithm are written down.

The effects of updating the singular event for each iteration are visible in Figure 60. In the span of four iterations, the singular event expands with four calendar years. From the fourth until the final iteration, the size of this singular event does not change anymore. Note, that the ages are not affected by the re-evaluation of the singular events in this example.

The effects of this newly added moving singular event within the iteration correction method will be discussed for the Nolfi Model and the LC Model below. In the parameter difference graphs below, the parameter difference between no correction and the moving iterative correction method is shown by the blue line. The difference between the single correction method and the moving iterative correction method is represented by the orange line. Finally, the difference between the stationary iterative correction method and the moving iterative correction method is represented by the green line.

4.2.2.1 Nolfi

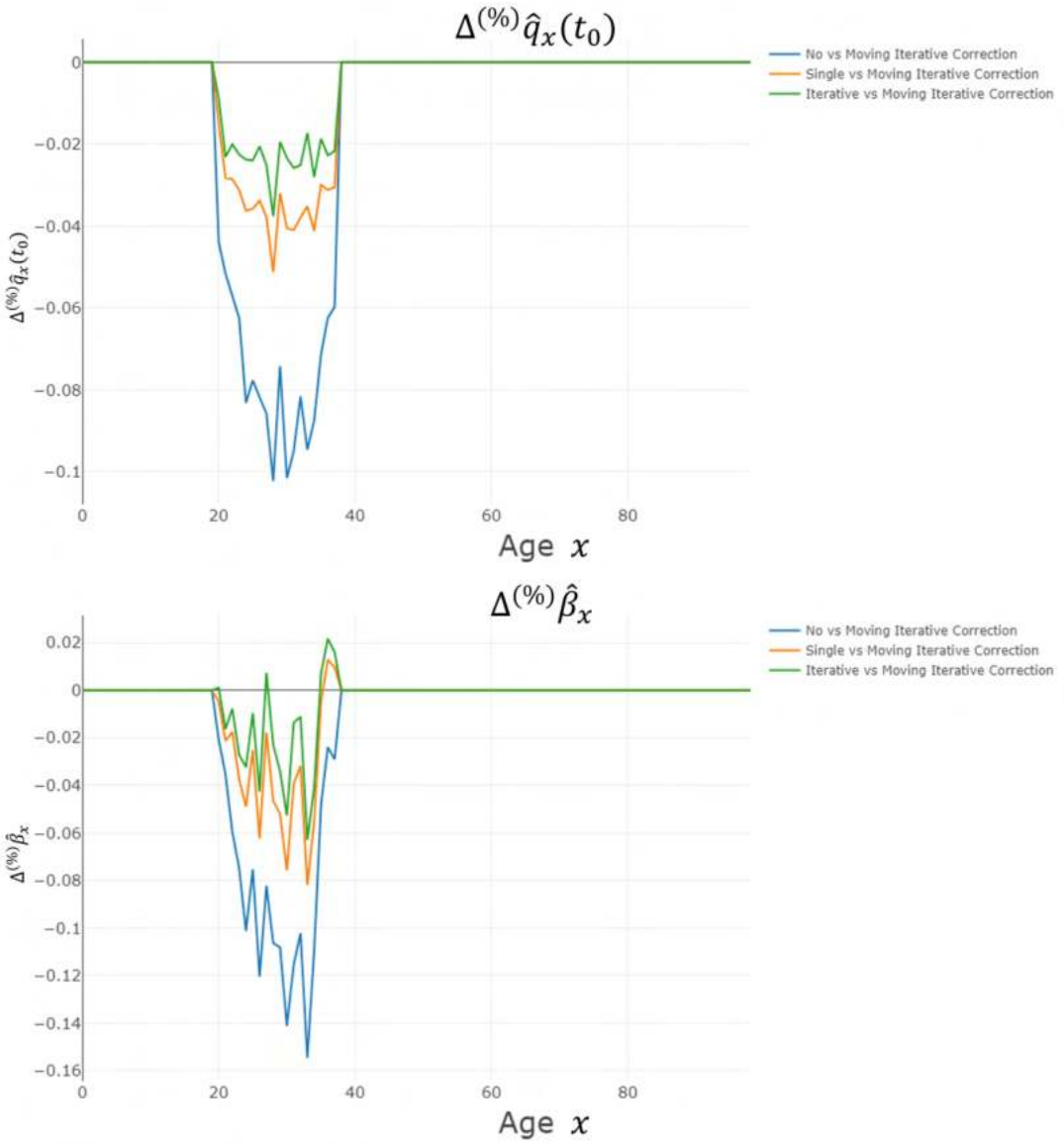

Figure 61: Nolfi Model parameters $\hat{q}_x(t_0)$ and $\hat{\beta}_x$ after the moving iterative correction method has been applied. The graphs show the relative difference (Equation (4.5)) in the parameter for ages 0-98 for men in Switzerland (calendar years 1970-2010). The blue lines show the difference between no correction and the moving iterative correction. The orange lines show the difference between the single correction and the moving iterative correction. The green lines show the difference between the stationary iterative correction and the moving iterative correction. All correction methods use credibility weight $z = 1$.

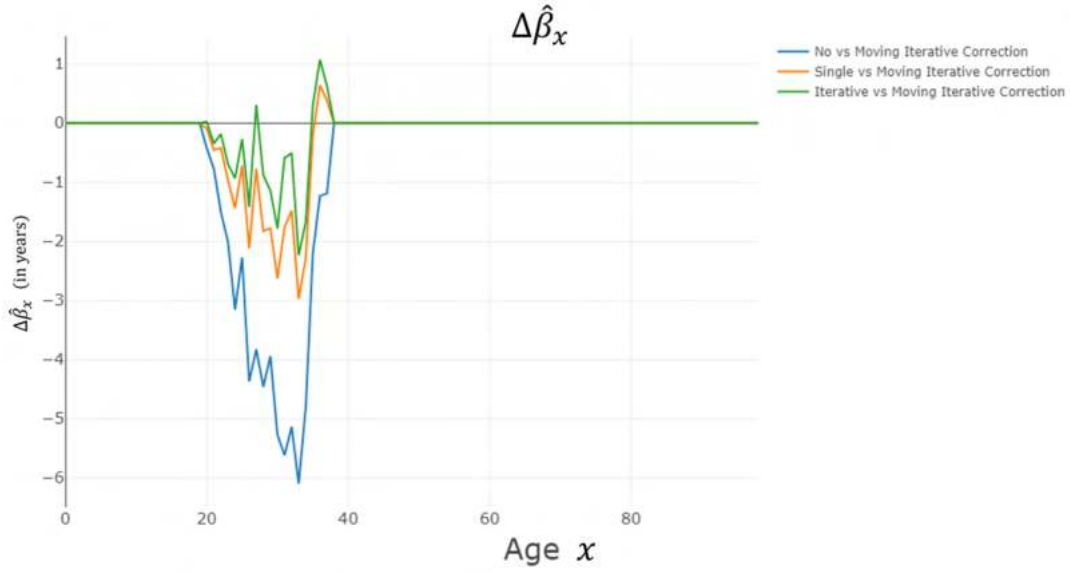

Figure 62: Nolfi Model parameter $\hat{\beta}_x$ after the moving iterative correction method has been applied. The graph shows the absolute difference (Equation (4.4)) in the parameter for ages 0-98 for men in Switzerland (calendar years 1970-2010). The blue line shows the difference between no correction and the moving iterative correction. The orange line shows the difference between the single correction and the moving iterative correction. The green line shows the difference between the stationary iterative correction and the moving iterative correction. All correction methods use credibility weight $z = 1$.

Before commenting on the results, the way to read these more complicated parameter difference graphs is explained. In these figures, the effects of all previous corrections compared to the newest correction are shown. To figure out the net effect of one of these previous versions compared to the no correction case, one can simply look at the differences between the coloured lines.

For example, for figuring out the approximate effect of the simple correction method compared to no correction, one can look at the difference between the blue line and the yellow line. In Figure 61 and Figure 62 these differences are quite large, showing that the simple correction is still responsible for a big portion of the improvement. The difference between the yellow and green line approximates the effect that the stationary iterative correction method had compared to the single correction method. This difference is relatively small, which corresponds with the information that was discussed in previous graphs in the stationary iterative correction section. The difference between the blue line and the green line shows the approximate difference between the stationary iterative correction and no correction. This method for reading the relative differences between corrections can be used for all parameter difference

graphs that are coming up.

Compared to the stationary iterative correction, the moving iterative correction still causes a large improvement compared to the single correction method. This can be seen by the yellow line still being a few percentage points below the x-axis. The difference between the stationary iterative correction and the moving iterative correction is more marginal, leading to an approximate improvement of 25% to 30%.

The half-value period graphs ($\hat{\beta}_x$) show some interesting effects. Here, for the older ages within the singular event, the moving iterative correction reduces the negative impact of the single and stationary correction method. Additionaly, it can be noted that the effects on the half-value period are also getting large for certain ages, with relative differences now growing up to -15%.

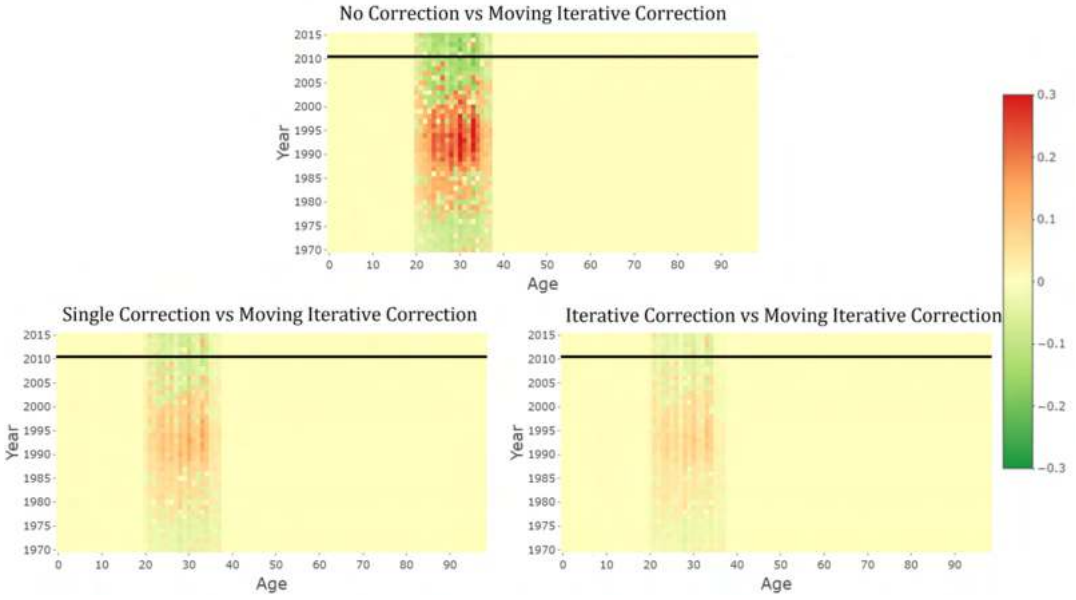

Figure 63: Absolute improvements (shown in green) or deteriorations (shown in red) between no correction, the single correction, the stationary iterative correction and the moving iterative correction for the Nolfi Model. The improvement is defined by Equation (4.3).

The overall increasing effects on the parameters can also be seen in the improvement graphs of Figure 63. Compared to no correction, the moving iterative correction now causes improvements around 15% in the areas outside the singular event and in the projected data. These relative improvements decrease when the moving iterative correction is compared to the single or the stationary iterative correction.

4.2.2.2 Lee-Carter

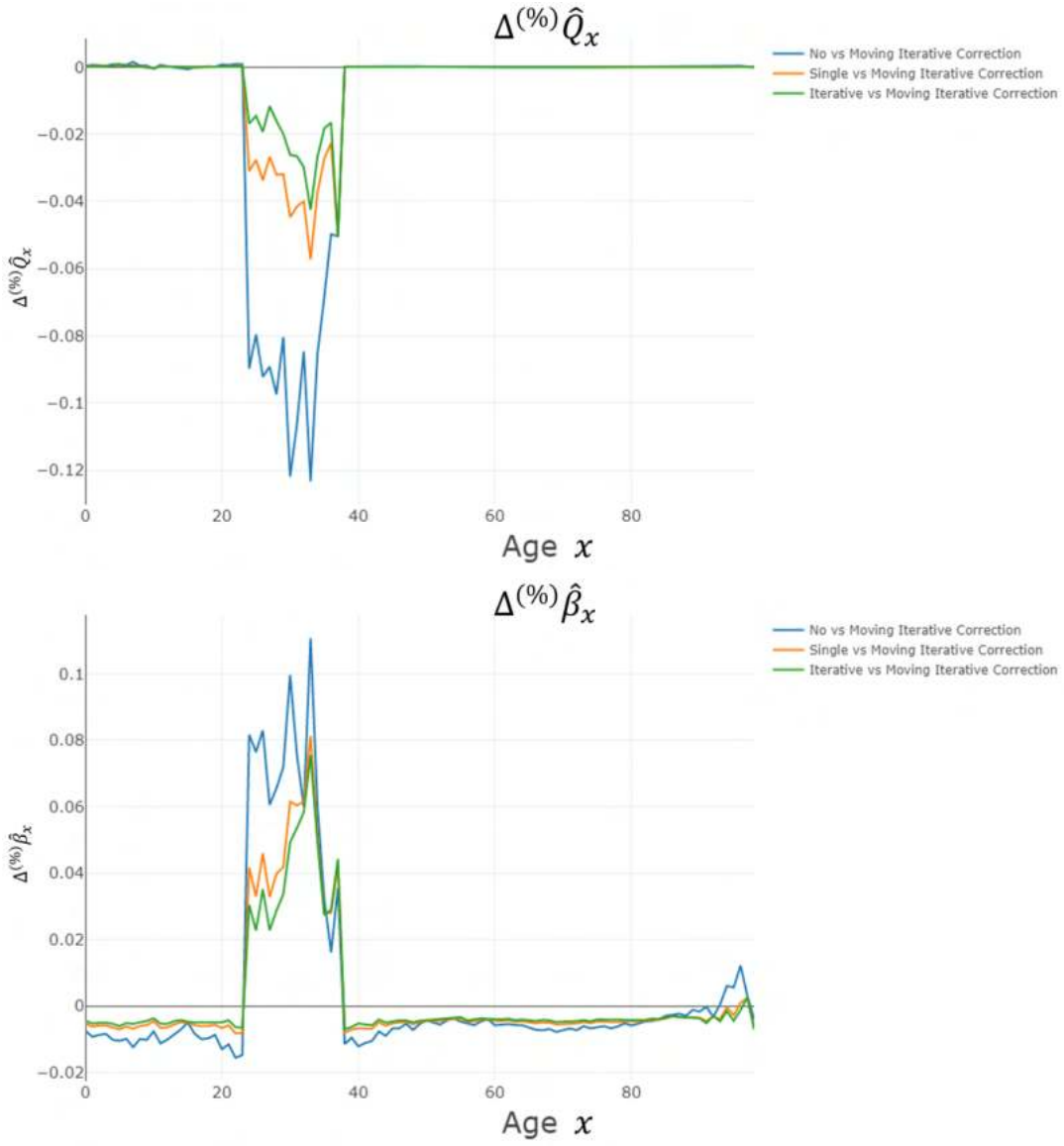

Figure 64: LC Model parameters $\hat{Q}_x$ and $\hat{\beta}_x$ after the moving iterative correction method has been applied. The graphs show the relative difference (Equation (4.5)) in the parameter for ages 0-98 for men in Switzerland (calendar years 1970-2010). The blue lines show the difference between no correction and the moving iterative correction. The orange lines show the difference between the single correction and the moving iterative correction. The green lines show the difference between the stationary iterative correction and the moving iterative correction. All correction methods use credibility weight $z = 1$.

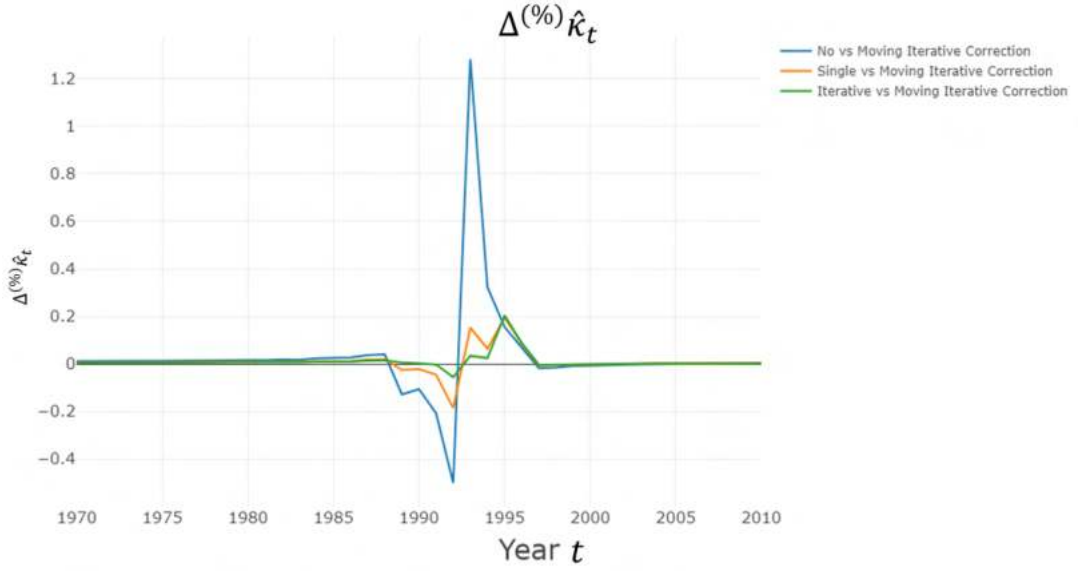

Figure 65: LC Model parameter $\hat{\kappa}_t$ after the moving iterative correction method has been applied. The graph shows the relative difference (Equation (4.5)) in the parameter for ages 0-98 for men in Switzerland (calendar years 1970-2010). The blue line shows the difference between no correction and the moving iterative correction. The orange line shows the difference between the single correction and the moving iterative correction. The green line shows the difference between the stationary iterative correction and the moving iterative correction. All correction methods use credibility weight $z = 1$.

The moving iterative correction method has a big impact on the parameter differences. In Figure 64 and Figure 65 it is clear that some of the parameter differences are only due to the moving iterative correction. These effects are visible for ages around 38 and calendar years 1995. It can be concluded that the singular event grew after some iterations and allowed for previously unaffected ages and calendar years to be adjusted.

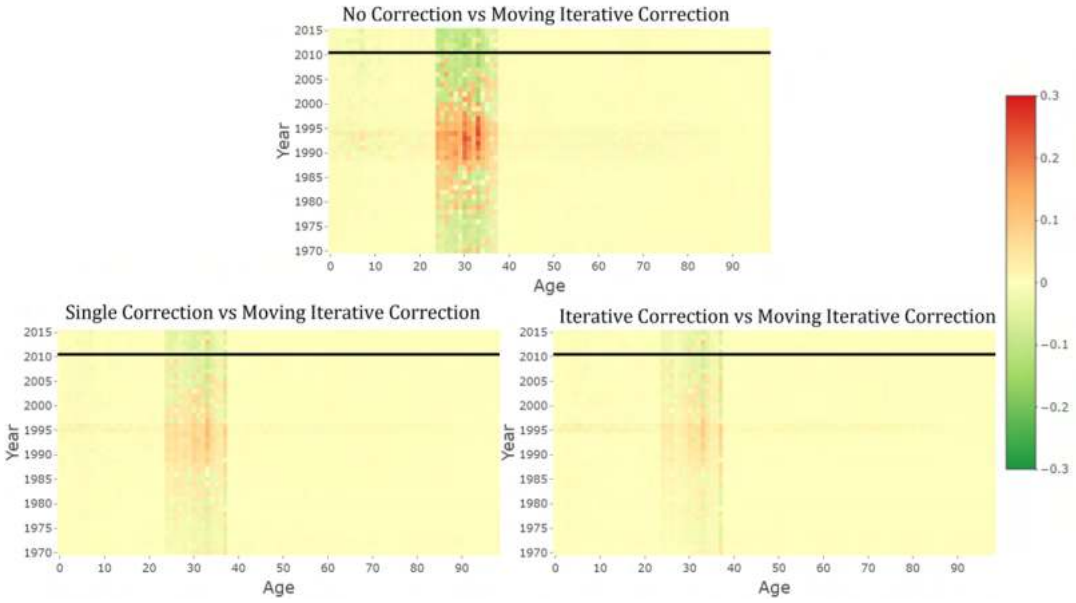

Figure 66: Absolute improvements (shown in green) or deteriorations (shown in red) between no correction, the single correction, the stationary iterative correction and the moving iterative correction for the LC Model. The improvement is defined by Equation (4.3).

In Figure 66, the areas of improvement and deterioration are now slightly larger than before with the stationary iterative correction method. This can be seen most clearly in the comparison between no correction and the moving iterative correction graph. The older ages of the singular event (approximately around age 36) have a slightly less bright colour, these ages were previously not changed in the other iterative correction method. The bottom right graphs shows small improvements between the stationary and moving iterative correction model, with the biggest changes happening around these older ages and calendar year 1995.

4.3 Final Fit Correction

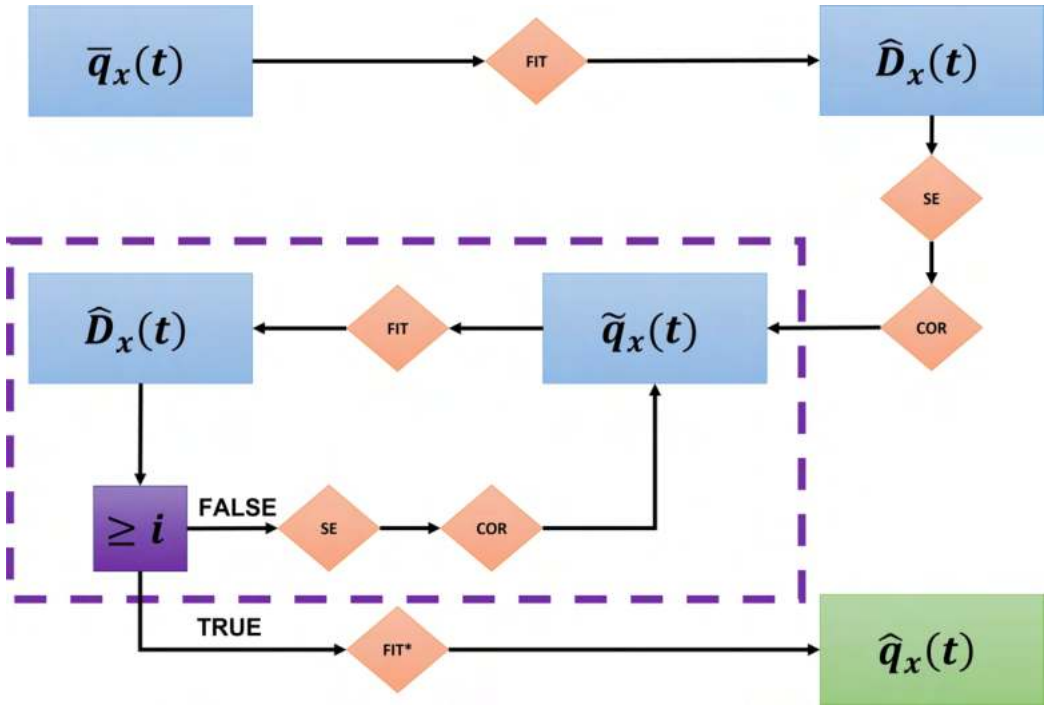

Figure 67: Diagram overview of the single model correction. Blue boxes represent obtained data, red diamonds represent a calculation step. The purple dashed square is the area in which an iterative process takes places. The arrow which leaves the purple dashed square happens after the iterative process. The (FIT*) red diamond represent fitting the data with an alternative model (either LC Model or RH Model).

The last correction method attempts to improve the LC Model moving iterative correction method. The differences between the Nolfi Model correction methods and the LC Model correction methods consistently showed that the singular events were larger for the Nolfi Model methods. Hence, it could be argued that one can get rid of the singular event using the Nolfi Model and then use this corrected data for a LC Model fit. As an experiment, a final fit with the RH Model will also be investigated.

This new correction approach is shown in Figure 67, where the last red diamond (FIT*) stands for the fitting process with the LC Model or the RH Model. All the other red diamonds are executed using the Nolfi Model. Summarized, the basis of this new correction method is the moving iterative correction method for the Nolfi Model. As a final fitting step, the LC Model or the RH Model is fitted with the adjusted data from the moving iterative correction method. Hence, the method is named the final fit correction method.

For each of the parameter difference graphs below, the comparison between no correction and the final fit correction is shown by the blue line. The difference between the single correction method and the final fit correction is represented by the yellow line. The deviation between the stationary iterative correction and the final fit correction is visualized by the green line. Finally, the difference between the moving iterative correction method and the final fit correction method is shown by the red line.

4.3.1 Lee-Carter

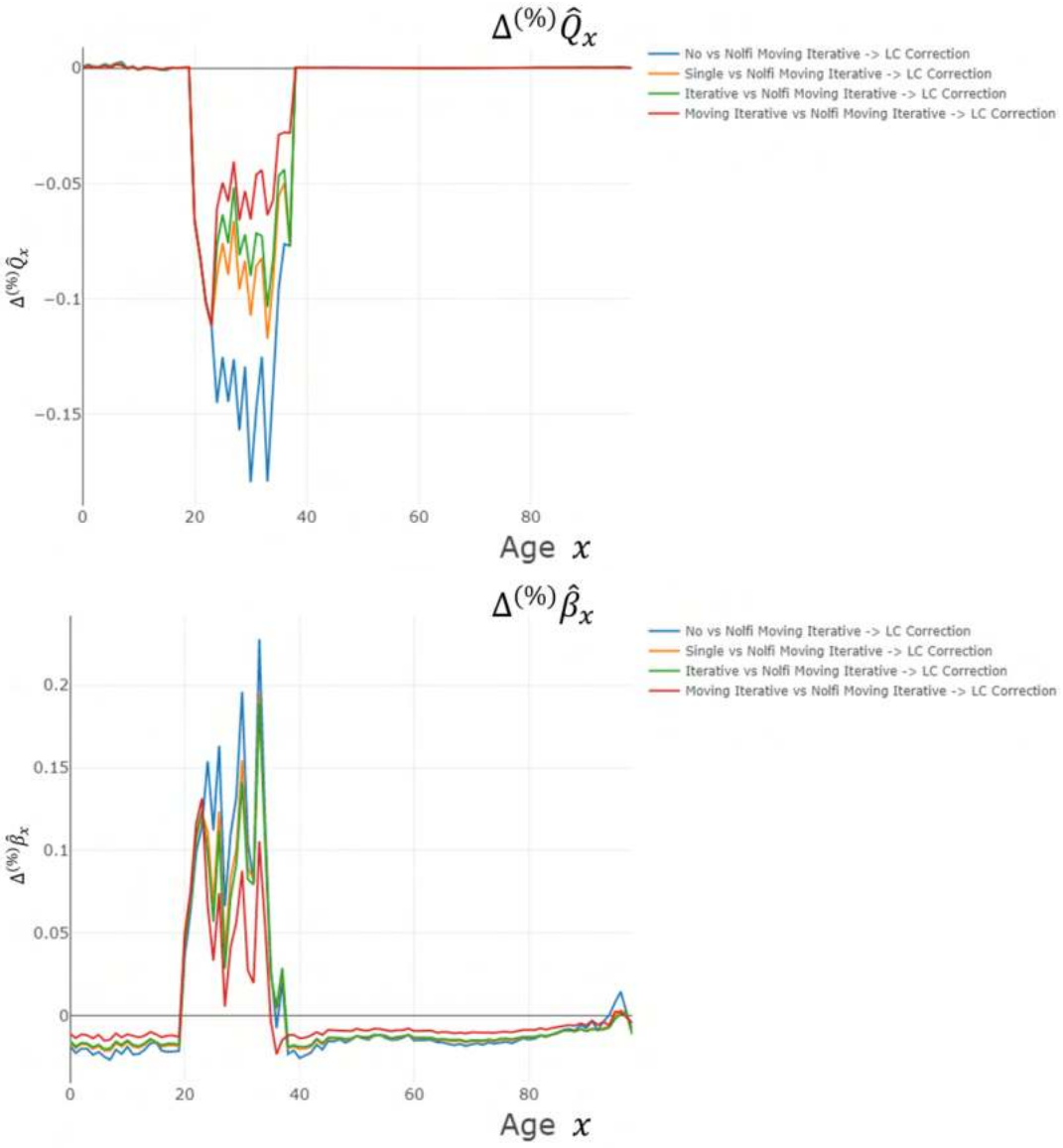

Figure 68: LC Model parameters $\hat{Q}_x$ and $\hat{\beta}_x$ after the final fit correction method (LC Model) has been applied. The graphs show the relative differences (Equation (4.5)) in the parameters for ages 0-98 for men in Switzerland (calendar years 1970-2010). The blue lines show the relative differences between no correction and the final fit correction (LC Model). The orange lines show the relative differences between the single correction and the final fit correction (LC Model). The green lines show the relative differences between the stationary iterative correction and the final fit correction (LC Model). The red lines show the relative differences between the moving iterative correction and the final fit correction (LC Model). All correction methods use credibility weight $z = 1$.

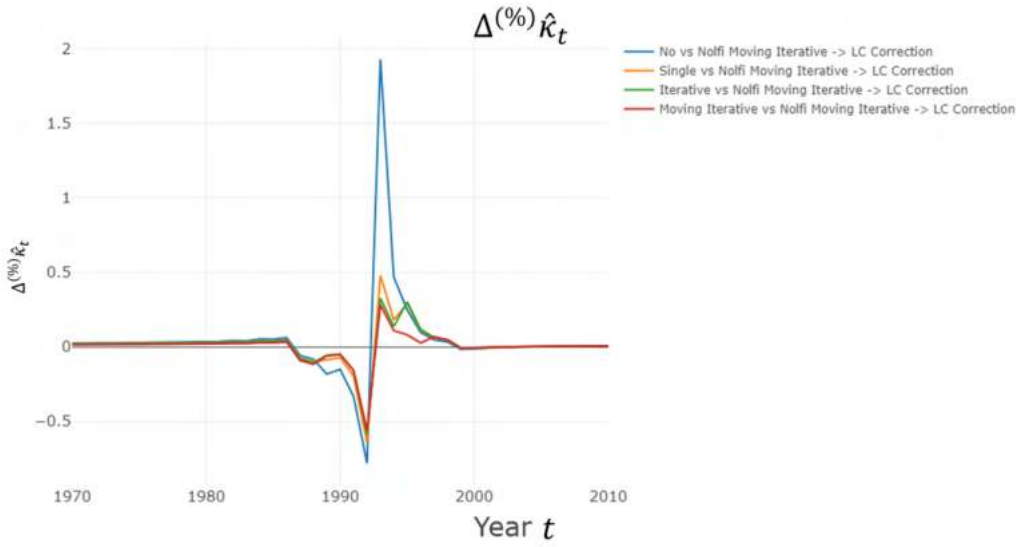

Figure 69: LC Model parameter $\hat{\kappa}_t$ after the final fit correction method (LC Model) has been applied. The graphs show the relative difference (Equation (4.5)) in the parameter for ages 0-98 for men in Switzerland (calendar years 1970-2010). The blue line shows the relative difference between no correction and the final fit correction (LC Model). The orange line shows the relative difference between the single correction and the final fit correction (LC Model). The green line shows the relative difference between the stationary iterative correction and the final fit correction (LC Model). The red line shows the relative difference between the moving iterative correction and the final fit correction (LC Model). All correction methods use credibility weight $z = 1$.

The graphs above are corrected using a final LC Model fit. The parameters $\hat{Q}_x$ and $\hat{\beta}_x$ now have large relative differences with effects up to 20% (see Figure 68). This is largely driven by the single correction and the final fit correction. For the younger ages of the singular event, the parameter differences in these two parameters are almost solely attributable to the final fit correction. The effects on the mortality trend $\hat{\kappa}_t$ are also mostly driven by the single correction and the final fit correction (see Figure 69). The lower calendar years within the singular event are mostly dominated by the final fit correction.

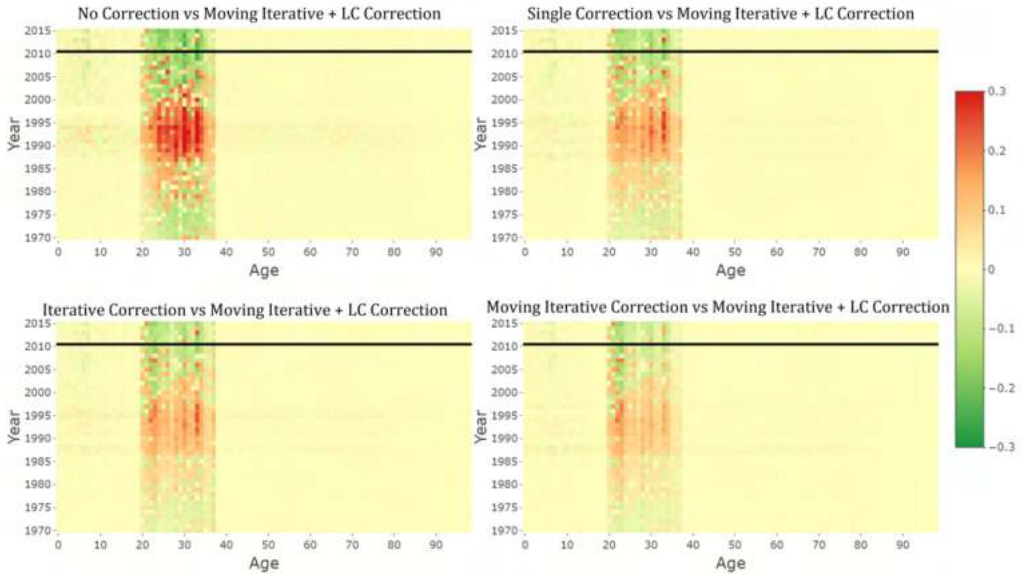

Figure 70: Absolute improvements (shown in green) or deteriorations (shown in red) between no correction, the single correction, the stationary iterative correction, the moving iterative correction and the final fit correction for the LC Model. The improvement is defined by Equation (4.3).

The absolute improvement and deterioration graphs now show large improvements outside of the sinuglar event area (see Figure 70). When comparing the final fit correction to the no correction LC Model (top left graph), certain improvements reach up to 25%. Even when comparing the moving iterative correction to the final fit correction one can still observe relatively large improvements, especially for ages around the early twenties (bottom right graph).

Below, the same analysis will be done for the RH Model.

4.3.2 Renshaw-Haberman

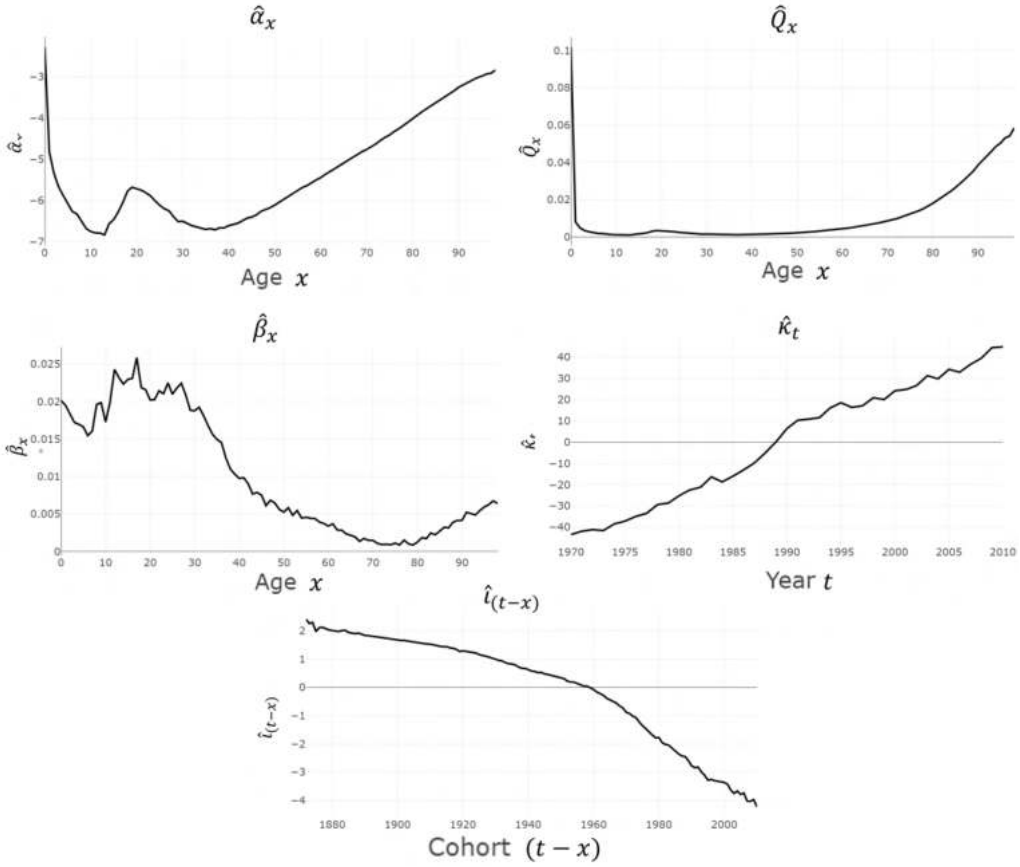

Figure 71: Parameters of the RH Model for calendar years 1970-2010 and ages 0-98 for men in Switzerland. The top left graph shows the logarithmic mean mortality rate $\hat{\alpha}_x$. The top right graph shows the mean mortality rate $\hat{Q}_x = \exp(\hat{\alpha}_x)$. The middle left graph shows age sensitivity for the mortality trend $\hat{\beta}_x$. The middle right graph shows the mortality trend $\hat{\kappa}_t$. The bottom graph shows the cohort trend $\hat{\iota}_{(t-x)}$.

Before looking at the parameter difference graphs, the original fitting parameters are shortly discussed. The parameters in the four upper graphs in Figure 71 have the same interpretation as the LC Model parameters, which were discussed earlier in this chapter. It is notable the infant mortality is much higher in the RH Model (around 10%) than with the LC Model (around 2%, see Figure 40). Furthermore, the mortality trend goes up in the RH Model, whereas it goes down in the LC Model. This is the case, because the RH Model still has a fifth parameter which acts as a counterweight to the rising mortality trend. This fifth parameter ($\hat{\iota}_{(t-x)}$) can be interpreted as a cohort trend, note that this trend appears to be decreasing exponentially.

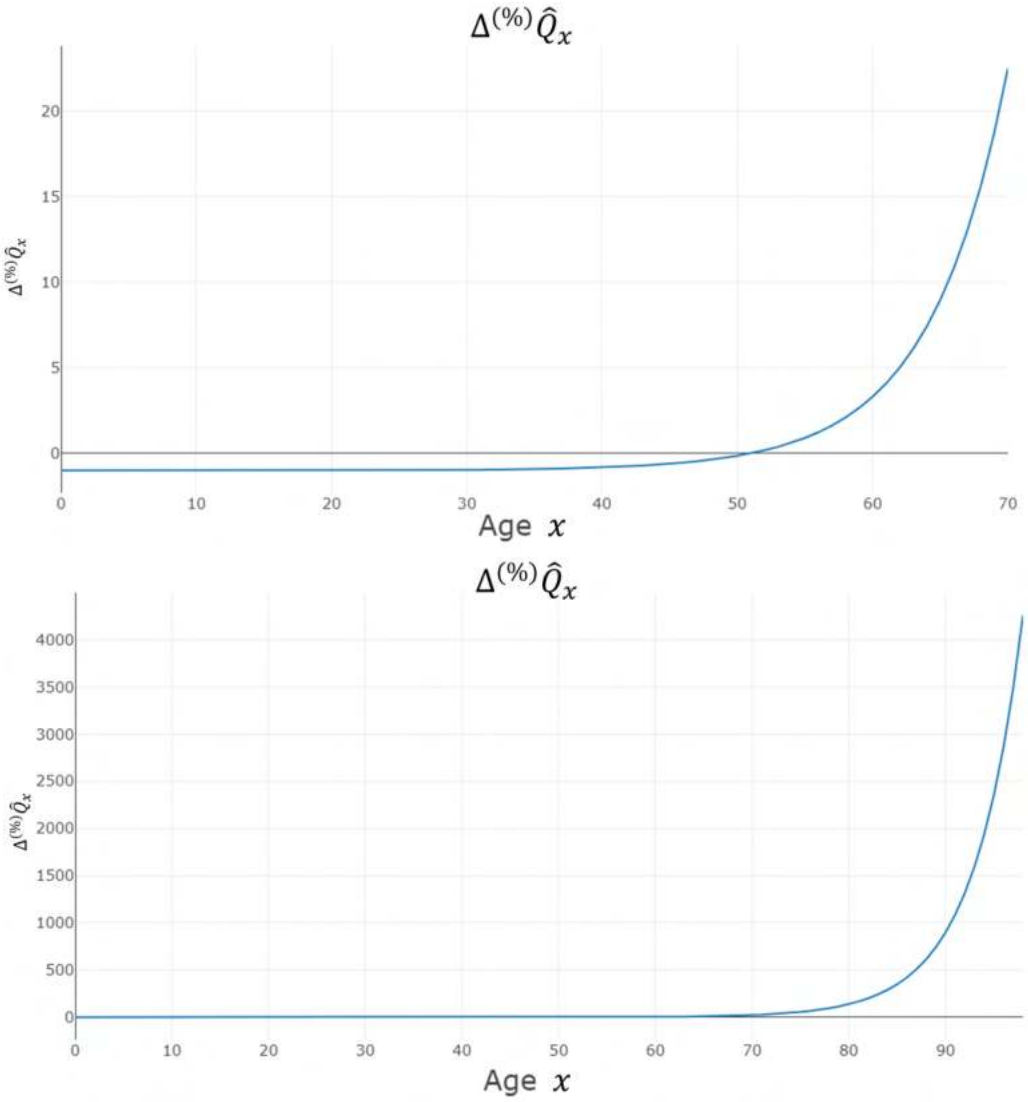

Figure 72: RH Model parameter $\hat{Q}_x$ after the final fit correction method (RH Model) has been applied. The blue line represents the difference between the RH Model without correction and the final fit correction (RH Model). The upper graph is cut off at age 70 allow for better visibility of the lower ages.

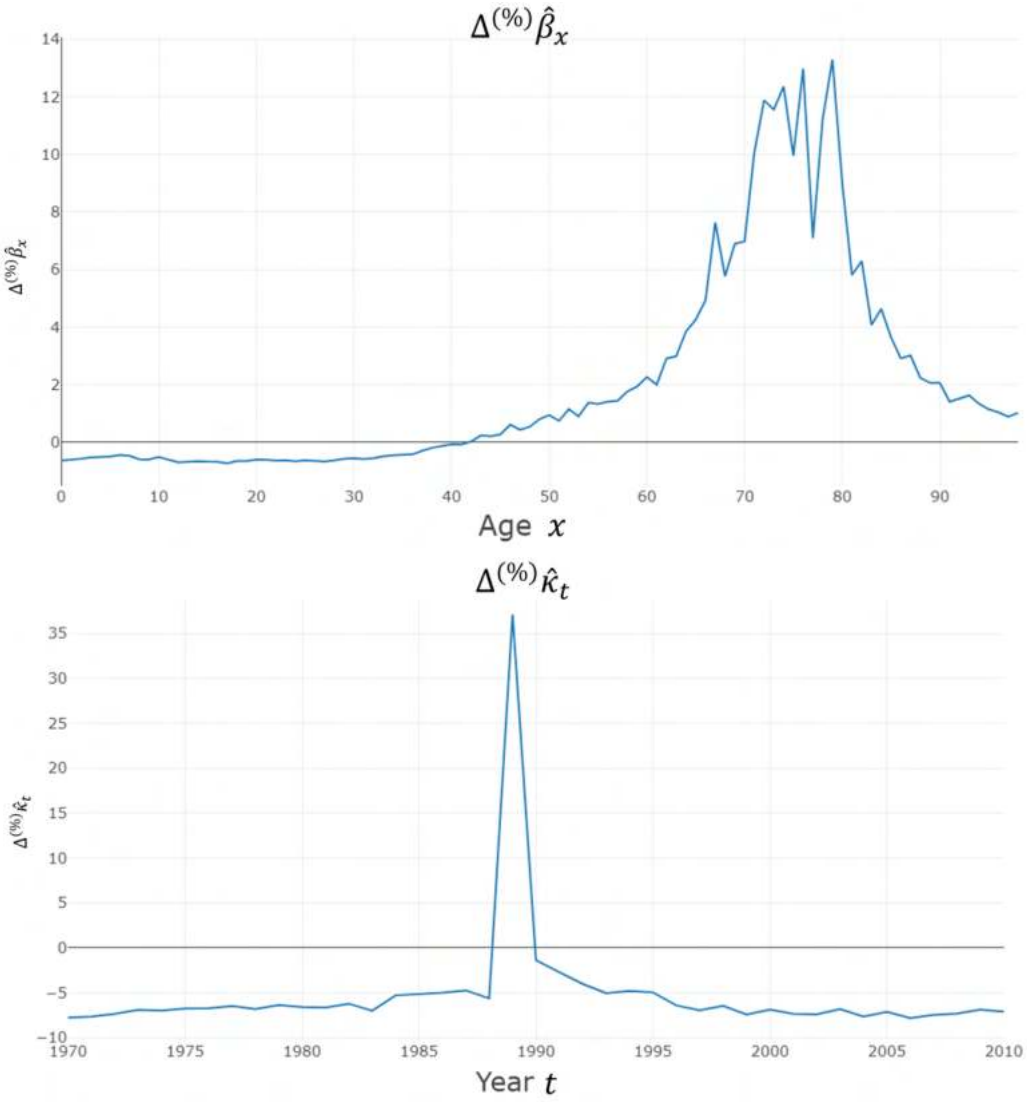

Figure 73: RH Model parameters $\hat{\beta}_x$ and $\hat{\kappa}_t$ after the final fit correction method (RH Model) has been applied. The blue lines represent the differences between the RH Model without correction and the final fit correction (RH Model).

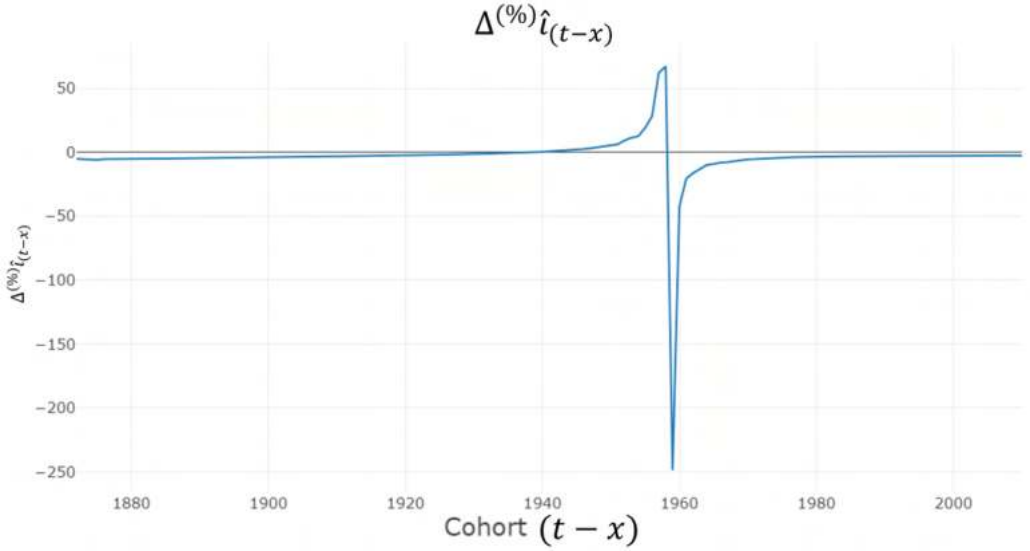

Figure 74: RH Model parameter $\hat{\iota}_{(t-x)}$ after the final fit correction method (RH Model) has been applied. The blue line represents the difference between the RH Model without correction and the final fit correction (RH Model).

Figures 72, 73 and 74 show extremely large parameter differences. The mean mortality rate increases up to 400′000% in the older ages, whereas the younger ages are decreased by up to 100%. Less extreme, but nonetheless large changes, are found for the parameters $\hat{\beta}_x$ and $\hat{\kappa}_t$. The parameter $\hat{\beta}_x$ increases the age sensitvity to the mortality trend mostly in the older ages, whereas it is decreased in the younger ages. The mortality trend $\hat{\kappa}_t$ has a large increase for calendar year 1989, whereas all the other calendar years are decreased significantly. The cohort trend $\hat{\iota}_{(t-x)}$ changes are so large, that the complete parameter curve is flipped, producing an upward cohort trend.

All of these parameter changes are difficult to explain intuitively. This is one of the side effects of the RH Model complexity. There is enough flexibility to overfit to the data even after the data has been corrected for the singular event. Moreover, the RH Model fitting process has a large variability when fitting. With the exact same data, the RH Model tends to produce significantly different model parameters. This appears to be due to the random parameter initialization for the Newton algorithm in R (see Chapter 2).

Figure 75: Absolute improvements (shown in green) or deteriorations (shown in red) between no correction and the final fit correction for the RH Model. The improvement is defined by Equation (4.3).

Figure 75 shows the absolute improvements and deteriorations when comparing the RH Model without correction to the RH Model with the final fit correction. Contrary to all other corrections, the RH Model is not significantly improved by the final fit correction. The only area of improvement is for the cohorts affected by the AIDS pandemic; the projected data seems to be more accurate when taking out the singular event for these cohorts (shown as the green area around age 40 in the projected area).

5 Conclusion

Singular events are part of humanity's past, present and its future. These singular events distort the underlying patterns of the normal mortality development. These distortions lead to distorted mortality forecasting model parameters, which in turn deteriorates their estimation and projection quality. Additionally, the projections for mortality tables will fluctuate more, given that some fitting time periods will contain singular events, whereas others will not. In other words, they have a greater dependency on the fitting period. Hence, this thesis attempted to set up a framework for dealing with singular events.

Firstly, this thesis looked at three common mortality forecasting models: Nolfi, Lee-Carter and Renshaw-Haberman. For each of these models, the fitting process, the parameters and the projection process were explained.

With these models introduced, the thesis focused on identifying the singular events. Two potential approaches were discussed: the "expert judgement" method and the "algorithm" method. The expert judgement method solely relies on the judgement of an expert, who judges visually where the event begins and ends. The downside of this approach is that it entails a manual process, which hinders any iterative solutions (like the moving iterative correction). Hence, the thesis utilized the algorithm approach, which was introduced in detail in Chapter 3. The algorithm approach still allows flexibility due to its parameters and does not require manual input for each event detection. The algorithm approach succesfully identifies singular events including AIDS, World War I, World War II and the Spanish Flu (see Appendix).

Afterwards, the consistently defined and identified singular event is exposed to multiple correction methods. The goal of these corrections is that the distorted parameters are corrected, so that they accurately represent the normal mortality development outside of singular events. The success of these correction methods is tested by comparing the observed mortality frequencies with the original and corrected mortality rate estimates. Additionally, the original and corrected model parameters are compared. The four correction methods discussed are the "single" correction method, the "stationary iterative" correction method, the "moving iterative" correction method and the "final fit" correction method. Of these four correction methods, the final fit correction method showed the largest improvements of them all.

Returning to COVID-19

With this new information, the thesis returns to the question posed in the Introduction: Is the decrease in life expectancy due to COVID-19 an accurate representation of the mortality development? The periodic mortality table used by the BfS to calculate the life expectancy allows for large distorting effects from singular events. This includes COVID-19. Hence, the thesis recommends to either take out the singular event and keep using the periodic mortality table, or to switch to a generation mortality table. This generation table will by default make an important distinction for each generation. This means that the generation table would take into account that the younger generations of today are unlikely to be affected by COVID-19 when they are older and more vulnerable.

Removing the effects of the COVID-19 from the mortality data will likely require the expert judgement method, given that the increase in mortality is barely impacting younger ages and the increase for the older ages is moderate. Hence, it is unlikely that the singular event would be detected by the algorithm if the large error threshold is set to a 30% underestimation. Reducing this threshold will likely lead to general fluctuations also being identified as singular events. To avoid this, the expert judgement method would be the safer option. Removing the COVID-19 singular event with the single correction method would likely remove the decrease in life expectancy as found by the BfS.

Future Research

There are still certain aspects that could be researched for this thesis topic. Firstly, more mortality forecasting models can be researched. This thesis only focused on three commonly used mortality models. There are still many different variations of the Lee-Carter Model that could be added. One promising Lee-Carter Model adjustment takes into account regime changes. Perhaps the regime change could also capture singular events.

Secondly, one can attempt to improve and add more singular event detection methods. The methods currently used do not take into account the generational effects, which could be added to the existing models. Furthermore, the use of certain machine learning algorithm might help with identification of singular events. Before settling on the current algorithm, the k-nearest-neighbour and k-means machine learning algorithms were tested. These algorithms did not produce desirable results and were thus discarded. However, one could continue experimenting with these algorithms or try out other clustering al-

gorithms. Another limitation of the currently used singular event detection algorithm is that it always classifies a singular event as a rectangle. It is possible to add an iterative gridsearch algorithm to see whether any surrounding data points also have large errors, which could then be added to the singular event. This can potentially be repeated until no more neighbouring large error data points are found. However, this leads to the potential danger of having too large singular events.

Thirdly, the correction methods can be improved or new correction methods can be tested. One could also test out the current correction methods with new mortality forecasting models. It can be attempted to estimate singular events as a separate model, thereby allowing the normal mortality development to be estimated without the singular event. With this approach the estimation quality within the singular event would not have to decrease, given that its separate model can fully attempt to fit to the singular event. The model within the singular event would then not have any projection quality, but could for example be used to forecast impacts of future possible singular events.

Lastly, one can increase the number of analyses done per correction method. Currently, only the parameter differences and the change in estimation quality were discussed. One could investigate the effects to the life expectancy, or analyse the effects on simple life insurance products. Additionally, one could investigate to what extend these correction methods decrease the jumps between mortality tables across time.

All in all, there are still many exciting directions to explore within this topic. Hopefully, this thesis serves as a partial starting point for future research on this topic.

Appendix

The upcoming Appendices all have the same structure. First, the singular event detection is shown. Next, each Appendix splits up into sections for each mortality forecasting model. Per mortality forecasting model, the errors before and after correction are shown. Afterwards, the absolute improvements and an overview of the correction steps is shown for each model. Each Appendix ends with a comparison of the mortality forecasting models, showing graphs that compare the errors before correction and after correction. Finally, the absolute improvement graphs are used to see which of the mortality forecasting models has lower errors in each data point.

The Lee-Carter Model and the Renshaw-Haberman Model will show a similar pattern when comparing the before and after correction fitting errors. Before correcting, the singular event is often not visible in the error graphs. This is due to the overfitting of these models. The singular event correction then makes this singular event reappear (i.e. it deteriorates the errors within the singular event significantly). This reduces the distortion of the model parameters, often leading to an improvement in estimation quality outside of the singular event.

Appendix A: WW I (France)

Singular Event

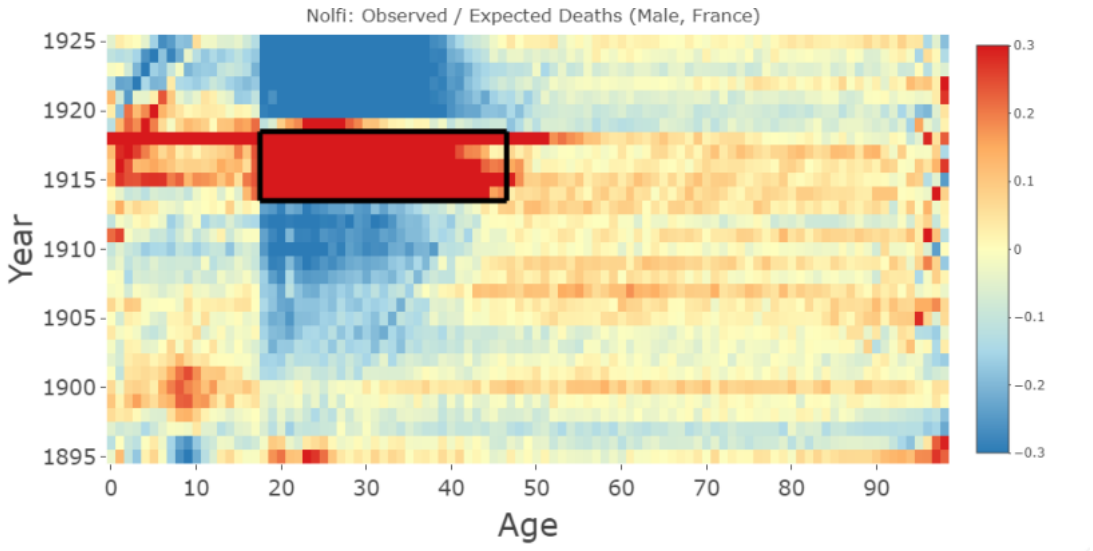

Figure 76: Nolfi Model mortality rate estimation errors for calendar years 1895-1925 and ages 0-98 (French, male). The black box highlights the singular event as identified by the algorithm with parameters $\varepsilon = 0.3$, $\gamma^{(year)} = 1/3$, $\alpha^{(year)} = 0.5$, $\gamma^{(age)} = 2/3$ and $\alpha^{(year)} = 0.4$.

Nolfi

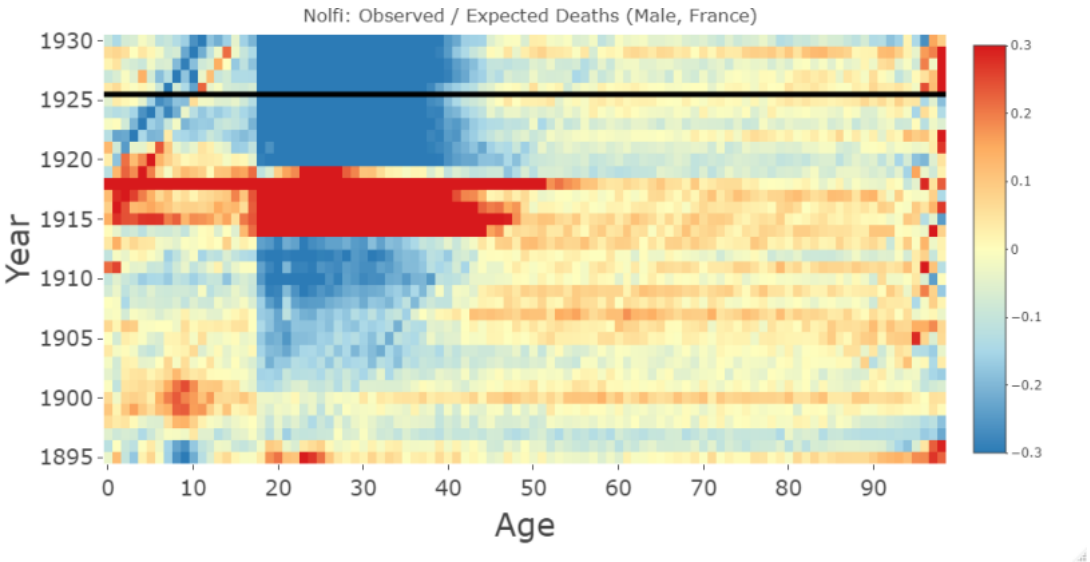

Figure 77: Nolfi Model mortality rate estimation errors before correction for calendar years 1895-1930 and ages 0-98 (French, male), the last five years were projected (above the black line).

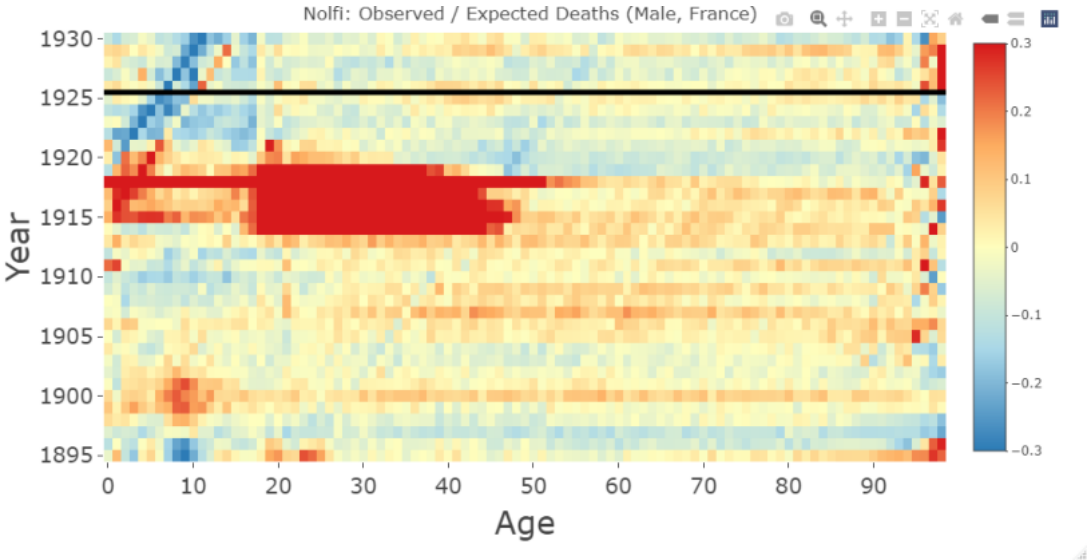

Figure 78: Nolfi Model mortality rate estimation errors after correction with the moving iterative correction method for calendar years 1895-1930 and ages 0-98 (French, male), the last five years were projected (above the black line).

Figure 79: Nolfi Model mortality rate estimation improvements for calendar years 1895-1930 and ages 0-98 (French, male), the last five years were projected (above the black line). The graph compares no correction to the moving iterative correction.

Figure 80: Nolfi Model mortality rate correction steps for calendar years 1895-1930 and age 30 (French, male), the last five years were projected (left of the black line).

Lee-Carter

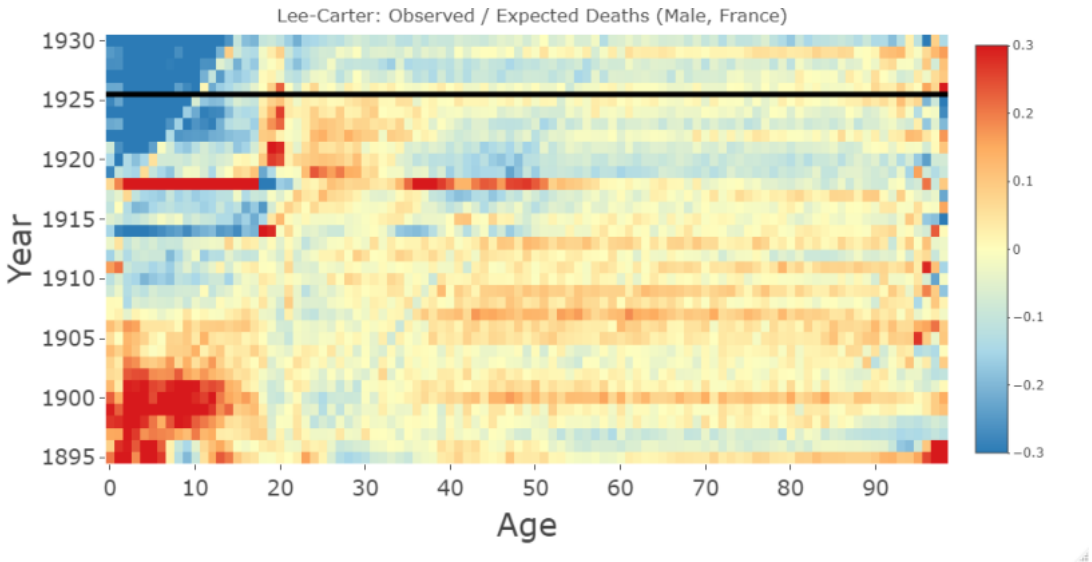

Figure 81: Lee-Carter Model mortality rate estimation errors before correction for calendar years 1895-1930 and ages 0-98 (French, male), the last five years were projected (above the black line).

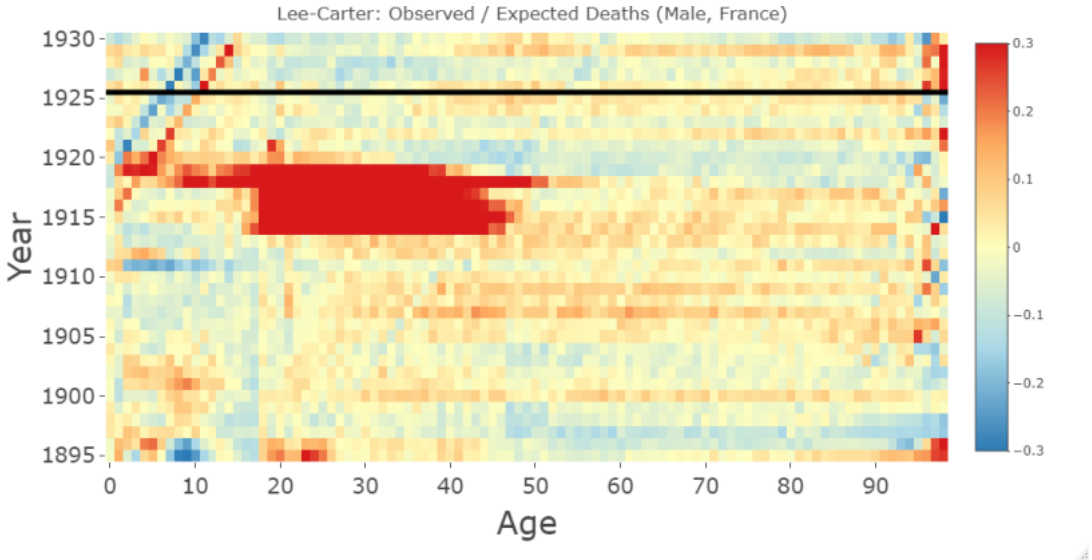

Figure 82: Lee-Carter Model mortality rate estimation errors after correction with the final fit correction method for calendar years 1895-1930 and ages 0-98 (French, male), the last five years were projected (above the black line).

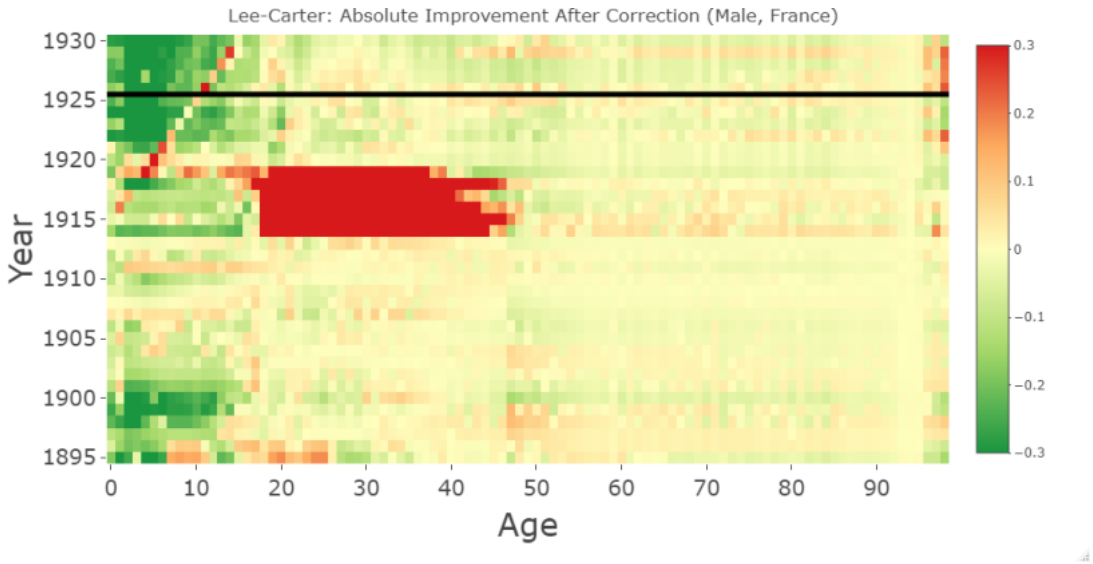

Figure 83: Lee-Carter Model mortality rate estimation improvements for calendar years 1895-1930 and ages 0-98 (French, male), the last five years were projected (above the black line). The graph compares no correction to the final fit correction.

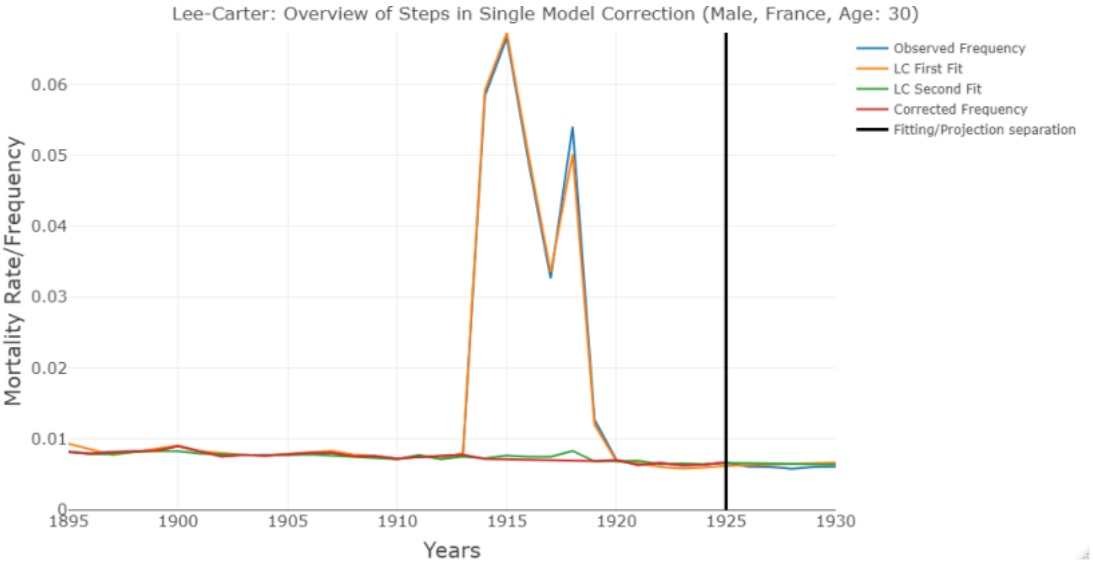

Figure 84: Lee-Carter Model mortality rate correction steps for calendar years 1895-1930 and age 30 (French, male), the last five years were projected (left of the black line).

Renshaw-Haberman

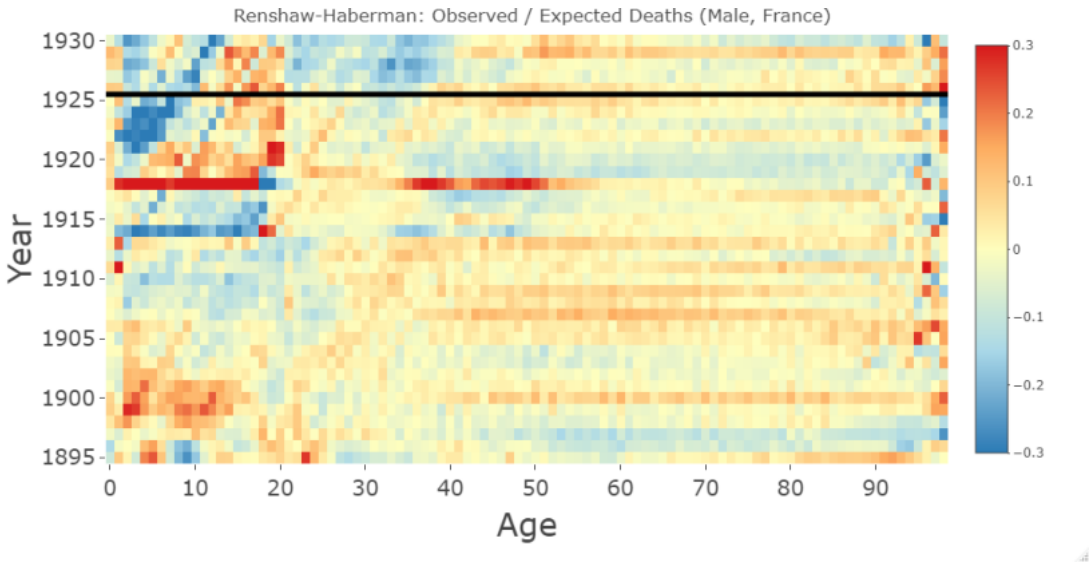

Figure 85: Renshaw-Haberman Model mortality rate estimation errors before correction for calendar years 1895-1930 and ages 0-98 (French, male), the last five years were projected (above the black line).

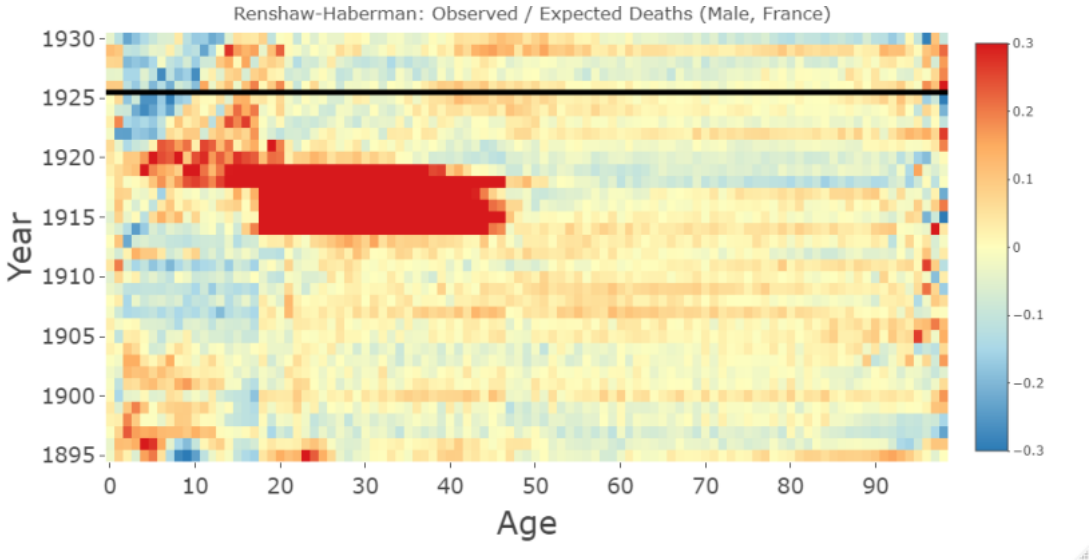

Figure 86: Renshaw-Haberman Model mortality rate estimation errors after correction with the final fit correction method for calendar years 1895-1930 and ages 0-98 (French, male), the last five years were projected (above the black line).

Figure 87: Renshaw-Haberman Model mortality rate estimation improvements for calendar years 1895-1930 and ages 0-98 (French, male), the last five years were projected (above the black line). The graph compares no correction to the final fit correction.

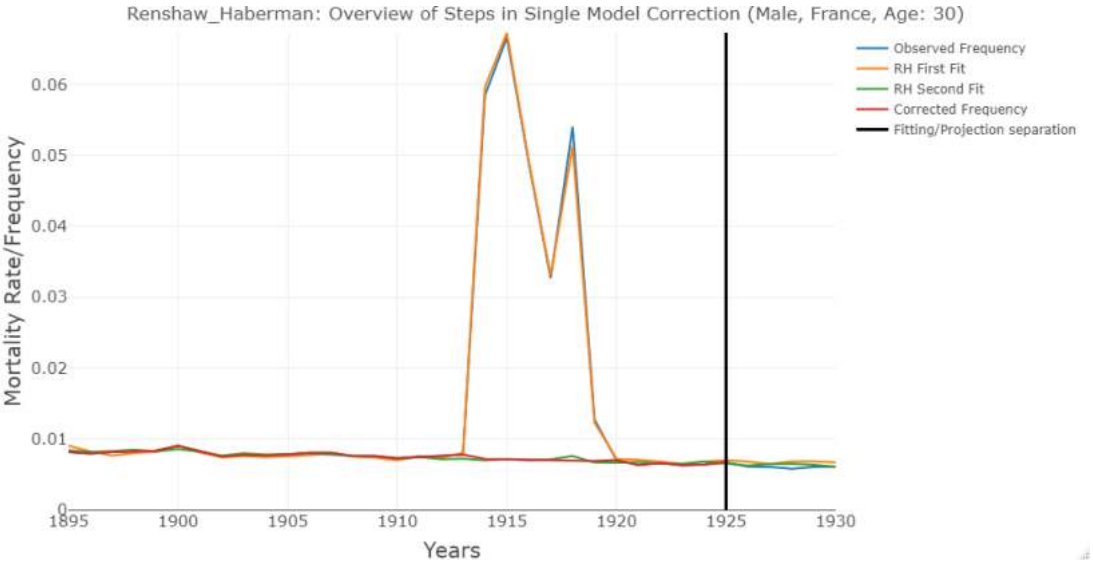

Figure 88: Renshaw-Haberman Model mortality rate correction steps for calendar years 1895-1930 and age 30 (French, male), the last five years were projected (left of the black line).

Model Comparison

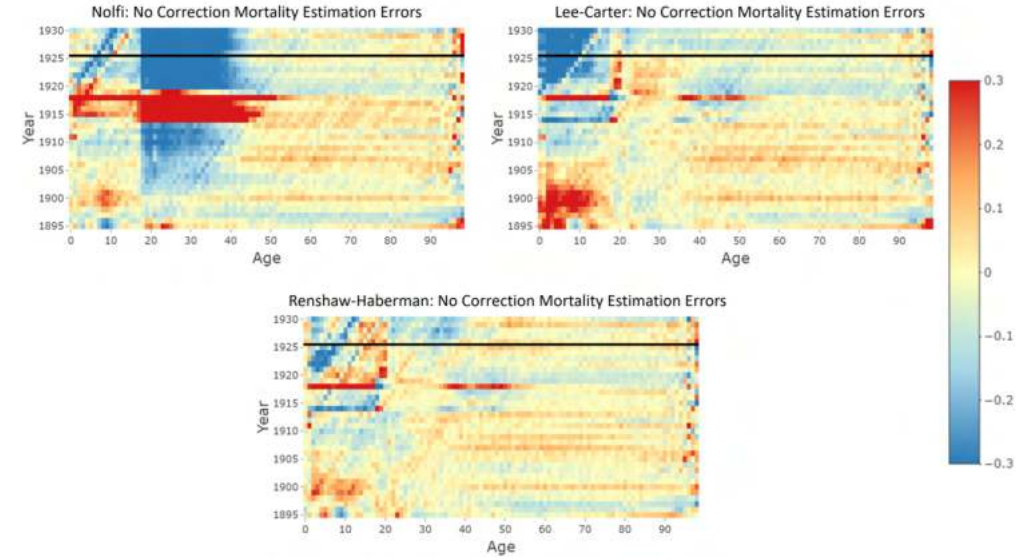

Figure 89: Mortality rate estimation improvements for calendar years 1895-1930 and ages 0-98 (French, male), the last five years were projected (above the black line). The graph shows the Nolfi, Lee-Carter and Renshaw-Haberman Model estimation errors before correction.

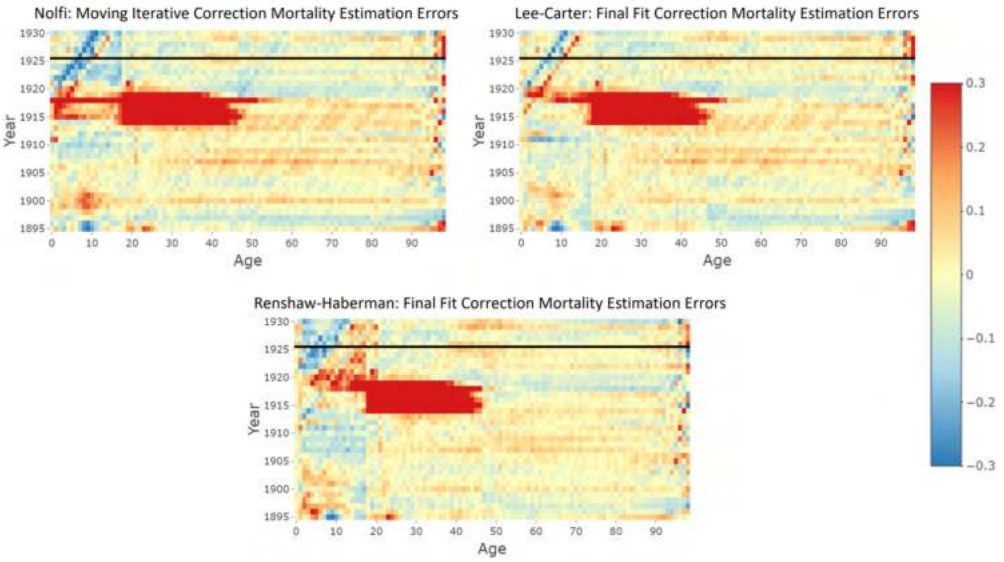

Figure 90: Mortality rate estimation improvements for calendar years 1895-1930 and ages 0-98 (French, male), the last five years were projected (above the black line). The graph shows the Nolfi, Lee-Carter and Renshaw-Haberman model estimation errors after correction.

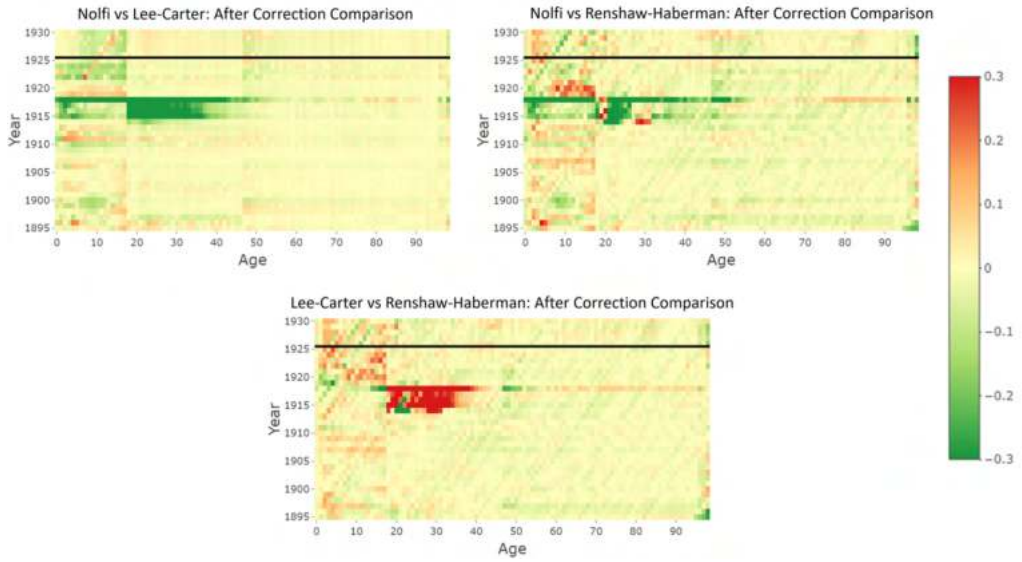

Figure 91: Mortality rate estimation improvements for calendar years 1895-1930 and ages 0-98 (French, male), the last five years were projected (above the black line). The graph compares the Nolfi, Lee-Carter and Renshaw-Haberman Models after correction. In the graphs the model before the"vs" is better when the colour is red, whereas the model after the "vs" is better when the colour is green.

Appendix B: WW II (France)

Singular Event

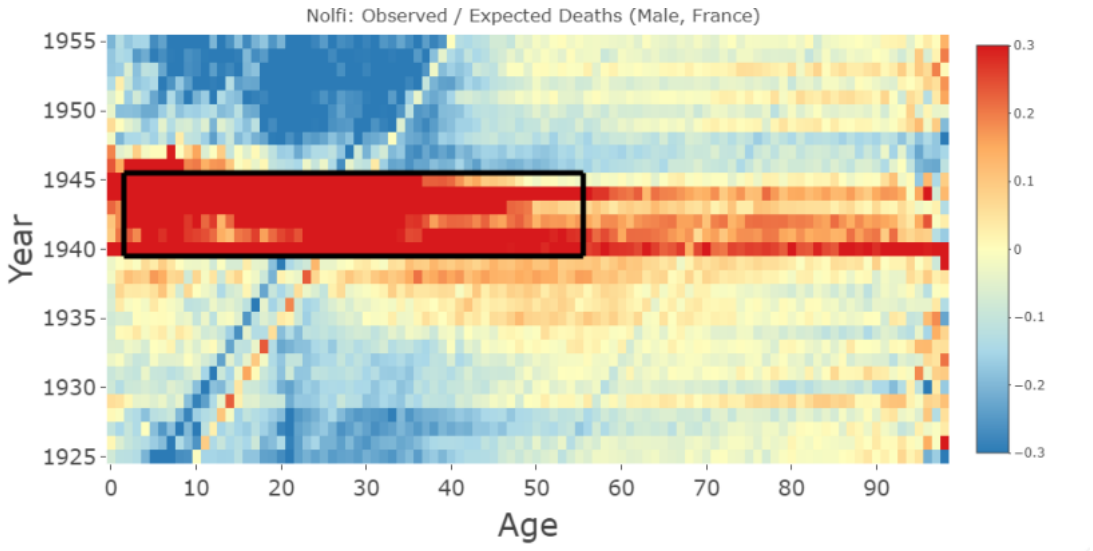

Figure 92: Nolfi Model mortality rate estimation errors for calendar years 1925-1955 (French, male). The black box highlights the singular event as identified by the algorithm with parameters $\varepsilon = 0.3$, $\gamma^{(year)} = 1/3$, $\alpha^{(year)} = 0.5$, $\gamma^{(age)} = 2/3$ and $\alpha^{(year)} = 0.4$.

Nolfi

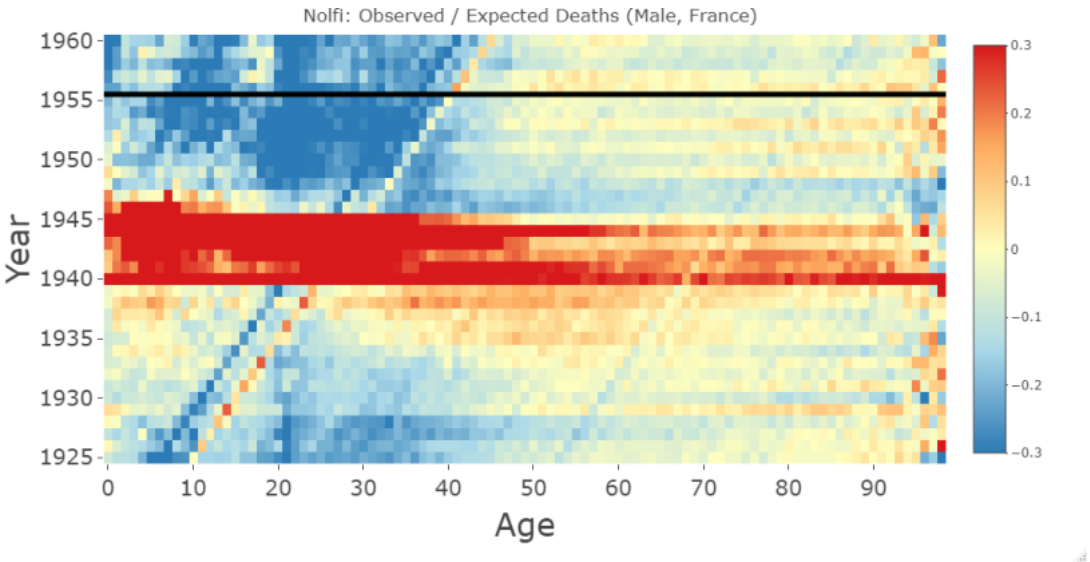

Figure 93: Nolfi Model mortality rate estimation errors before correction for calendar years 1925-1960 and ages 0-98 (French, male), the last five years were projected (above the black line).

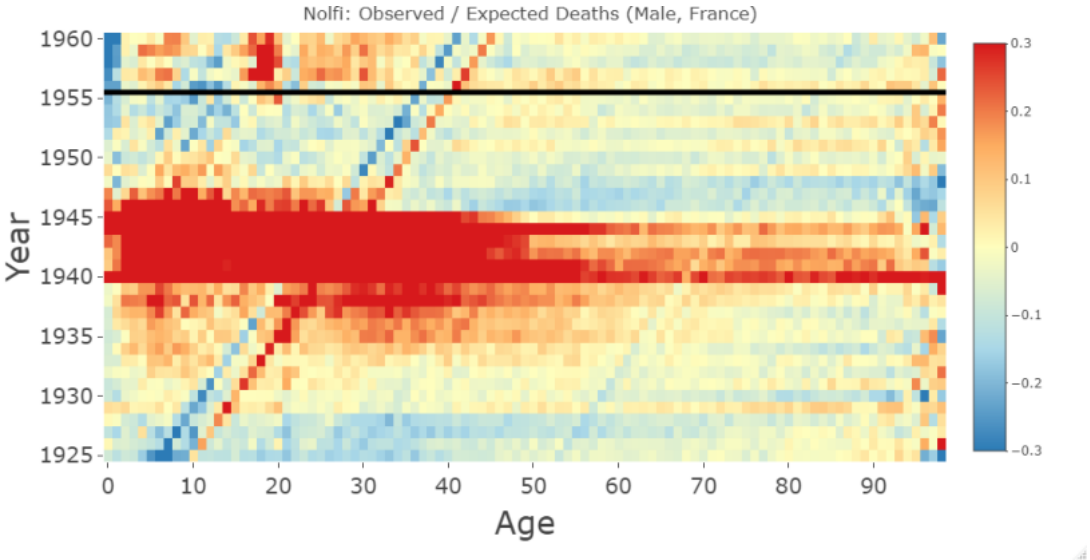

Figure 94: Nolfi Model mortality rate estimation errors after correction with the moving iterative correction method for calendar years 1925-1960 and ages 0-98 (French, male), the last five years were projected (above the black line).

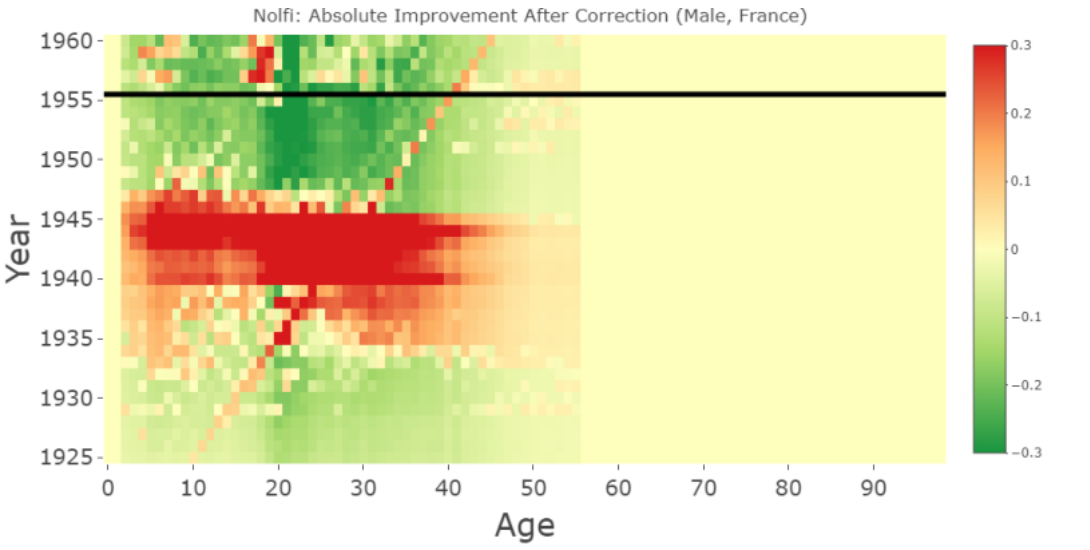

Figure 95: Nolfi Model mortality rate estimation improvements for calendar years 1925-1960 and ages 0-98 (French, male), the last five years were projected (above the black line).The graph compares no correction to the moving iterative correction method.

Figure 96: Nolfi Model mortality rate correction steps for calendar years 1925-1960 and age 30 (French, male), the last five years were projected (above the black line).

Lee-Carter

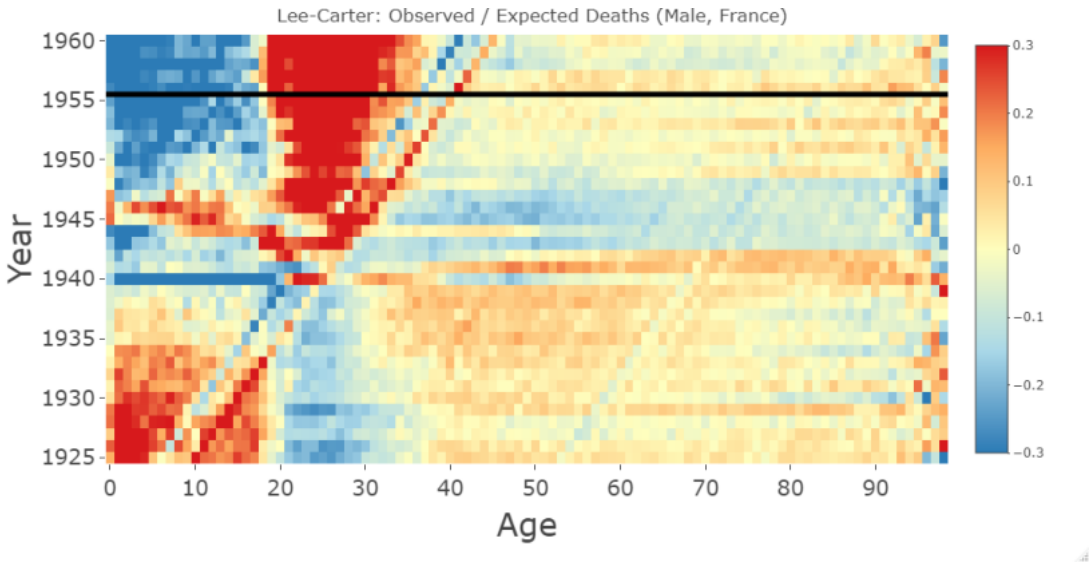

Figure 97: Lee-Carter Model mortality rate estimation errors before correction for calendar years 1925-1960 and ages 0-98 (French, male), the last five years were projected (above the black line).

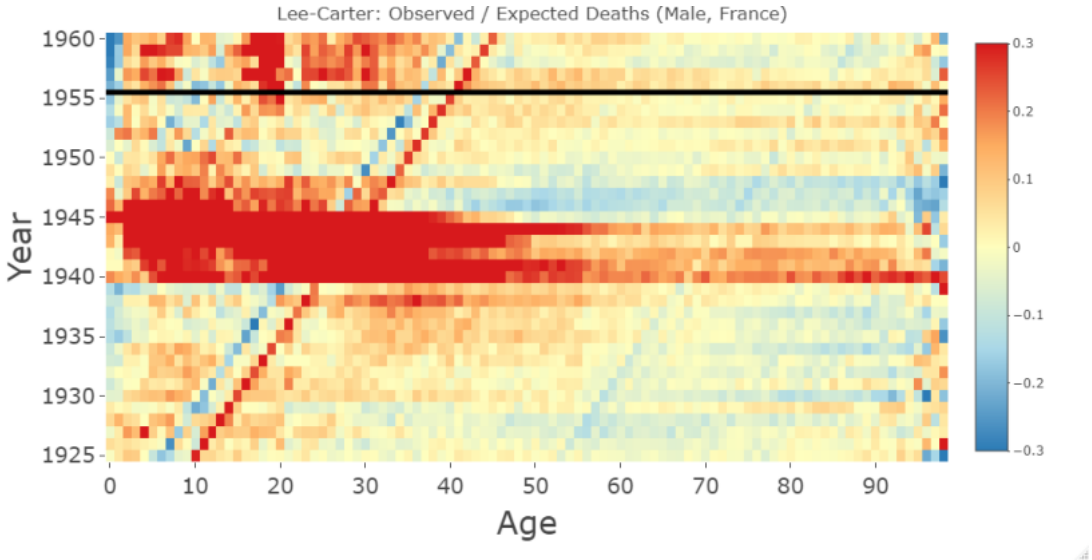

Figure 98: Lee-Carter Model mortality rate estimation errors after correction with the final fit correction method for calendar years 1925-1960 and ages 0-98 (French, male), the last five years were projected (above the black line).

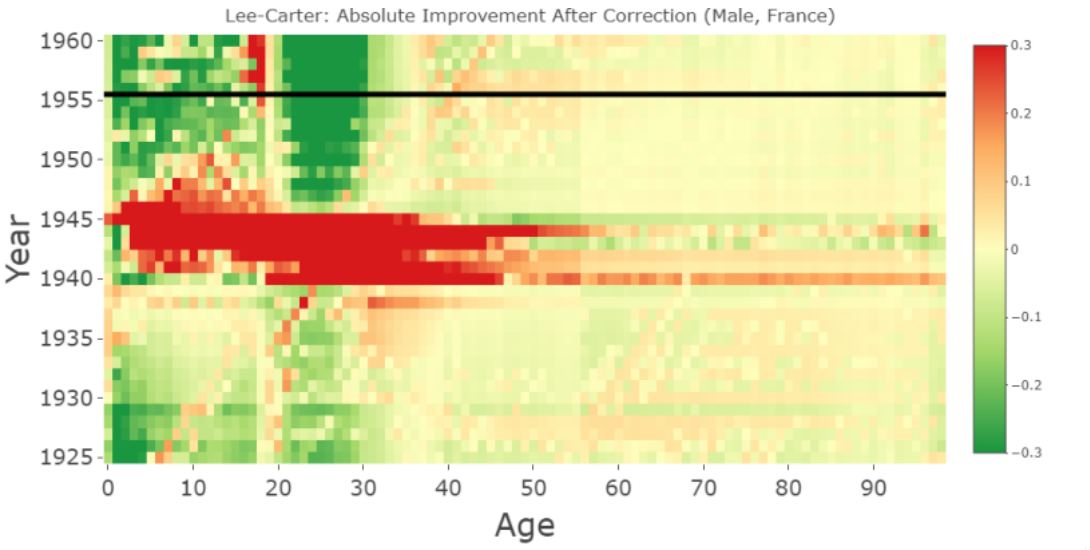

Figure 99: Lee-Carter Model mortality rate estimation improvements for calendar years 1925-1960 and ages 0-98 (French, male), the last five years were projected (above the black line). The graph compares no correction to the final fit correction method.

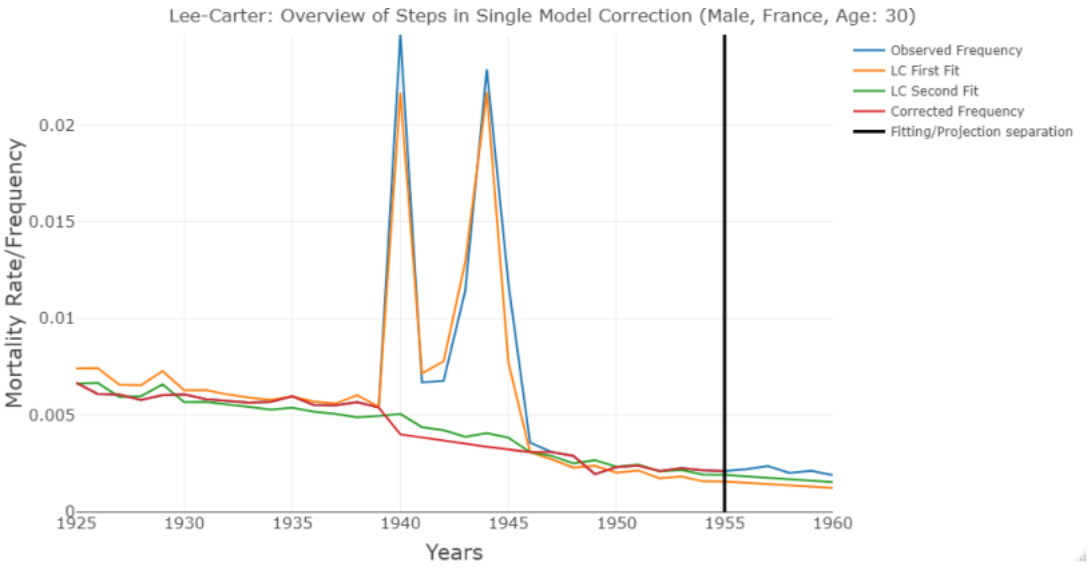

Figure 100: Lee-Carter Model mortality rate correction steps for calendar years 1925-1960 and age 30 (French, male), the last five years were projected (above the black line).

Renshaw-Haberman

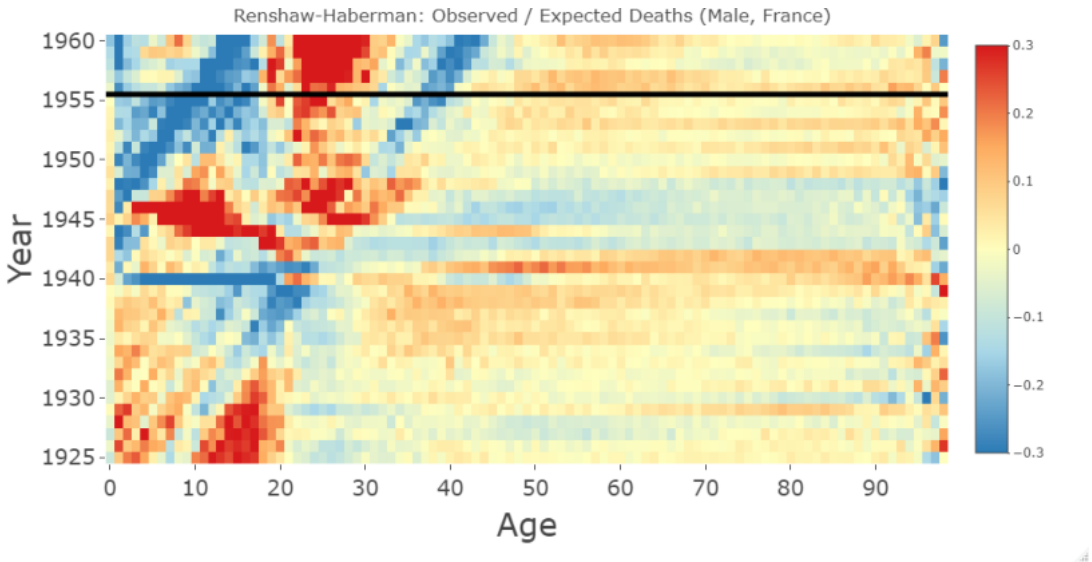

Figure 101: Renshaw-Haberman Model mortality rate estimation errors before correction for calendar years 1925-1960 and ages 0-98 (French, male), the last five years were projected (above the black line).

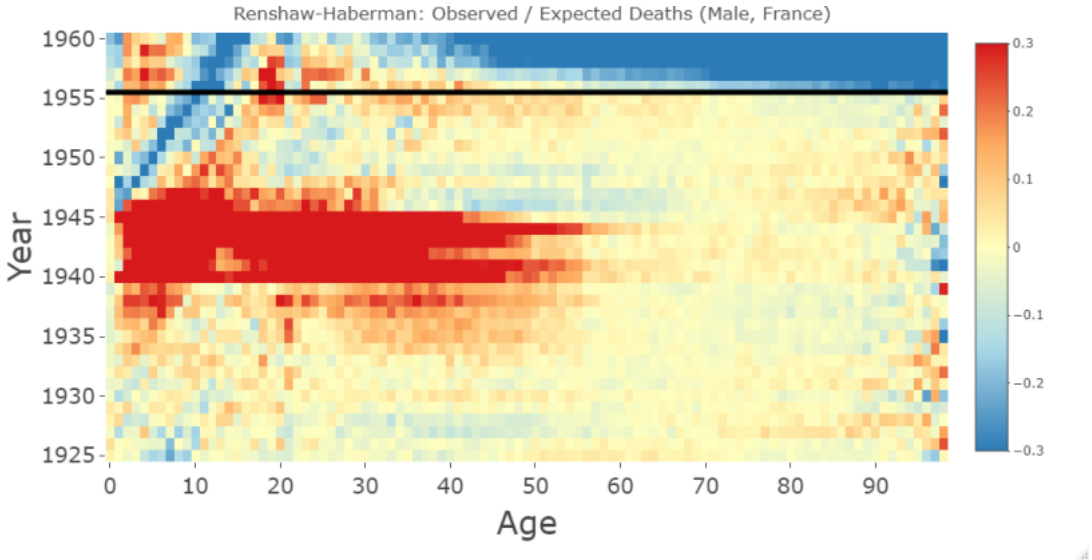

Figure 102: Renshaw-Haberman Model mortality rate estimation errors after correction with the final fit correction method for calendar years 1925-1960 and ages 0-98 (French, male), the last five years were projected (above the black line).

Figure 103: Renshaw-Haberman Model mortality rate estimation improvements for calendar years 1925-1960 and ages 0-98 (French, male), the last five years were projected (above the black line).The graph compares no correction to the final fit correction method.

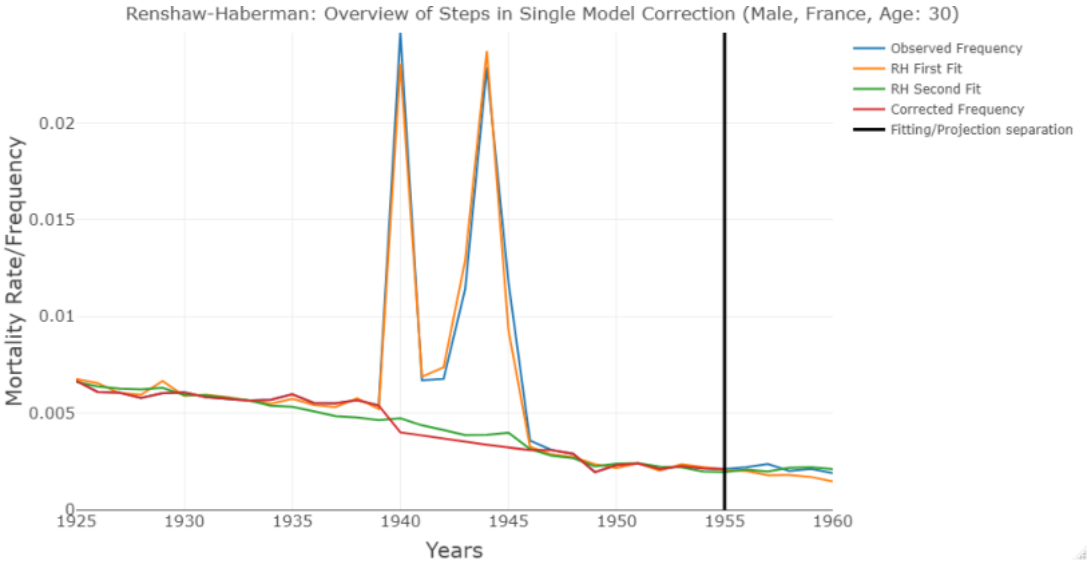

Figure 104: Renshaw-Haberman Model mortality rate correction steps for calendar years 1925-1960 and age 30 (French, male), the last five years were projected (above the black line).

Model Comparison

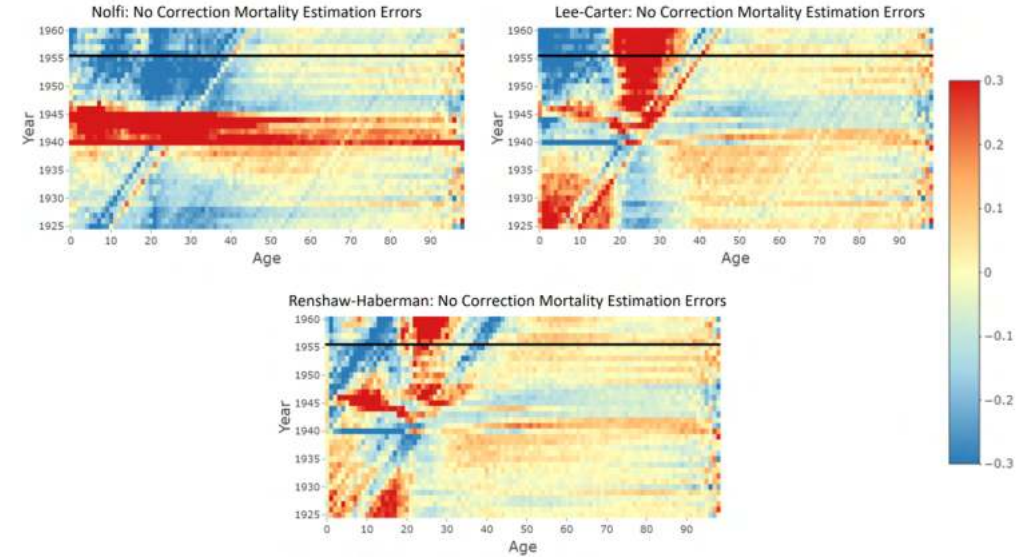

Figure 105: Mortality rate estimation improvements for calendar years 1925-1960 and ages 0-98 (French, male), the last five years were projected (above the black line). The graph shows the Nolfi, Lee-Carter and Renshaw-Haberman Model estimation errors before correction.

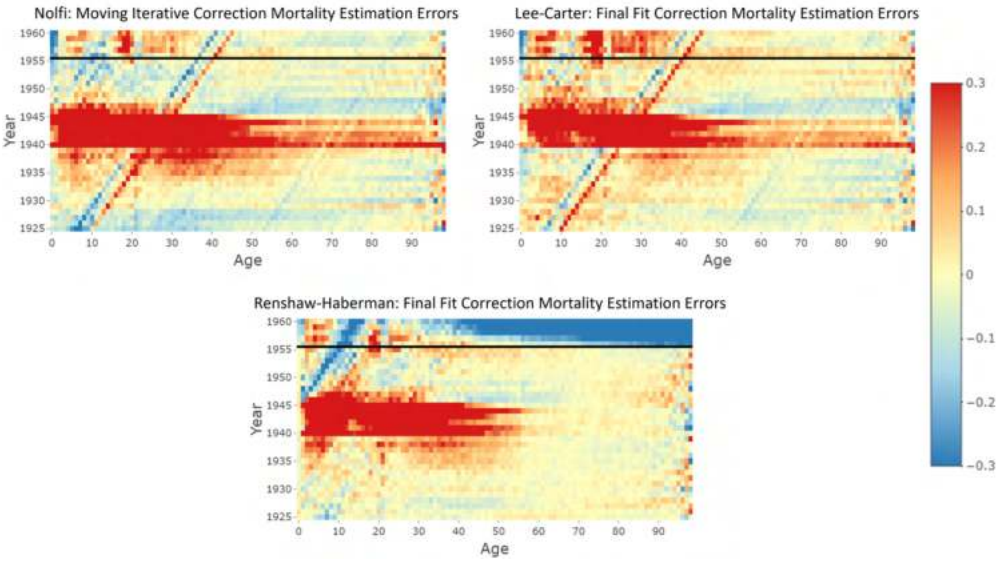

Figure 106: Mortality rate estimation improvements for calendar years 1925-1960 and ages 0-98 (French, male), the last five years were projected (above the black line). The graph shows the Nolfi, Lee-Carter and Renshaw-Haberman Model estimation errors after correction.

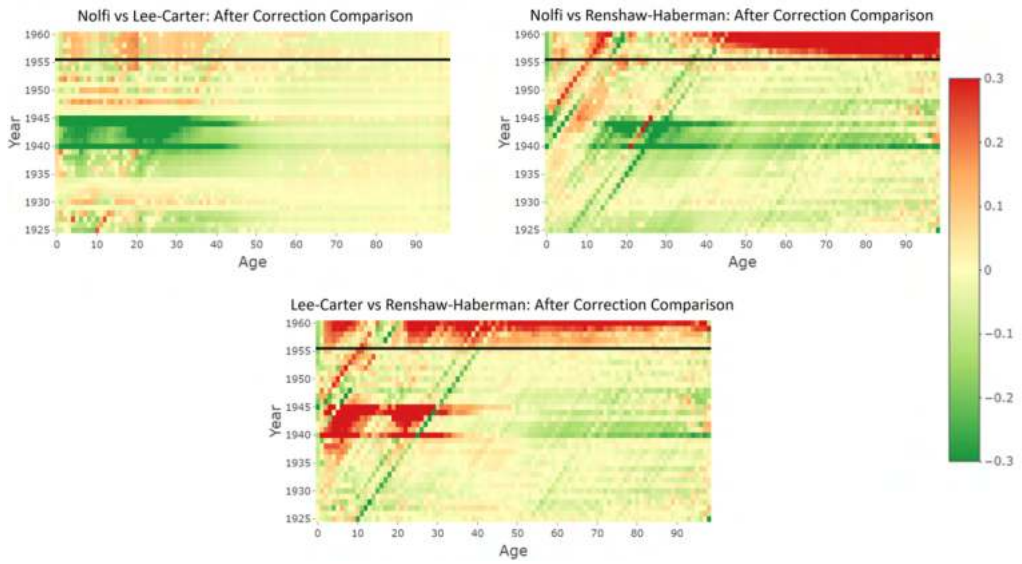

Figure 107: Mortality rate estimation improvements for calendar years 1925-1960 and ages 0-98 (French, male), the last five years were projected (above the black line). The graph compares the Nolfi, Lee-Carter and Renshaw-Haberman Models after correction. In the graphs the model before the"vs" is better when the colour is red, whereas the model after the "vs" is better when the colour is green.

Appendix C: Spanish Flu (Switzerland)

Singular Event

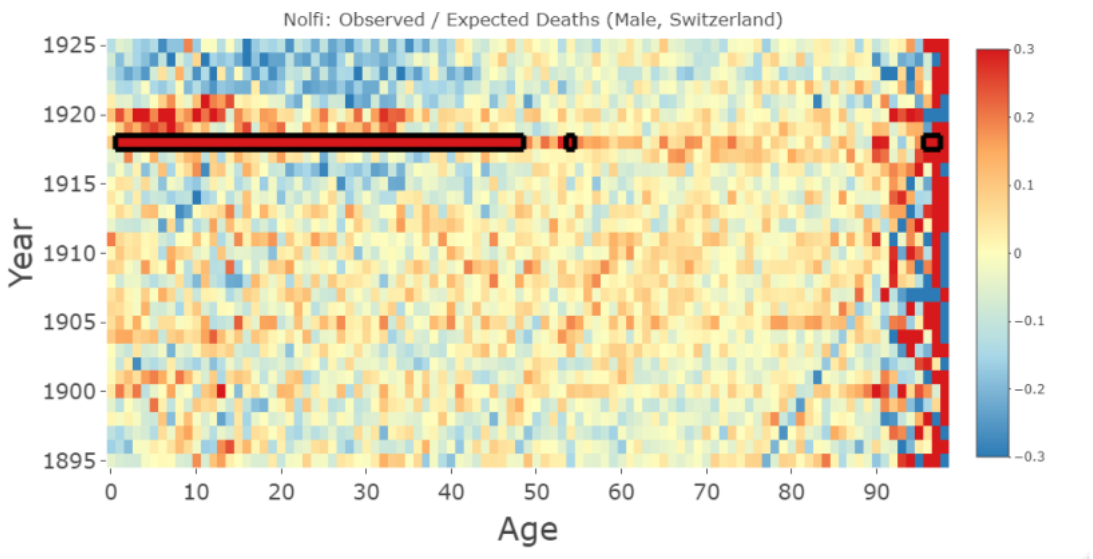

Figure 108: Nolfi Model mortality rate estimation errors for calendar years 1895-1925 (Swiss, male). The black box highlights the singular event as identified by the algorithm with parameters $\varepsilon = 0.3$, $\gamma^{(year)} = 1/3$, $\alpha^{(year)} = 0.5$, $\gamma^{(age)} = 2/3$ and $\alpha^{(year)} = 0.4$.

Nolfi

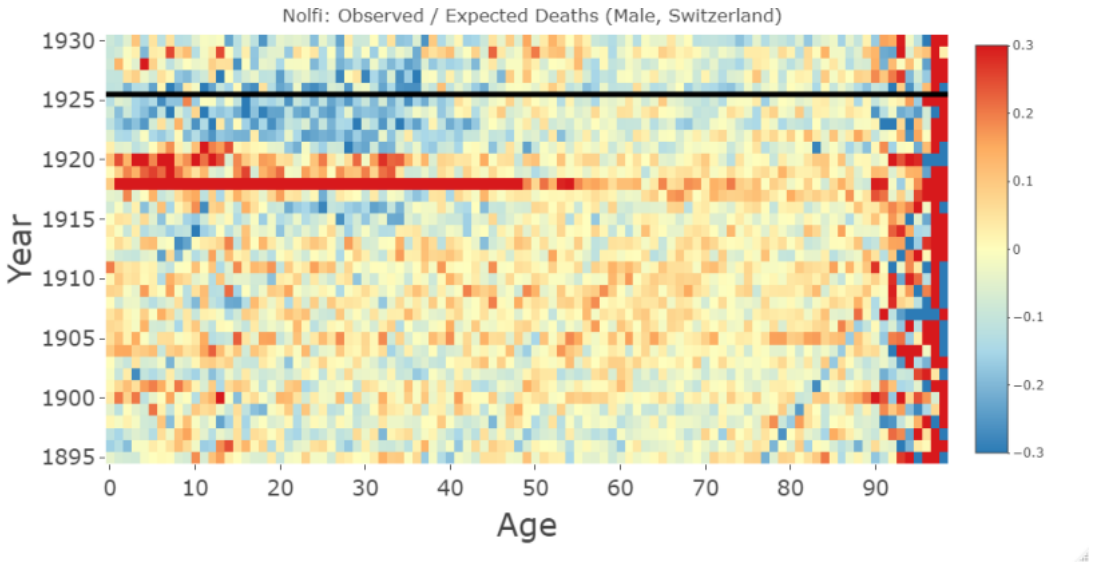

Figure 109: Nolfi Model mortality rate estimation errors before correction for calendar years 1895-1930 and ages 0-98 (Swiss, male), the last five years were projected (above the black line).

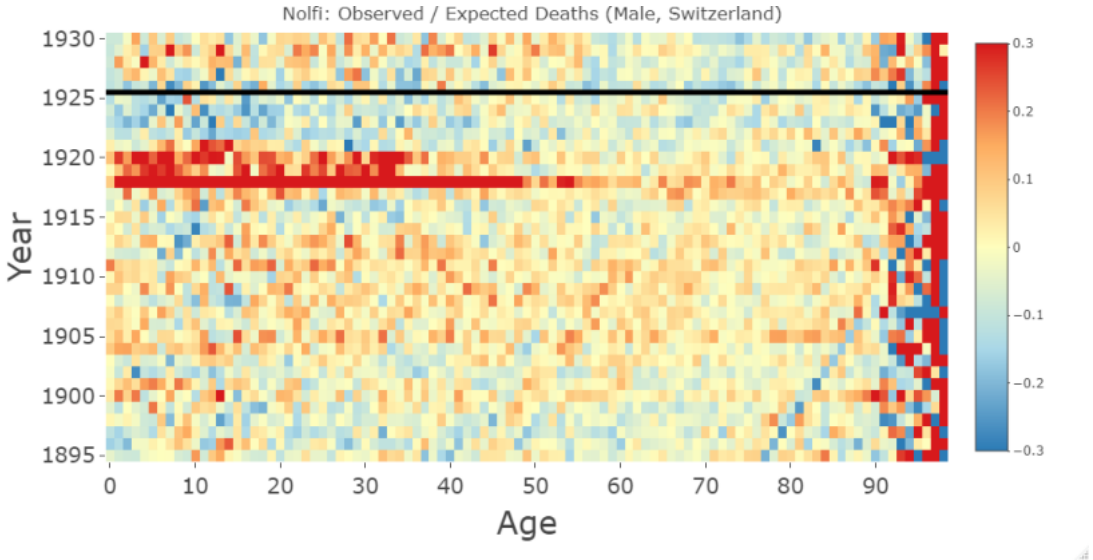

Figure 110: Nolfi Model mortality rate estimation errors after corretion with the moving iterative correction method for calendar years 1895-1930 and ages 0-98 (Swiss, male), the last five years were projected (above the black line).

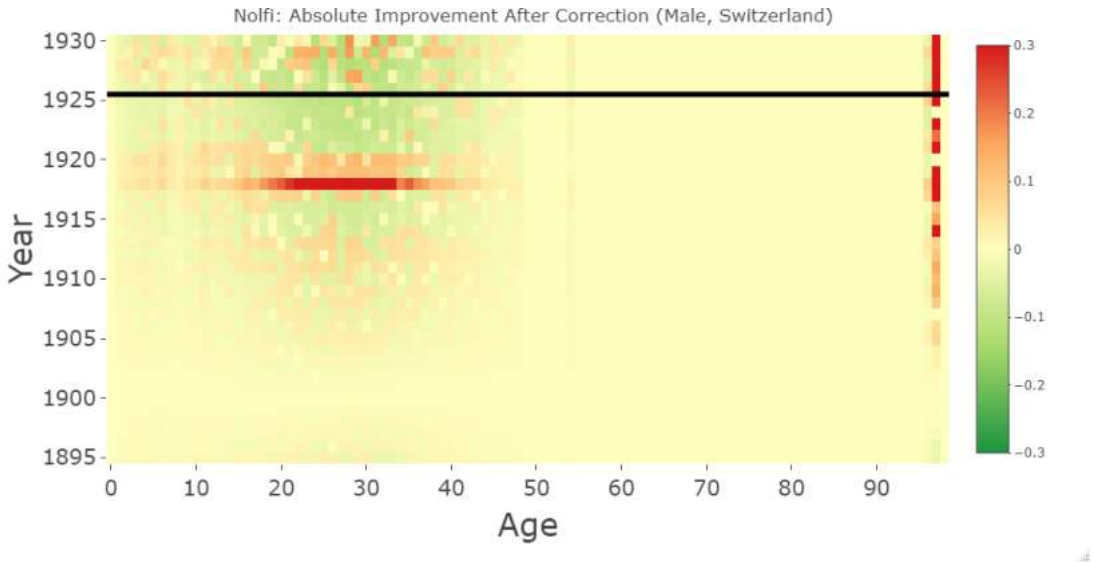

Figure 111: Nolfi Model mortality rate estimation improvements for calendar years 1895-1930 and ages 0-98 (Swiss, male), the last five years were projected (above the black line). The graph compares no correction to the moving iterative correction method.

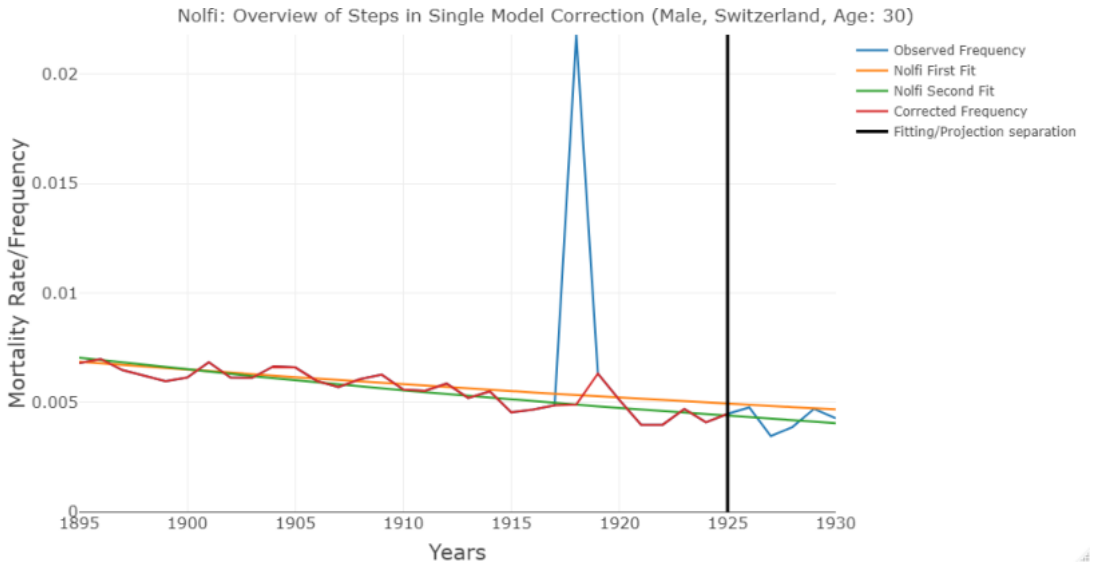

Figure 112: Nolfi Model mortality rate correction steps for calendar years 1895-1930 and ages 30 (Swiss, male), the last five years were projected (left of the black line).

Lee-Carter

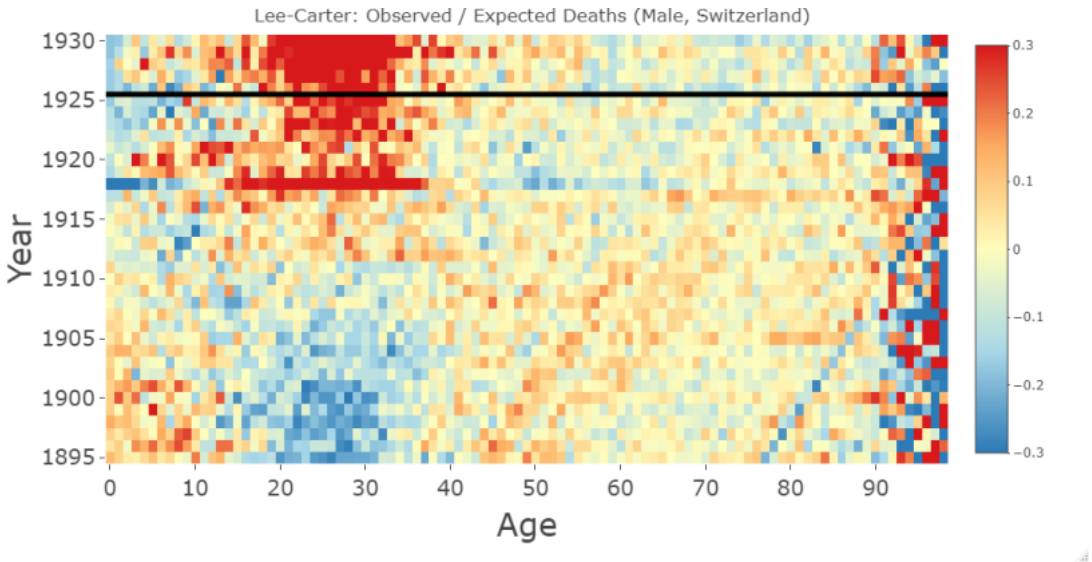

Figure 113: Lee-Carter Model mortality rate estimation errors before correction for calendar years 1895-1930 and ages 0-98 (Swiss, male), the last five years were projected (above the black line).

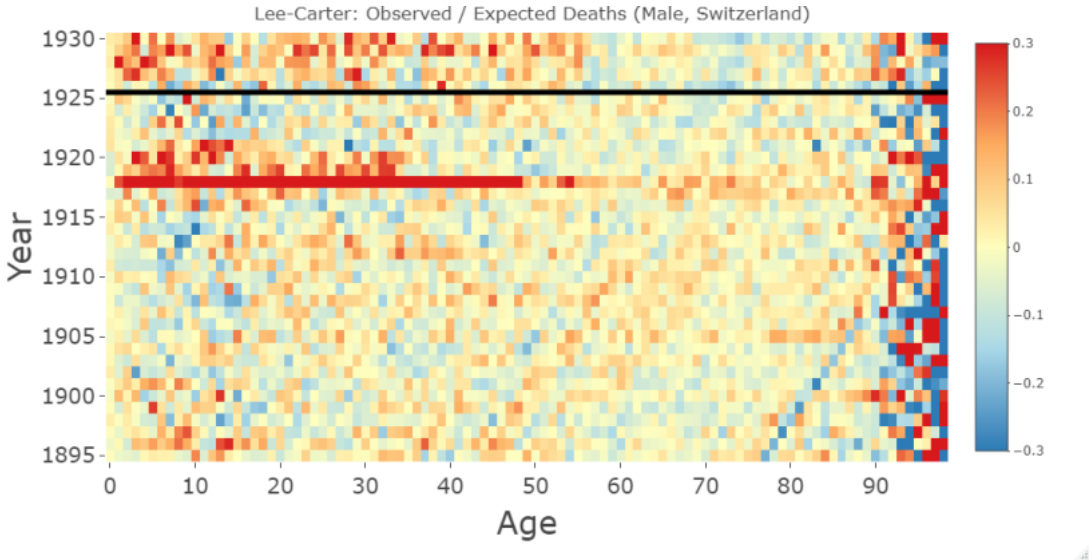

Figure 114: Lee-Carter Model mortality rate estimation errors after corretion with the final fit correction method for calendar years 1895-1930 and ages 0-98 (Swiss, male), the last five years were projected (above the black line).

Figure 115: Lee-Carter Model mortality rate estimation improvements for calendar years 1895-1930 and ages 0-98 (Swiss, male), the last five years were projected (above the black line). The graph compares no correction to the final fit correction method.

Figure 116: Lee-Carter Model mortality rate correction steps for calendar years 1895-1930 and ages 30 (Swiss, male), the last five years were projected (left of the black line).

Renshaw-Haberman

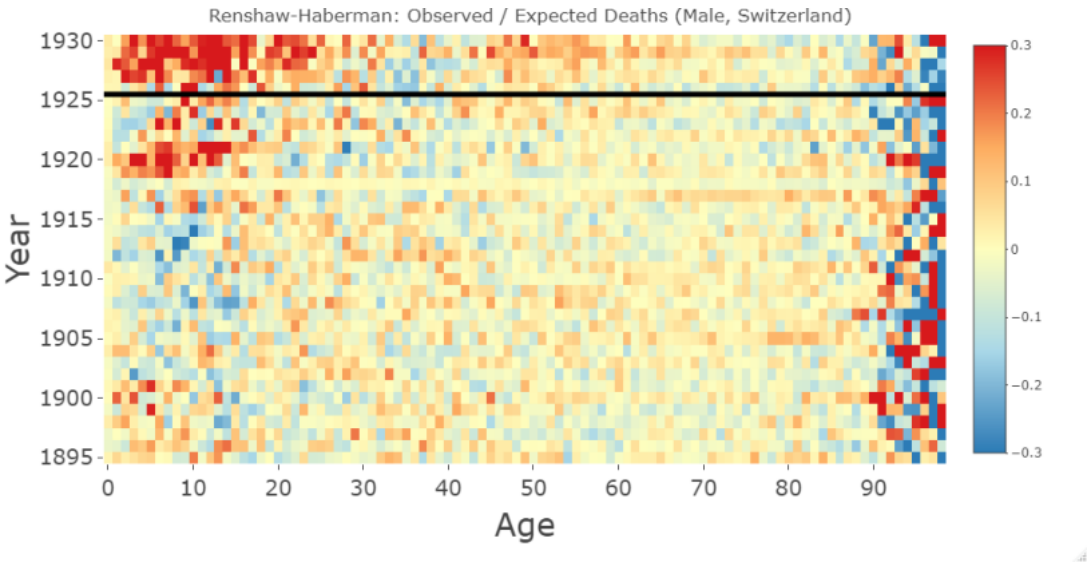

Figure 117: Renshaw-Haberman Model mortality rate estimation errors before correction for calendar years 1895-1930 and ages 0-98 (Swiss, male), the last five years were projected (above the black line).

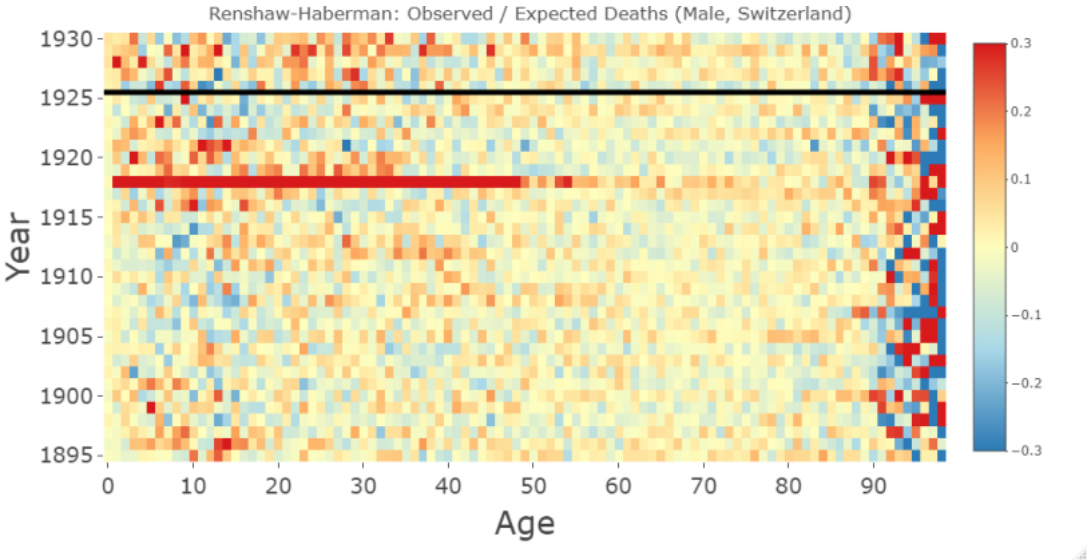

Figure 118: Renshaw-Haberman Model mortality rate estimation errors after corretion with the final fit correction method for calendar years 1895-1930 and ages 0-98 (Swiss, male), the last five years were projected (above the black line).

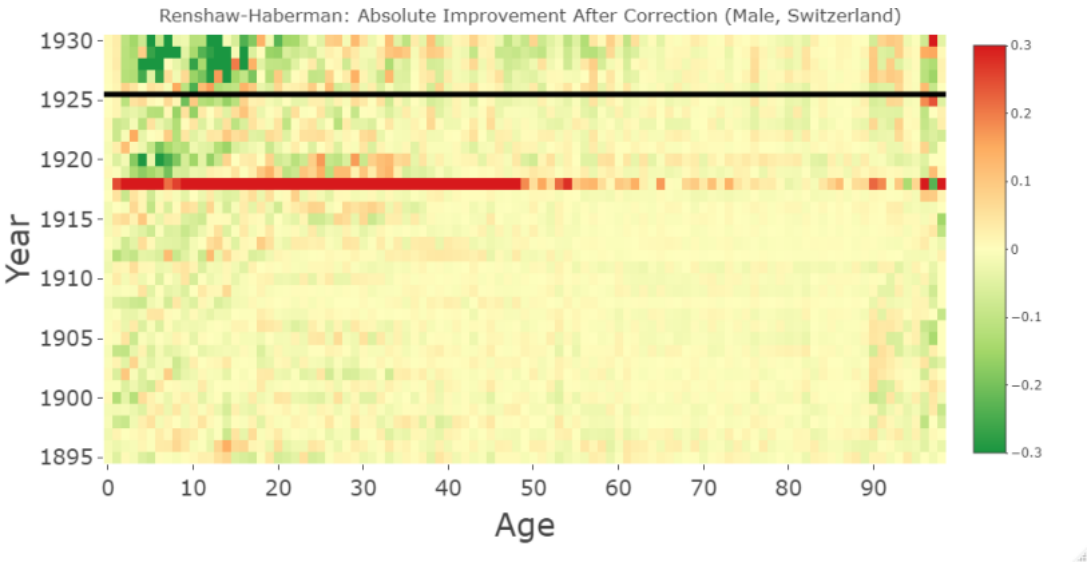

Figure 119: Renshaw-Haberman Model mortality rate estimation improvements for calendar years 1895-1930 and ages 0-98 (Swiss, male), the last five years were projected (above the black line). The graph compares no correction to the final fit correction method.

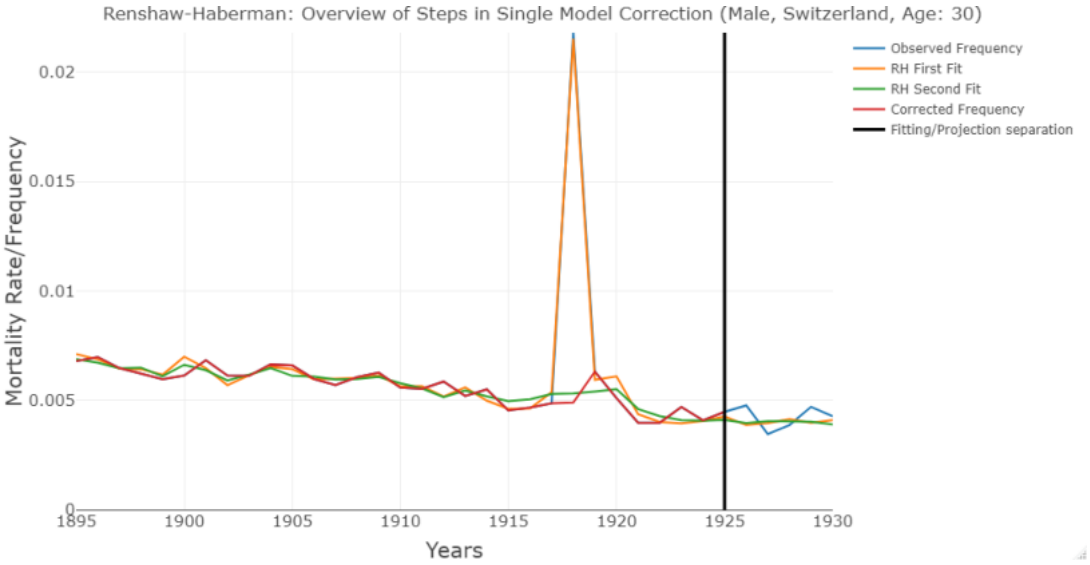

Figure 120: Renshaw-Haberman Model mortality rate correction steps for calendar years 1895-1930 and ages 30 (Swiss, male), the last five years were projected (left of the black line).

Model Comparison

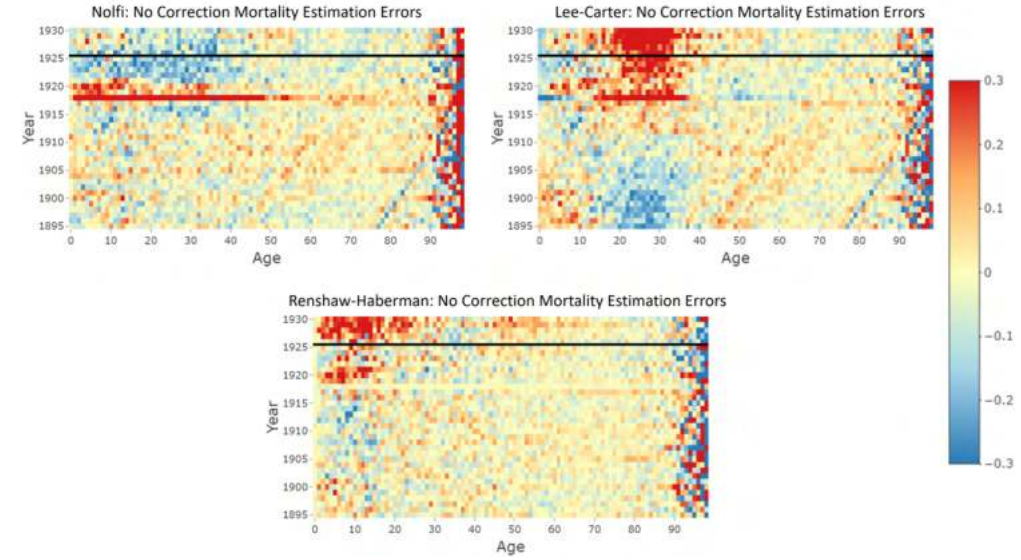

Figure 121: Mortality rate estimation improvements for calendar years 1895-1930 and ages 0-98 (Swiss, male), the last five years were projected (above the black line). The graph shows the Nolfi, Lee-Carter and Renshaw-Haberman Model estimation errors before correction.

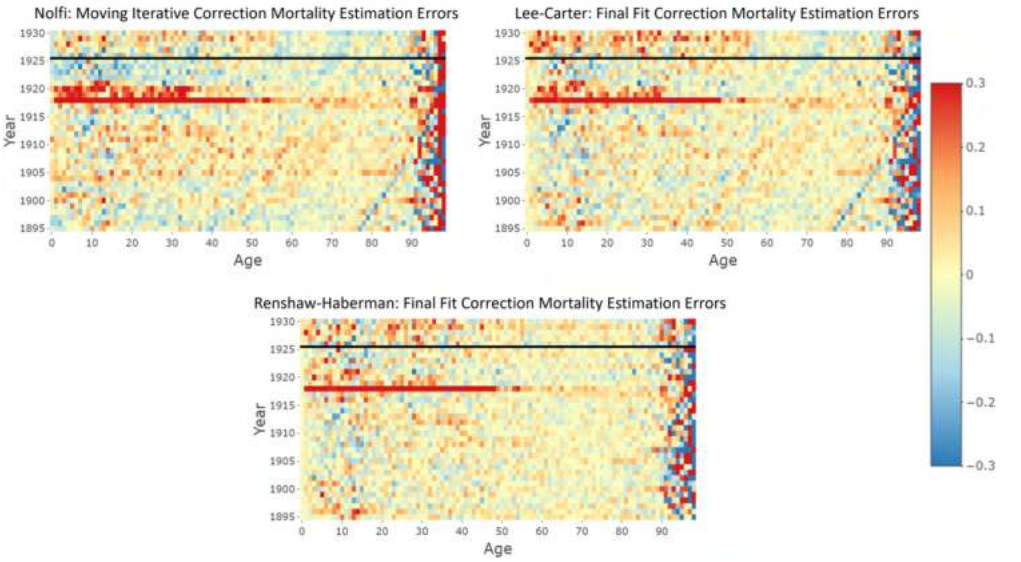

Figure 122: Mortality rate estimation improvements for calendar years 1895-1930 and ages 0-98 (Swiss, male), the last five years were projected (above the black line). The graph shows the Nolfi, Lee-Carter and Renshaw-Haberman Model estimation errors after correction.

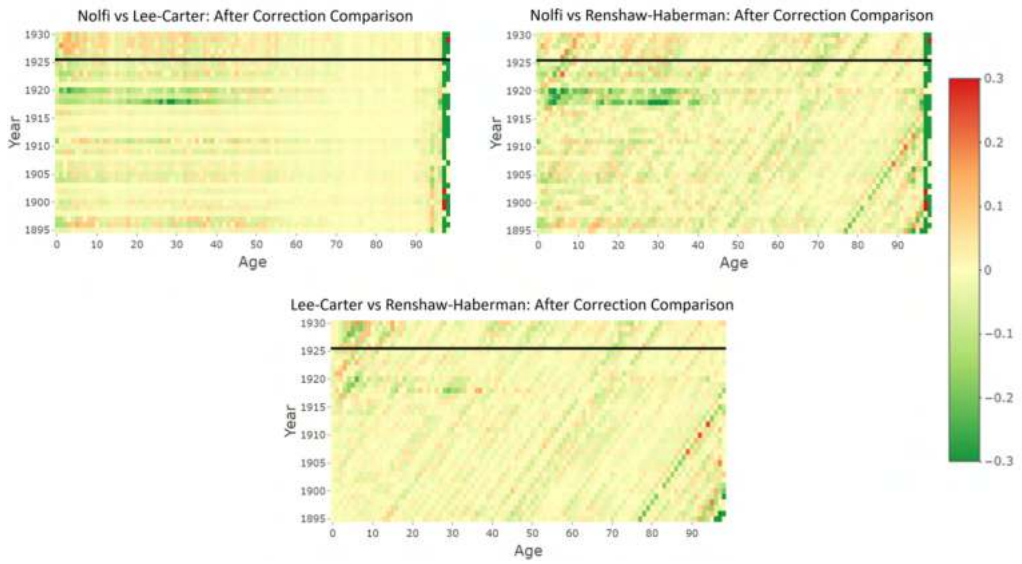

Figure 123: Mortality rate estimation improvements for calendar years 1895-1930 and ages 0-98 (Swiss, male), the last five years were projected (above the black line). The graph compares the Nolfi, Lee-Carter and Renshaw-Haberman Models after correction. In the graphs the model before the"vs" is better when the colour is red, whereas the model after the "vs" is better when the colour is green.

References

[1] F. Weber, "Lebensversicherungmathematik," Sep. 2021.

[2] *Auswirkungen der Covid-19-Pandemie auf die Sterblichkeit in der Schweiz*, DE, 19305028. Neuchâtel: Bundesamt für Statistik (BFS), Oct. 2021, p. 8. [Online]. Available: https://dam-api.bfs.admin.ch/hub/api/dam/assets/19305028/master.

[3] T. Tharmagulasingam, "Untersuchungen zur sterblichkeitsentwicklung," Jan. 2020.

[4] T. van Rijn, "Backtesting nolfi und lee-carter," Apr. 2021.

[5] M. Merz, "Statistische verfahren zur tarifierung und reservierung in der schadenversicherung," in Sep. 2020, ch. 2.

[6] R. Lee and L. Carter, "Modeling and forecasting u.s. mortality," *Journal of The American Statistical Association - J AMER STATIST ASSN*, vol. 87, pp. 659–671, Sep. 1992. DOI: 10.1080/01621459.1992.10475265.

[7] A. M. Villegas, V. K. Kaishev, and P. Millossovich, "Stmomo: An r package for stochastic mortality modeling," *Journal of Statistical Software*, vol. 84, no. 3, pp. 1–38, 2018. DOI: 10.18637/jss.v084.i03. [Online]. Available: https://www.jstatsoft.org/index.php/jss/article/view/v084i03.

[8] N. Brouhns, M. Denuit, and J. Vermunt, "A poisson log-bilinear regression approach to the construction of projected life tables," *Insurance: Mathematics and Economics*, vol. 31, pp. 373–393, Dec. 2002. DOI: 10.1016/S0167-6687(02)00185-3.

[9] S. Haberman and A. Renshaw, "On age-period-cohort parametric mortality rate projections," *Insurance: Mathematics and Economics*, vol. 45, no. 2, pp. 255–270, 2009, ISSN: 0167-6687. DOI: https://doi.org/10.1016/j.insmatheco.2009.07.006. [Online]. Available: https://www.sciencedirect.com/science/article/pii/S016766870900081X.

[10] A. Hunt and A. M. Villegas, "Robustness and convergence in the lee–carter model with cohort effects," *Insurance: Mathematics and Economics*, vol. 64, pp. 186–202, 2015, ISSN: 0167-6687. DOI: https://doi.org/10.1016/j.insmatheco.2015.05.004. [Online]. Available: https://www.sciencedirect.com/science/article/pii/S0167668715000852.

[11] H. L. Turner and D. Firth, "Generalized nonlinear models in r: An overview of the gnm package," 2007.